THE UNIVERSITY OF MICHIGAN

COLLEGE OF ENGINEERING
Department of Aeronautical and Astronautical Engineering
Aircraft Propulsion Laboratory

Final Report Part I

THE PERFORMANCE OF SUPERSONIC NOZZLES AS USED IN THE OXYGEN CONVERSION PROCESS

D. R. Glass
P. O. Hays

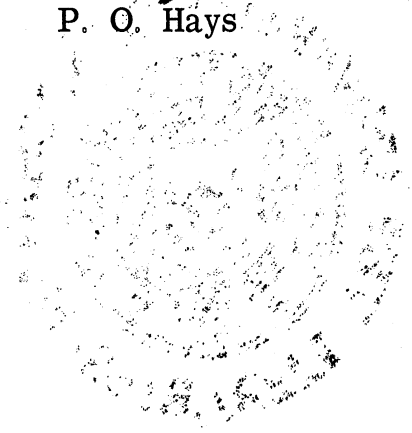

ORA Project 04806

under contract with:

McLOUTH STEEL CORPORATION
TRENTON, MICHIGAN

administered through:

OFFICE OF RESEARCH ADMINISTRATION ANN ARBOR

August 1963

TABLE OF CONTENTS

LIST OF ILLUSTRATIONS

Figure

LIST OF TABLES

ABSTRACT

The ideal relation between the oxygen flow rate through a sonic or supersonic nozzle, the nozzle throat area, and the pressure impressed on the nozzle is presented and is shown to be accurate within one or two percent for several nozzles typical of those used in the Oxygen Conversion Process of Steelmaking. This relation states that the oxygen flow rate in cubic feet per minute is equal to 17.45 times the pressure upstream of the nozzle (psia) times the nozzle throat area (square inches) under the conditions specified.

Results of a large number of tests wherein the nozzle exhausted into room air are presented. The gas exhausting from the nozzles was in most cases air; test results are presented which show the interchangeability of oxygen and air for such tests. These tests show that when a gas jet impacts on a surface, normal to the jet axis, the force per unit area (i.e., pressure) exerted by the gas on the surface near the center of the impact area will in general increase when:

1. the pressure imposed on the nozzle inlet increases,
2. the nozzle size increases, and
3. the distance between the nozzle and the point of impact decreases.

Certain exceptions to this general rule are presented and discussed.

Data regarding the extent of the supersonic core within the jet and the rate of jet spread in room air are presented for supersonic nozzles of the type used in the Oxygen Conversion Process.

The deleterious affect on the penetration capability of a gas jet due to the use of improperly designed nozzles is discussed. In particular it is shown that the use of a converging (i.e., sonic) nozzle at an operating pressure near or above 100 psig results in a jet which has appreciably

less penetration capability than does the jet from a reasonably well designed converging-diverging (i. e., supersonic) nozzle operating at the same pressure.

Results are presented for a large number of tests wherein a gas jet was directed downward onto a liquid surface from directly above the bath. These tests involved many different combinations of gases and liquids. In all cases, to the extent that conditions within the bath could be observed and/or measured it was found that:

1. The jet tended to create within the liquid a "Basic Circulation Pattern" which is characterized by the liquid moving up and out of the cavity created by the jet, outward toward the vessel walls along and above the bath surface, downward near the vessel walls, in toward the center of the vessel in the bottom regions of the bath and upward toward the cavity from the region below the cavity created by the jet.
2. The depth to which the jet penetrates into the liquid generally increases when the nozzle size is increased, when the gas pressure imposed on the nozzle is increased, or when the height of the nozzle above the bath is decreased.

A method, based on nozzle test data, of estimating the depth to which a jet will penetrate into a liquid bath is presented. It is shown, however, that the use of data from nozzle tests conducted in room air will result in an underestimate of the penetration to be expected in the case of an oxygen jet blowing onto molten iron. Surrounding a gas jet with a heated atmosphere (as is done when oxygen is blown on molten iron) usually results in the jet having a greater penetration capability (at a given distance from the nozzle) than the jet would have in room air. The results of a number of tests made to determine the relation between nozzle size, nozzle height above the bath, the oxygen pressure

imposed on the nozzle and the depth to which the oxygen jet penetrates a molten iron bath are presented. These tests were conducted in The University of Michigan's Cast Metals Laboratory, under the direction of Professors R. A. Flinn and R. D. Pehlke. The results of these penetration tests are presented in the form of an "Empirical Penetration Curve."

OBJECTIVE

The overall objective in these studies is to understand and define the way in which nozzle configuration and operating conditions affect the operation of the Oxygen Conversion Process of Steelmaking; primarily as regards jet penetration into the liquid bath and the movement of the bath.

INTRODUCTION

The Oxygen Conversion Process is used in steel production to remove impurities from the iron. This process employs nozzles which direct an oxygen jet into the molten iron from directly above the bath. The depth to which the jet penetrates and the extent of the resulting movement of the bath are dependent on the nozzle configuration, nozzle driving pressure, and nozzle height above the bath surface. The work reported herein was done to obtain a better understanding of the physical mechanisms of penetration and bath movement and how these are affected by changes in the various nozzle parameters.

SECTION A

NOZZLE EQUATIONS AND COEFFICIENTS

The ideal equation for the flow of oxygen through a nozzle is:

$$Q = 17.45\ P_o\ A_t \qquad (1)$$

where Q = flow rate - standard cubic feet per minute, based on a standard atmospheric pressure of 14.7 psia and temperature of 60°F.

P_o = stagnation or reservoir pressure immediately upstream of the nozzle - pounds per square inch absolute.

A_t = the area of the nozzle throat-square inches.

The coefficient (17.45) in Equation 1 is based on the characteristics of oxygen and the assumption that the stagnation temperature of the oxygen upstream of the nozzle is 60°F. Equation 1 is in general applicable only if P_o is over about twice the absolute pressure of the region into which the nozzle is exhausting, thus producing sonic velocity at the nozzle throat.

The stagnation or reservoir pressure of a gas can be measured directly when the gas is essentially at rest, but it is usually desirable to write Equation 1 in terms of the static pressure (as measured by a pressure tap flush with the inside wall of the pipe approaching the nozzle) instead of in terms of stagnation pressure. This can be done by re-writing Equation 1;

$$Q = \frac{17.45\ P\ A_t}{(P/P_o)} \qquad (2)$$

where P is the static pressure upstream of the nozzle—pounds per square inch absolute (psia). The ratio P/P_o is determined, for a particular gas, by the ratio of the nozzle throat diameter to the approach pipe diameter. Figure 1 is a plot of P/P_o versus the ratio of the throat diameter to approach pipe diameter. Note that when the nozzle throat diameter is less than one half the approach pipe diameter the correction factor P/P_o is nearly unity.

The flow through a nozzle is generally somewhat less than the ideal equation would predict. A nozzle discharge coefficient, C_w, is used to correct the ideal nozzle equation where:

$$C_w = \frac{\text{Actual flow rate}}{\text{Theoretical flow rate}} \tag{3}$$

Thus Equation 2 becomes:

$$Q = \frac{C_w \, 17.45 \, A_t \, P}{(P/P_o)} \tag{4}$$

The nozzle discharge coefficient, C_w, is in general an empirical constant determined by tests of individual nozzles. However, a "well designed" nozzle should have a nozzle discharge coefficient of 0.99 (Ref. 5, page 99). A special well designed "test nozzle" was built according to recommendations contained on page 29 of Reference 7. It was concluded that the nozzle discharge coefficient for this "test nozzle" was 0.99, based on References 5, 6, and 7.

This "test nozzle" was then used to determine the nozzle discharge coefficients for three other nozzles with results as listed in Table A-1.

Table A-1

NOZZLE DATA AND COEFFICIENTS

Throat Diameter	Pipe Diameter	A_t	C_w	(P/P_o)	$\frac{17.45\ C_w\ A_t}{(P/P_o)}$
	in.	$in.^2$			
35 mm (Linz I)	2.466	1.492	0.972	0.977	25.92
1 5/8 in. (McL. OP-1)	2.625	2.075	0.967	0.963	36.25
1 5/8 in. (McL. OP-2)	3.25	2.075	0.967	0.983	35.6

For example, the oxygen flow rate through the McLouth 1 5/8 in. nozzle with the 2.625 approach pipe (used in McLouth's OP-1), from Table A-1 is:

$$Q = 36.25\ P \tag{5}$$

where P is the static pressure a few pipe diameters upstream of the nozzle throat and is in pounds per square inch—absolute, and the reservoir temperature is assumed to be $60^{\circ}F$.

When the flow rate, Q, is based on reference conditions other than the standard temperature of $60^{\circ}F$ (or 520° Rankine) and the standard pressure of 14.7 psia, the above equation can be adapted as follows:

$$Q_{reference} = Q\,\frac{14.7}{520}\,\frac{T_{ref.}\ (^{\circ}\text{Rankine})}{P_{ref.}\ (\text{psia})} \tag{6}$$

The "ideal" exit area for a supersonic nozzle is determined for a specific gas, by the ratio of exit pressure to driving pressure (psia), where the "ideal" area is defined as that area which for a given nozzle throat area and driving pressure will result in the nozzle exit pressure being just equal to ambient or surrounding pressure. Values of

the ratio, A_{exit}/A_{throat}, are tabulated with the ratio, P_{exit}/P_o, as well as exit Mach number, M (M = local gas velocity divided by local speed of sound) in Reference 8. Conversely, the "ideal" or "design" driving pressure is herein defined as the driving pressure which, for a given nozzle, results in the pressure at the nozzle exit just equaling ambient pressure.

Figures 2, 3, and 4 are plots of theoretical nozzle data of interest in the design of supersonic nozzles. The term P_d, nozzle driving pressure, when used in the presentation of theoretical data in this report denotes the stagnation pressure upstream of a nozzle (e. g., Figures 2, 3, and 4), but when test results are presented P_d is the measured static pressure upstream of the nozzle.

Table A-2 is a list of most of the various nozzles used throughout these studies together with their more pertinent characteristics.

Table A-2

DIMENSIONS OF VARIOUS NOZZLES UTILIZED

Nozzle		D_t-Throat Diameter in.	D_e-Exit Diameter in.	Convergent Half Angle Degrees	Divergent Half Angle Degrees	Approach Pipe Diameter in.	Throat Length in.	$\frac{A_e}{A_t}$	"Ideal" Driving Pressure psig
A	McLouth (OP-1)	1.625	1.875	6 1/2	~2 1/2	2 5/8	~1 3/8	1.33	57
B	Laboratory Nozzle built to conform to dimensions of Linz I 35 mm Lance	1.378	2.165	8	8	2 1/2	~D_t	2.47	210
C	Laboratory Nozzle	1.100	1.730	8	8	2 1/2	~D_t	2.47	210
D	Laboratory Nozzle	0.780	1.228	8	8	2 1/2	~D_t	2.47	210
E	Laboratory Nozzle (14 mm)	0.552	0.867	8	8	2 1/2	~D_t	2.47	210
F	Laboratory Nozzle	0.392	0.613	8	8	2 1/2	~D_t	2.47	210
G	Laboratory Nozzle (8 mm)	0.315	0.394	8	8	2 1/2	~D_t	1.56	84
H	McLouth (OP-2)	1.625	2.25	7	10	3 1/4	~1/2	1.92	130
I	Water Cooled Lance for Laboratory use 8 mm No. 1	0.315	0.349	30	10	1/2	~D_t	1.23	46
J	Water Cooled Lance for Laboratory use 8 mm No. 2	0.316	0.368	30	10	1/2	~D_t	1.36	60
K	Water Cooled Lance for Laboratory use	0.162	0.173	30	10	1/2	~D_t	1.152	36
L	McLouth	1.875	2.759	5 1/2	10	2 5/8	1 1/4	2.16	164

Nozzle A - Lance No. 1 of McLouth Steel Corp. Dwg. No. 10301; 6-15-55
Nozzle H - McLouth Steel Corp. Dwg. No. 13090
Nozzle I - see Figure 5
Nozzle L - Lance No. 2 of McLouth Steel Corp. Dwg. No. 10301; 6-15-55

Several other small nozzles have been built and used in model tests. These general purpose nozzles were usually convergent, for ease of construction.

Note that Nozzle A is usually operated well above its design or ideal driving pressure while Nozzle B is normally operated well below its design driving pressure.

SECTION B

NOZZLE TEST RESULTS

A number of nozzles have been tested which are pertinent to the oxygen conversion process. The nozzles tested include McLouth production type nozzles and smaller nozzles made for purposes of this study. In almost all cases the immediate objective of these tests was to determine the penetration capability of the jet produced by one set of nozzle conditions relative to that of a jet produced by another set of conditions.

Throughout this section the nozzle performance is expressed primarily in terms of $(P_i)_{max}$, where by definition:

$(P_i)_{max}$ = the gauge pressure measured along the jet centerline and on the upstream side of a flat plate so located that the jet strikes the plate at right angles. $(P_i)_{max}$ may be expressed in many ways, such as inches of mercury, inches of water, or inches of liquid iron. 1 in. mercury = 13.6 in. water $\cong$ 2 in. iron. As a general rule an increase in $(P_i)_{max}$, when measured at an appropriate distance, results in an increase in the penetration capability of the jet.

This section deals only with nozzle tests wherein the nozzle exhausted into room air. The effect of a heated atmosphere on $(P_i)_{max}$ is discussed in Section D.

Figure 6 is a schematic drawing of the setup used to obtain the majority of the $(P_i)_{max}$ data presented herein.

Most of the more recent nozzle tests (other than those dealing directly with the jet penetrating into a liquid) have been conducted for the purpose of obtaining $(P_i)_{max}$ data. The results of these tests are presented in Figures 8 through 19. Although much of this data has been previously presented in preliminary reports it is included here for completeness. The data for Figures 8, 10, 11 and 12 were obtained using the heated atmosphere facility shown in Figure 7. The center of the jet impinged on a slightly cupped impact surface instead of the flat plate shown in Figure 6. Because the impact plate was so nearly flat the pressures measured on the upstream side of this plate are also presented herein as $(P_i)_{max}$ data.

Figure 8 is a plot of $(P_i)_{max}$ vs. driving pressure at various blowing distances for a water cooled lance having a throat diameter of 0.162 in. (Nozzle K of Table A-2). This lance was built for use in hot iron tests in the Cast Metals Laboratory of the Department of Chemical and Metallurgical Engineering. The $(P_i)_{max}$ data was desired for comparison with the hot iron tests.

Figure 9 is a plot of $(P_i)_{max}$ vs. blowing distance at various driving pressures for an 8 mm laboratory nozzle (Nozzle G of Table A-2).

Figures 10 and 11 are plots of $(P_i)_{max}$ vs. driving pressure at various blowing distance for two 8 mm water cooled lances (I and J respectively of Table A-2). These lances were also built for hot iron tests in the Cast Metals Laboratory. Both lances were tested rather exhaustively to determine what, if any, differences existed between the two as regards to $(P_i)_{max}$ performance. Clearly there are only slight differences between the two and these show up primarily at the lower blowing distances.

Figure 12 is a plot of $(P_i)_{max}$ vs. driving pressure for an 8 mm lance (I of Table A-2). The data for this graph were obtained using both air and oxygen, separately. This figure clearly demonstrates that insofar as these nozzle tests are concerned, results obtained using air are applicable to the use of oxygen.

Although the nozzles used in oxygen converters are blowing oxygen, it was impractical to conduct all nozzle tests with oxygen. Since air and oxygen behave similarily in flowing through a nozzle, air was used for most nozzle tests discussed in this section. Figure 12 justifies that procedure. As further proof of the interchangeability of air and oxygen for these tests, a brief test was made using a nozzle having a 35 mm throat (B of Table A-2) wherein oxygen was delivered to the nozzle at 119 psig. The $(P_i)_{max}$ measured at a blowing distance of 43.3 inches was 25.4 inches of mercury. Air at the same driving pressure and blowing distance resulted in a $(P_i)_{max}$ of 25 inches of mercury. The difference in $(P_i)_{max}$ was less than 2% which is within the accuracy expected for these tests.

Figure 2 (obtained from Ref. 8) can be used for determining the theoretically "correct" ratio of nozzle exit area to throat area for any given operating condition. Any given converging-diverging (Laval) nozzle exhausting into the atmosphere has a "design" or "ideal" driving pressure which is by definition the driving pressure which results in the nozzle exit pressure being just equal to atmospheric pressure. Thus when a given convergent-divergent nozzle is being tested over a range of driving pressures it will in general be operating at a driving pressure which is not its "ideal" or "design" driving pressure. The results of such off-design operation are discussed below. The "ideal" or "design" driving pressure is listed in Table A-2 for comparison with the various nozzle test conditions used when evaluating $(P_i)_{max}$ data.

Figures 13, 14, 15, 16, and 17 are plots of $(P_i)_{max}$ vs. nozzle driving pressure for nozzles F, E, D, C, and B, respectively, of Table A-2. These 5 nozzles are all geometrically similar, in that these nozzles all have the same convergent and divergent angles, a throat length equal to the throat diameter and the same exit area to throat area ratio. The 14 mm nozzle (E) and the 35 mm nozzle (B) were of interest because of the use of similar nozzles in test work at Linz, Austria. Nozzles F, D, and C were built and tested to determine the repeatability of the $(P_i)_{max}$ curves for this family of five nozzles. Clearly there is a high degree of similarity in the results obtained, especially with the smaller nozzles of this family. Consider Figures 14A and 14B. The "hump" in the $(P_i)_{max}$ curves near a driving pressure of 50 psig results because the flow separates from the walls of the nozzle before the nozzle exit, at driving pressures less than 50 psig. As the driving pressure increases above 50 psig the flow follows the nozzle walls for a greater distance. The resulting over-expansion of the jet produces severe shocks which result in a decreased velocity downstream of the shock. Thus the continued decrease in $(P_i)_{max}$ as driving pressure increases from say 50 to 80 psig. Eventually the overall effect of these severe losses decreases as the nozzle driving pressure continues to increase and $(P_i)_{max}$ again increases with driving pressure. Sharp changes in $(P_i)_{max}$ occur at the higher driving pressures (above 100 psig) as a result of rather subtle changes in the shock pattern within the jet and the mixing along the jet. These changes in $(P_i)_{max}$ at the higher driving pressures are more dependent on the individual nozzle and are not as repeatable from one nozzle to another, within this family of similar nozzles, as were the changes near a driving pressure of 50 psig. The data show that the sharp changes in $(P_i)_{max}$ with driving pressure are less severe as the nozzle height (blowing distance) increases.

Figure 18 is a plot of $(P_i)_{max}$ vs. nozzle driving pressure for a McLouth 1.625 inch nozzle (A of Table A-2). For a blowing distance of 1100 mm (43.3 inches) it is clear that no sharp changes in $(P_i)_{max}$ occur. This nozzle is operating at a driving pressure above its design point while the nozzles of the family of 5 nozzles discussed before were all operating at pressures well below their design pressure. Refer to Table A-2 for tabulation of "Design Pressures."

Figure 19 is a composite plot of $(P_i)_{max}$ vs. blowing distance for several nozzles of interest. This summary plot clearly shows that the pressure exerted by a jet on a surface onto which the jet is impinging:

a. generally increases with nozzle driving pressure for a given nozzle, or
b. it generally increases with nozzle size for a fixed nozzle driving pressure, and
c. it generally decreases with increasing distance between the nozzle and the point of impact of the jet onto the surface.

Mixing between a jet and the gas surrounding it begins at the nozzle exit and continues to take place along the length of the jet. This makes the exact location of the jet boundary difficult to determine. Ideally the jet boundary is precisely the "surface" separating the region of zero axial velocity from a region wherein velocity is not zero, namely the jet.

Since this is difficult to determine in practice, some arbitrary definition of the jet is usually made. The practice used in this report is to define the jet boundary, at any given distance from the nozzle, as the radial position where the velocity head was not discernible within the accuracy of the measuring system being used. For example, when using total head tubes connected to 50 inch mercury manometers,

any reading below about 0.02 inch of mercury (this corresponds to a velocity of about 30 ft/sec) would be beyond the accuracy of the measuring system. Thus when the radial position is determined at which the local total head was about 0.02 inch of mercury this point was taken to be a point on the jet boundary. The above pressures are all gauge pressures.

The mixing between the jet and the surrounding gas results in the deceleration of the gas in the jet and the acceleration (entrainment) of some of the surrounding gas. Thus $(P_i)_{max}$ in general decreases with increasing distance between the nozzle and the plane of measurement.

Supersonic Core

The oxygen conversion process normally employs an oxygen jet which is supersonic at the nozzle exit. The central core of the jet will remain essentially supersonic for some distance downstream of the nozzle. The length of this supersonic core will depend primarily on the nozzle configuration, the nozzle driving pressure, and the ambient conditions of the region surrounding the jet; the ambient pressure is assumed constant at 14.7 psia unless otherwise stated.

Within the supersonic core a variety of shocks may occur which effect sudden and sometimes severe changes in local velocity and pressure. The result of these shocks is a general decrease in $(P_i)_{max}$. The exact pattern of the shocks within this supersonic core is in many cases difficult to predict and will in general change with operating conditions. For example the shock pattern downstream of a particular nozzle at one driving pressure may differ appreciably from that occurring under a different driving pressure. This change in shock pattern usually results in a direct change in the $(P_i)_{max}$

measured at some downstream position. The extent of change in $(P_i)_{max}$ is dependent on (a) the nature of the shock patterns and, (b) the position, relative to the nozzle, at which $(P_i)_{max}$ is measured.

Examples of two types of shock patterns occurring in the gas jet are shown in Figures 20 and 21. (Figure 4 and Figure 6 of Ref. 1) These two figures are shadow photographs (or shadowgraphs) taken during early work (1955) with nozzles which were then in use or which were being considered for use in McLouth Steel Corporation's Oxygen Converters.

The salient features related to these shadowgraphs are:

Fig. 20 — Nozzle No. 1 of McLouth Steel Corp., Dwg. 10301 Throat diameter = 1.625, exit diameter = 1.875. Air flow rate approximately 3900 CFM (A of Table A-2)*

Fig. 21 — Nozzle No. 2 of McLouth Steel Corp., Dwg. 10301 Throat diameter = 1.875, exit diameter = 2.759. Air flow rate approximately 3900 CFM (L of Table A-2)*

Note that the air flow is from the nozzle on the left into room air.

Although these two nozzles were both producing a flow rate of about 3900 CFM, tests showed that at a distance of 72 inches from the nozzle the centerline velocity head for nozzle 1 was 6.7 inches of mercury but the centerline velocity head for nozzle 2 was 2.3 inches of mercury (Ref. 1). The important point here is that nozzle 2 was simply not designed for operation at or near 3900 CFM. Because of the nozzle size and configuration the velocity at the exit of nozzle 2 was greater than that of nozzle 1. However the normal (i.e.,

*Nozzles similar to Nozzle A of Table A-2 were actually used by McLouth in commercial operation in OP-1 from July 1955 to September 1955 and in OP-2 from April 1958 to October 1958. Nozzles similar to Nozzle L of Table A-2 have never been used by McLouth in commercial operation.

at right angle) shock which resulted from this "off design" operation of nozzle 2 decreased the downstream velocity of the jet. A further result of this "off design" operation (Figure 21) is an increase in downstream jet diameter. The jet diameter, at the 72 inch position, corresponding to Figure 20 was about 16 inches while the jet diameter corresponding to Figure 21 was over 20 inches.

Most nozzles tested in this current series of tests have produced shock patterns much less severe than that of Figure 21. In such less severe cases the loss in velocity due to shocks would be less significant, and such velocity decreases that did occur due to normal shocks would occur primarily along the jet centerline. Such velocity losses near the jet centerline would tend to be smoothed out as distance from the nozzle is increased, because of mixing within the jet. The result of this is shown in the fact that in many cases (such as Fig. 14) sharp breaks occur in the plot of $(P_i)_{max}$ vs. driving pressure at the relatively low blowing distances, but as blowing distance (distance between nozzle and impact plane where $(P_i)_{max}$ is measured) is increased the breaks become less pronounced.

The fact that sharp breaks occur in the $(P_i)_{max}$ curves of Figures 14a and 14b for a given nozzle at a close blowing distance of 350 mm (about 14 inches), for example, is of little practical interest if the nozzle is normally used at blowing heights of 1000 mm (about 40 inches). Blowing height is defined as the distance from the nozzle to the free surface of the bath in its quiescent state.

The extent of the supersonic core is also an indication of the performance of a nozzle. In general increasing the length of the supersonic core results in increased penetration capability. Figure 22 shows the approximate outline of the supersonic core for nozzles 1 and 2 of Table A-2. Several comments are pertinent to the nature and extent of supersonic cores.

Regions may exist within this core, primarily along the jet axis, where the local velocity is less than the speed of sound. This can occur when the shock pattern is such that the velocity along the axis drops to below the local speed of sound while the velocity at the same axial distance from the nozzle but at some greater radial positions is still greater than the speed of sound. This higher velocity annular region can then re-accelerate the locally subsonic core to supersonic velocities, thus retaining an essentially overall supersonic core for some further distance downstream.

An extreme example of this can be seen clearly in Figure 21. Here the first normal shock (located about 1 1/4 inches downstream of the nozzle) produces a subsonic core of about 0.7 inches in diameter inside a supersonic jet while at a point about 4 1/2 inches from the nozzle the entire core of the jet is essentially supersonic again.

The extent of the supersonic core may be very sensitive to slight changes in nozzle driving pressure. This is true for the test conditions employed in obtaining the results shown in the lower part of Figure 22:

Test Conditions and Results

Nozzle	35 mm, B of Table A-2
Driving pressure	94 psig
Distance to end of supersonic core	1,000 mm

Now referring to Figure 17, it is observed that $(P_i)_{max}$ measured at 1,000 mm and with P_d around 94 psig, will change drastically with only a slight change in nozzle driving pressure. Thus, when the extent of the supersonic core is measured within the region where sharp breaks occur in the $(P_i)_{max}$ curve it must be assumed that the length of the supersonic core is only approximate.

The extent of the supersonic core is determined experimentally by carefully probing the jet with a total head probe. The Mach number (for air and oxygen) is just equal to 1 when

$$P_a = 0.528\,(P_a + P_t) \tag{7}$$

provided the static pressure in the jet is atmospheric downstream of the probe position, where P_a = ambient pressure, absolute; P_t = gage pressure measured by a total head probe. Considering the average atmospheric pressure in Ann Arbor, Michigan, to be about 29.2 inches of mercury and for M = 1:

$$\begin{aligned} P_t &= (P_a/.528) - P_a \\ &= 29.2/.528 - 29.2 \\ P_t &= 26.1 \text{ in. mercury} \end{aligned} \tag{8}$$

Throughout these nozzle tests it has been observed that $(P_i)_{max}$ is always greater than the impact pressure measured by a probe without a flat plate (i.e., P_t). Within the range of interest here, an average value of $(P_i)_{max}/P_t$ was determined to be about 0.9. That is:

$$P_t \approx 0.9\,(P_i)_{max}$$

Thus Equation 8 becomes:

$$P_t = 26.1 \text{ in Hg} \approx 0.9\,(P_i)_{max} \tag{9}$$

i.e., $(P_i)_{max} \approx 29$ in. mercury when M = 1. The various figures showing plots of $(P_i)_{max}$ can thus be used to determine the approximate extent of a supersonic core. For example, with the atmospheric pressure assumed to be 29.2 inches of mercury and going to Figure 19:

For the McLouth Nozzle 1 (A of Table A-2)

The 3900 CFM curve intersects the 29 inches of mercury line at the 1220 mm line. Therefore the supersonic core extends 1220 mm (48.1 inches) downstream of the nozzle exit.

For the 35 mm Nozzle (B of Table A-2)

The 2820 CFM curve intersects the 29 inches of mercury line at the line of 835 mm (32.9 inches). Therefore the supersonic core extends 835 mm (note discussion below) downstream of the nozzle exit.

This second example is used to point out one area where large discrepencies may occur with some nozzles. Referring to Figure 22; this plot shows the extent of the supersonic core (as measured by a total head tube in the jet stream) for the 35 mm nozzle, at the same operation conditions, to be 1000 mm. Now, refer to Figure 17. This plot shows $(P_i)_{max}$ vs. nozzle driving pressure (for the 35 mm nozzle) at blowing heights of 1000 mm and 1100 mm. At these blowing distances note the fluctuations in $(P_i)_{max}$ in the driving pressure range from 78 to 105 psig. Obviously with this type of fluctuation in the jet stream the actual extent of the supersonic core at any given instant can be considered to be, at best, only an approximation.

For the first example above (McLouth Nozzle) the variation (Figure 22 shows 1250 mm, Figure 19 data results in 1220 mm) in the extent of the supersonic core is 30 mm or about 2 1/2%. This is due primarily to the fact that the factor of 0.9, used to convert P_t to $(P_i)_{max}$, is an approximate value.

Jet Spread

The angle at which a jet spreads is in general not a constant. The shock pattern within the supersonic core and mixing conditions on the jet boundary can have considerable effect on the jet spread angle. In spite of this it is desirable to know at least approximately the angle of jet spread to be expected since the greater the spread of the jet the less the penetration capability of the jet.

The divergence of the jet will in general decrease with increasing jet velocity (page 148 of Ref. 10). However, changes in the shock structure within the jet and changes in the nature of the mixing between the jet and its surroundings can alter this trend.

The angle of jet divergence or the angle of the apex of the cone which the jet approximates and which may be referred to as θ, is defined by the following equation:

$$\text{Tangent } (\theta/2) = r_j/x$$

or

$$d_j = 2 \times \tan (\theta/2)$$

where r_j = radius of the jet in inches at a distance x from the nozzle exit

d_j = diameter of the jet in inches at a distance x from the nozzle exit

x = distance in inches from the nozzle exit, measured along the jet axis.

Note that the angle of jet divergence, θ, is not constant along the length of a jet and it may vary with the flow rate. However, an average value of θ may be employed over some prescribed range of positions along the jet axis with reasonable accuracy.

Data from References 1 and 3 for nozzle A of Table A-2 show that $\theta/2$ may decrease as gas flow rate is increased, but not in a linear fashion.

CFM	x	r_j	$\theta/2$	Tan $(\theta/2)$
2900	72"	9.15"	7.23°	0.127
3400	72"	8.3"	6.58°	0.113
3900	72"	8.0"	6.36°	0.111
4350	72"	7.5"	5.96°	0.104
5200	60"	6.3"	6.0°	0.105

The angle of jet divergence may also vary with nozzle size and design. For example from Reference 2 a nozzle having a throat diameter of 0.377 inches with a flow rate of about 130 CFM of air produced a jet which had an angle of jet divergence of over 18° (i.e., $\theta/2 = 9^{\circ}$) for blowing distances of from 13 to 20 inches.

The angle of jet divergence may be used to determine the jet diameter at any point downstream of the nozzle. Thus for nozzle A of Table A-2 operating in room air at an air flow rate of from 3400 through 5200 CFM a reasonable estimate of the jet diameter (d_j) can be made for blowing distances (x) of the order of 3 to 6 feet, by using an average value of $\theta/2 = 6\ 1/4^{\circ}$.

Thus roughly, for nozzle A,

$$d_j = 0.22\ (x)$$

The effect of a heated atmosphere on the jet spread angle is discussed in Section D.

Performance of a Converging-Diverging Nozzle Compared with a Converging Nozzle

The oxygen conversion process as practiced by McLouth Steel Corporation and also at Linz, Austria, makes use of a converging-diverging (Laval) nozzle. Such nozzles produce supersonic velocities at the nozzle exit under conditions normally employed. The terms converging-diverging, convergent-divergent, Laval or de Laval all refer to the type of nozzle which, moving in the direction of flow within the nozzle, first converges to a throat of minimum cross-sectional area and then diverges to an exit area larger than the throat. A converging nozzle simply converges to a throat section and then ends; the throat section may have some length but there is no diverging section following the throat. It has been suggested that converging nozzles may be used in the oxygen conversion process.

A series of tests was conducted to compare the characteristics of a jet and in particular the penetration capabilities of a jet emerging from a converging-diverging nozzle with the characteristics of a jet emerging from a converging nozzle.

The results of these tests show that for blowing heights and driving pressures representative of those used in the oxygen conversion process a jet emerging from a converging nozzle may have a penetration capability 30% less than a jet emerging from a well designed converging-diverging (Laval) nozzle.

The converging-diverging nozzle used in these tests was built to conform to the dimensions of the 35 mm nozzle used at Linz, Austria. In order to obtain the converging nozzle, the diverging section of the 35 mm converging-diverging nozzle was machined away leaving only the converging section and the throat.

The machining operation was performed in several steps in order that tests could be made of several intermediate nozzles. The dimensions of the nozzles tested and the sequence of the machining operations are as follows:

Nozzle	D_t = Throat Diameter in.	D_e = Exit Diameter in.	$(A_e/A_t)^*$	"Ideal"* P_d (Approx.)	Remarks
B	1.378	2.165	2.47	210	Nozzle B of Table A-2
B'	1.377	2.16	2.46	210	Similar to Nozzle B of Table A-2
B'_1	1.377	1.98	2.07	150	Machined from Nozzle B'
B'_2	1.377	1.76	1.63	94	Machined from Nozzle B'_1
B'_3	1.377	1.55	1.27	50	Machined from Nozzle B'_2
B'_4	1.377	1.377	1	14	Machined from Nozzle B'_3

*Defined in Section A

The test set-up is shown schematically in Figure 6 and the test conditions for this series were as follows:

1. Nozzle Driving Pressure

   The nozzles were tested at driving pressures ranging from 15 to 150 psig.

2. Nozzle Blowing Distance

   A distance of 75 inches between the downstream end of the nozzle throat and the 4 ft by 4 ft flat plate against which the jet impinged was used for these tests so that no change in the test set-up would be required except the nozzle itself. This resulted in a difference of 4% in the blowing distance,

as measured from the nozzle exit to the impact plane, in testing the two nozzles. The flat plate was normal to the jet and the pressure on the upstream side of the plate, on the jet axis, was measured. This pressure has been defined as $(P_i)_{max}$ in Section B of this report.

Test Results

The maximum flat plate impact pressures obtained in these tests are shown in Figure 31, a plot of $(P_i)_{max}$ vs. driving pressure for each of the nozzles tested.

Note that with the converging-diverging nozzle in the vicinity of 94 psig driving pressure, rather sharp changes in $(P_i)_{max}$ occur at a blowing distance of 75 inches, measured from the throat. (See Figure 17 for measured changes in $(P_i)_{max}$ at shorter blowing distances for a similar 35 mm converging-diverging nozzle.)

The converging-diverging nozzle has an "ideal" pressure of approximately 210 psig. That is, the nozzle exit pressure is 14.7 psia when the nozzle driving pressure is 210 psig. At lower driving pressures the nozzle exit pressure is less than 14.7 psia. Thus when the converging-diverging nozzle is exhausting to the standard atmosphere and the driving pressure is less than 210 psig the nozzle is operating in an "under driven" condition; i.e., the jet is said to be "over expanded" since it has expanded to a pressure lower than that into which the jet is exhausting.

The "ideal" pressure for the converging nozzle is about 14 psig. The values of $(P_i)_{max}$ obtained with this nozzle were similar to those of the converging-diverging nozzle up to a driving pressure of approximately 80 psig. As the driving pressure was increased above 80 psig, the $(P_i)_{max}$ data points for the converging nozzle fell further and

further below these data points for the converging-diverging nozzle. It is therefore quite evident that the maximum impact pressure is significantly decreased by the use of the converging nozzle when compared with a converging-diverging nozzle at driving pressures above 80 psig at a blowing distance of about 75 inches.

Before considering broader implications of the above statements consider Figures 32 and 33. These figures show shadow photographs (shadowgraphs) of the jet at the nozzle exit. These shadow photographs were obtained during the series of tests under discussion here. The test conditions for these figures are as follows:

Figure 32

All of the shadow photographs of this figure were taken when the nozzle driving pressure was 150 psig. The nozzles used for the five shadow photographs of Figure 32 were B', B'_1, B'_2, B'_3, and B'_4, respectively, reading from left to right and top down.

The shock waves in these pictures are shown by the adjacent dark and light bands in the core of the jet. These bands are caused in general by sudden changes in the density of the gas (across the shock wave) which results in the "bending" of the light rays. Shock waves are also accompanied by a sudden increase in static pressure and a sudden decrease in velocity. These changes are in general more severe across a normal shock than across an oblique shock. Here the word "normal" means that the shock wave is perpendicular to the direction of the gas flow.

Although all of the various shock waves within a jet contribute to ultimate losses in the velocity of the jet, and hence in penetration capability, the normal shock results in more severe losses than the oblique shocks. The velocity downstream of a normal shock is subsonic. The following discussion will consider only the losses in jet

velocity (and therefore, $(P_i)_{max}$) evidenced by the nature of the normal shock immediately downstream of the nozzle and centered on the jet axis.

Nozzle B' has a "design" pressure of 210 psig but the top left picture of Figure 32 was taken when the nozzle driving pressure was 150 psig. Thus this picture shows the effect of an overexpanded jet (as discussed previously). This particular set of conditions results in a normal shock which is relatively small in diameter, thus a relatively small proportion of the gas in the jet suffers the greater velocity losses associated with a normal shock.

Nozzle B'_1 has a "design" pressure of 150 psig thus the top right picture shows the flow from a nozzle operating essentially at its design point. Note the absence of the normal shock.

Nozzle B'_2 has a "design" pressure of 94 psig. At a driving pressure of 150 psig the jet from this nozzle is underexpanded (i. e., the pressure at the nozzle exit is greater than the pressure of the region into which the nozzle is exhausting). Again a relatively small normal shock is evident. Recall here that nozzles B', B'_1, and B'_2 produced nearly the same value of $(P_i)_{max}$ at a "blowing distance" of 75 inches when the driving pressure was 150 psig.

Nozzle B'_3 has a "design" pressure of 50 psig. Now the normal shock (see second picture from top on the right of Figure 32) has become quite appreciable and a significant portion of the gas in the jet passes through the shock. Again note from Figure 31 the decreased value of $(P_i)_{max}$ at a driving pressure of 150 psig.

Finally the converging* nozzle, B'_4, which has a "design" pressure of 14 psig produces a very large normal shock when operated at 150 psig. This explains the low value of $(P_i)_{max}$ obtained with this nozzle at 150 psig driving pressure.

Figure 33

This figure was obtained with a sequence of conditions similar to that of Figure 32 except the driving pressure used in obtaining all of the shadow photographs of Figure 33 was 94 psig. The remarks made in regard to Figure 32 in general apply to Figure 33.

Figure 34

Each of the shadow photographs of this figure were obtained for Nozzles B'_1, B'_2, B'_3, and B'_4, respectively when each nozzle was operated at nearly its "design" pressure. This figure demonstrates that the normal shock does not occur when nozzles are operated at their design pressure even when the nozzles are entirely different as regards to nozzle exit diameter.

Throughout this discussion the distance between the nozzle and the plane of impact of the jet has been considered essentially constant. This was done in order to evaluate the variation in jet performance due only to differences in nozzle design. The velocity of the jet generally decreases with increasing distance from the nozzle because of losses due to the mixing of the jet with its surroundings. At extremely great blowing distances the "mixing" losses dominate the situation while at close distances the losses due to shocks in the

---

*The terms converging or convergent are used to describe a nozzle which has its minimum area or throat at the nozzle exit. The throat section may in general have some length without appreciably altering flow conditions at the nozzle exit.

jet will dominate. If this series of nozzle tests had been conducted at relatively close blowing distances (such as 30 inches for example) the differences in performance of the various nozzles tested would have been more pronounced. Such a series of tests would be interesting and useful in defining the overall characteristics of these nozzles tested. The problem under consideration here, however, is to define the effect of nozzle design on the penetration capabilities of an oxygen jet in an oxygen converter. Thus we are concerned with those changes in nozzle design which result in significant overall losses of the jet velocity for the range of blowing distances of interest. For this reason the relatively long mixing distance of 75 inches was chosen. This distance is believed to be representative of the distances normally existing, for a nozzle of this size, in an Oxygen Converter between the nozzle and the point of maximum penetration of the jet.

The relative penetration capabilities of converging and converging-diverging nozzles are discussed in Section C of this report.

SECTION C

PENETRATION OF A GAS JET INTO A LIQUID BATH

Until the early part of 1961 this work for the McLouth Steel Corporation was mainly that of design and comparative testing of various full size nozzles as used in the Oxygen Conversion Process (Ref. 1, 2, 3). The question of what happens to and within the liquid bath when it is subjected to a jet of gas from above was not considered in detail until that time.

Since it was quite obvious that full scale work, even with nonreactive baths, would require larger apparatus than was available, scale models were used as a means of studying the effects of varying the more important parameters.

The first attempt made by the authors to obtain concrete proof of the capability of a gas jet to penetrate into a liquid was made in January 1961. A 14 mm nozzle (E of Table A-2) was mounted 13 3/4 inches above the surface of a quick setting cement (Floorstone). The cement was in a fluid state (specific weight = 121 lb/ft^3) and was contained by a metal tub approximately 1 1/2 feet in diameter by 1 foot in height. The nozzle was directed downward so that the air jet was normal to the undisturbed liquid surface. A nozzle driving pressure of 17 1/2 psig was maintained for approximately 20 minutes; thus allowing the cement to harden while the cavity was maintained by the jet.

Initially, circulation of the liquid was demonstrated by cement being continuously carried up the side walls of the cavity in the form of ragged waves. As the cement hardened, the waves were left standing. The depth of penetration at the beginning of the test was not noticeably different from the depth of the hole left in the cement at the conclusion of the test, approximately 7 inches.

The maximum flat plate impact pressure, $(P_i)_{max}$, for this same nozzle at a blowing distance of 13 3/4 inches and at a driving pressure of 17 1/2 psig, was determined to be about 1 inch of mercury which is equivalent to 7 inches of cement.

This work demonstrated that a correlation existed between the impact pressure produced by a gas jet and the distance to which the same gas jet would penetrate into a liquid bath.

A series of model tests was then made (starting in February 1961) using a number of different liquids and gases including tests in which the jetted gas reacted chemically with the liquid. The primary purpose of this series was to observe penetration of the gas jet into the liquid and the circulation pattern set up in the liquid by the gas jet, as well as the relation between penetration and circulation. A summary of these tests is included in Table C-1. The depth of penetration of the gas jet into the liquid bath is set forth for a number of these tests in Table C-2. Table C-3 is reference data on the various properties of the gases and liquids used in this phase of the work.

In all of this model work the same general pattern of circulation was set up in the liquid bath by the gas jet. This "Basic Circulation Pattern" is characterized by the following motion of the liquid throughout the bath:

1. The liquid moves upward and outward along the side walls of the cavity created by the jet.
2. The liquid moves outward from this cavity along the upper surface of the bath. (Under "strong" blowing conditions a significant amount of the liquid is carried into the space above the bath as droplets or "sheets" of liquid. Most of this liquid returns to the bath at some distance from the cavity, but some may also be returned to the center of the bath due to its being entrained in the gas jet.)

3. The liquid travels downward along the outer walls of the vessel.
4. The liquid moves inward toward the cavity throughout the lower portions of the bath.
5. The liquid moves upward toward the cavity from the region below the cavity.

Observe here that the primary force acting to produce this circulation is a shearing force which occurs at the interface between the gas and the liquid along the walls of the cavity created by the jet. The gas flowing out of the cavity along its walls tends to continuously carry the adjacent liquid with it. Clearly the rate at which liquid is carried out along the walls of the cavity will increase as the size of the cavity increases or as the velocity of gas leaving the cavity increases. Thus, generally speaking, increasing the gas flow rate will increase the size of the cavity (assuming here that conditions are adjusted to hold depth of penetration constant), and thus increase the "rate" at which the bath circulates. Also, increasing the depth of penetration tends to increase the velocity of the gas leaving the cavity, which results in an increase in the "rate" of bath circulation.

Another test which demonstrated the "Basic Circulation Pattern" made use of a multi-vaned rudder assembly. The vessel used was 2 feet in diameter by 4 feet in height (No. 3 of Table C-1). A plexiglass window was installed in the side of this vessel so that most of the bath was visible to an observer. An air jet was directed downward toward the water bath. The jet axis was along the axis of the vessel and perpendicular to the undisturbed bath surface.

The dimensions and position of the rudder assembly were as follows:

1. The pivot axis of the individual vanes was 5.47 inches from the vertical axis of the vessel.
2. The individual vanes were free to pivot in a horizontal plane about a vertical axis which was perpendicular to the undisturbed bath surface. Thus each vane would swing in the direction of the horizontal component of the local velocity.
3. The rudder assembly included 8 vanes, each independent of all the others; each vane was 0.85 inches in height by 2.73 inches in length, measured from the pivot point; and the vertical space between each vane was 1/8 inch.
4. The top of the top vane was 1/8 inch above the undisturbed bath surface.
5. The water bath was 9 3/16 inches in depth at the center of the vessel and a layer of balsa wood chips formed a layer of simulated "slag" approximately 1/4 inches in thickness.
6. A convergent nozzle having a throat diameter of 0.228 inches was located 10 inches above the undisturbed bath surface.

Picture No. 1 of Figure 30 shows the vessel used for this test as well as the light source used to illuminate the interior of the bath. The rudder assembly is also shown with the vanes positioned in the inward position.

This multivaned rudder test was started by manually positioning all the vanes so that they were essentially at right angles to a radius of the vessel drawn through the pivot axis of the vanes. This condition is shown by picture No. 2 of Figure 30. (Note that as viewed through the plexiglass window all vanes point toward the back of the vessel and thus the vanes cannot be seen.) The air was then turned on and the nozzle driving pressure was brought immediately to 15 psig and held there until the end of the run. Photographs of the rudder assembly were taken 6, 8, 19, and 30 seconds after the initiation of the air

flow (Pictures 3, 4, 5, and 6, respectively of Figure 30). The test was terminated at 30 seconds. The position of the vanes remained essentially unchanged in the interval between 19 and 30 seconds, with vanes 1 and 2 directed outwardly from the center of the bath while vanes 3 through 8 were directed inwardly toward the center of the bath.

The final position of the individual vanes clearly demonstrate that the gas jet produced the "Basic Circulation Pattern" in the liquid as described previously.

One other important point is clearly shown by this rudder test. The layer of liquid in the upper region of the bath which is moving out from the center of the vessel is thin relative to the bath depth. In this test the outward moving liquid is confined to a top layer about 1.9 inches in thickness where the bath is about 9.2 inches in depth. This is for a radial position of 5.47 inches. While the thickness of the outward moving, top layer will not necessarily always be the same for different bath depths, all the various circulation tests conducted in this study have shown that the portion of the bath within which the fluid is moving in an outward direction is limited to a relatively thin layer at the free surface of the bath.

The following conclusions may be drawn from these model tests:

1. Increasing the gas flow rate generally produces greater jet penetration into the liquid bath as well as increased "rate" of circulation. This assumes that the increased flow rate is accomplished by either an increase in nozzle size at fixed driving pressure or an increase in nozzle driving pressure with a fixed nozzle size, or both.
2. Reducing nozzle blowing height generally increases depth of penetration and rate of circulation.

3. Increasing the viscosity of the liquid by factors of nearly 1,000 reduced only slightly the depth of penetration, but the "rate" of circulation was decreased considerably.

> Note: The presence of simulated slags on the bath or excessive bubbles within the bath also resulted in decreased "rates" of circulation, but the "Basic Circulation Pattern" as described above was always observed. Even the "reactive tests," the last two tests listed in Table C-1, showed the same "Basic Circulation Pattern" as long as any overall circulation pattern was discernable throughout the bath.

Estimating Penetration from $(P_i)_{max}$ Data

One of the principal objectives in the nozzle testing program was to develop a means of estimating penetration of an oxygen jet issuing from the nozzle toward a molten iron bath spaced a known distance from the nozzle. For full scale, commercial-size nozzles the amount of penetration can be estimated or "computed" using flat plate impact pressure data accumulated from tests of those nozzles. Flat plate impact pressure or $(P_i)_{max}$ is defined in Section B.

In order to estimate the penetration it may be reasoned that any nozzle-blowing height-driving pressure combination producing a particular maximum impact pressure would penetrate into a particular liquid bath to a depth corresponding to that pressure. Consider, for example, a particular nozzle at a fixed driving pressure jetting into a bath of mercury. Assume that this nozzle at a blowing distance of 30 inches will produce a maximum flat plate impact pressure of 10 inches. Then the blowing height or distance from the nozzle to the quiescent surface of the bath in order to produce that amount of penetration in mercury would be 20 inches.

Since the specific gravity of mercury (13.57) is approximately twice that of molten pig iron (6.7 at 2500° Centigrade), the value of $(P_i)_{max}$ can be expressed in inches of iron. For example, 10 inches of mercury is equal to approximately 20 inches of iron. Thus for the example given we would expect to penetrate 20 inches into an iron bath with a blowing height of 10 inches. This approach is represented by the following relationships:

$$H = S - (P_i)_{max} \tag{10}$$

where H = nozzle blowing height above the bath surface—inches,

S = distance between nozzle and the impact plate during nozzle tests—inches,

$(P_i)_{max}$ = the gauge pressure measured on the axis of the jet and on the upstream surface of a flat plate normal to the jet—expressed in inches of bath material under consideration.

Equation (10) may also be expressed as:

$$S = H + D \tag{11}$$

where D (the depth of penetration) is equal to $(P_i)_{max}$.

This approach of estimating penetration does not account for certain conditions (for example high temperature) existing in an oxygen converter but not present during the flat plate nozzle tests made to obtain $(P_i)_{max}$ data. These conditions will be discussed in subsequent portions of this report (see Section D).

The relation defined by Equation (11) above was used to obtain the several curves of Figure 23 and the bottom curve of Figure 28.

The $(P_i)_{max}$ data of Figure 31 may be used to obtain a relative indication of the penetration capability of a converging nozzle relative to that of a converging-diverging nozzle.

Consider first the converging nozzle (B'_4 of Fig. 31) results presented in Figure 31.

1. Blowing Height = 75 inches
2. $(P_i)_{max}$ at 150 psig nozzle driving pressure $\cong$ 6 inches of mercury or 12 inches of iron
3. From Equation (11)

$$S = H + D$$

or

$$H = S - D = 75 - 12 = 63$$

Thus, this 35 mm (1.377 in.) nozzle when operated at a driving pressure of 150 psig and at a height above the molten iron bath of 63 inches should produce a jet capable of penetrating 12 inches into the molten iron bath—based on cold $(P_i)_{max}$ data.

Consider next a converging-diverging nozzle such as either B' or B'_1 of Figure 31:

1. Blowing Height = 75 inches
2. $(P_i)_{max}$ at 150 psig nozzle driving pressure $\cong$ 10 inches or 20 inches of iron.
3. From Equation (11)

$$H = S - D = 75 - 20 = 55$$

Thus, this nozzle when operated at a driving pressure of 150 psig and at a height above the molten iron bath of 55 inches should produce a jet capable of penetrating 20 inches into the molten iron bath—again based on cold $(P_i)_{max}$ data.

This does not give a direct comparison between the converging nozzle B'_4 and the converging-diverging nozzle B' and B'_1, but a more direct comparison may be obtained if we also make use of Figure 23. The converging-diverging nozzles B' and B'_1 at 150 psig nozzle driving pressure produce a penetration (computed from cold $(P_i)_{max}$

data) of about 20 inches of iron at 55 inches blowing height. Using these values to determine a point on Figure 23 and drawing a curve parallel to the adjacent curves already on Figure 23, it is found that the penetration for these converging-diverging nozzles would be about 17 inches at 63 inches nozzle blowing height. Thus we have the result that the penetration computed from $(P_i)_{max}$ data is about 12 inches for the converging nozzle (B'_4) while it is 17 inches for the converging-diverging nozzles (B' and B'_1).

The above was obtained for a nozzle driving pressure of 150 psig and a nozzle blowing height of 63 inches. A similar procedure applied to the $(P_i)_{max}$ data from these same nozzles at 100 psig nozzle driving pressure results in the following computed penetration:

Converging-diverging nozzles (B' and B'_1)—almost 9 inches of iron

Diverging nozzle (B'_4)—over 7 inches of iron

The computed blowing height in both cases is about 68 inches.

The results for the particular nozzles and blowing heights noted above are that the penetration capability of the converging nozzle is almost 30% below that of the converging-diverging nozzles (B' and B'_1) at 150 psig nozzle driving pressure, and 15% below that of these converging-diverging nozzles at 100 psig.

These comparative results should apply in general to nozzles having throat diameter of the order of 35 mm and at blowing heights of 4 to 6 feet. Note that as nozzle driving pressures are reduced below 100 psig the penetration capability of the jet produced by the converging nozzle more nearly approaches that of a well designed converging-diverging nozzle.

A converging-diverging nozzle which is not properly designed for the driving pressure employed may result in a less effective jet than the use of a converging nozzle of the same size. For example,

it appears from Figure 31 that at a nozzle driving pressure of just below 70 psig the converging nozzle (B'_4) results in about the same maximum impact pressure as does the use of the converging-diverging nozzle (B').

Penetration of Air into a Mercury Bath

One of the unknown factors in the estimating of penetration from $(P_i)_{max}$ data is the effect of the cavity formed in the liquid by the jet. The velocity distribution within a gas jet will normally be different for the case of a jet impacting on a flat plate than it will be for the case of a gas jet penetrating into a liquid bath, thus actual penetration will presumably not be precisely that calculated by Equation (11) from $(P_i)_{max}$ data. A series of tests was made in order that a comparison could be made between penetration computed by Equation (11) from $(P_i)_{max}$ data, obtained at room temperature, and the actual penetration measured at room temperature. The effect of a heated atmosphere surrounding the jet is discussed in Section D of this report.

Nozzle I of Table A-2 was used in this series of tests, the gas used was air and the mercury bath was contained in Vessel No. 1 of Table C-1 (i. e., a pyrex jar one foot in diameter by two feet in height). For each test of this series the vessel was filled to a preselected depth of mercury (17/32, 1 1/8, 1 27/32, 2 11/16, 3 11/16 or 4 1/2 inches). At various blowing heights (11 through 21 inches), the driving pressure required to expose the bottom surface of the vessel was recorded for each bath depth. The data from this series resulted in the two curves of Figure 28 labeled "Continuous Penetration in Hg." and "Intermittent Penetration in Hg." Although these values of penetration were actually measured in inches of mercury, they were converted to inches of iron in order that they might be compared with the actual penetration of an oxygen jet into a molten iron bath (see Section E).

The "Intermittent Penetration in Hg." curve of Figure 28 was obtained by recording the nozzle driving pressure necessary to expose the bottom of the vessel an estimated 50% of the time. The "Continuous Penetration of Hg." curve was obtained by recording the nozzle driving pressure necessary to expose the bottom of the vessel essentially continuously. Note that for a given nozzle driving pressure, the depth to which the jet intermittently penetrates is about 10% greater than the depth to which the jet continuously penetrates. This should be taken into account in considering any measurements of depth of penetration.

The bottom curve of Figure 28 was computed by the use of Equation (11) and data obtained by testing Nozzle I in the Heated Atmosphere Facility shown by Figure 7.

Note that the penetration measured exceeded the computed penetration which was based on $(P_i)_{max}$ data obtained with this facility when the gas surrounding the jet was at room temperature.

SUMMARY OF MODEL TESTS

	Vessel Number	Nozzle Throat Dia. in.	Blow Height in.	Driving Pressure psig	Bath Depth in.	Slag Used
Air into Water	1, 2, 3, 4	0.059 to 0.250	-4 to +12	5-90	4 to 11	Balsa chips for some tests
Air into Glycerine	1	0.081 & 0.115	5	5-30	4 1/2	None
Air into Trichloroethane	1	0.115	5	5-20	4 3/8	Balsa chips for some tests
Air into Trichloroethylene	1	0.115	5	5-20	4 1/8	Balsa chips for some tests, 1/4" of Glycerine for some tests
Air into Acetylene Tetrabromide	1	0.115	5	5-15	4 1/2	None
Air into Karo Syrup	1	0.115	5	5-30	4 1/2	None
Air into Mercury*	1	0.116 & 0.162	3 to 9	5-90	4 1/2	Lead shot for some tests
Air into Mineral Oil	1	0.081 & 0.116	5 to 11	5-30	4 1/2 to 9	None
Air into Castor Oil	1	0.115	5	5-30	4 1/2	None
Helium into Water	1	0.115	5	5-20	4 1/4 4 3/4	Balsa chips for some tests
Helium into Glycerine	1	0.115	5	5-20	4 3/8	None
Helium into Trichloroethane	1	0.115	5	5-20	4 3/8	Balsa chips for some tests
Helium into Trichloroethylene	1	0.115	5	5-25	4 1/2	Balsa chips for some tests
Helium into Acetylene Tetrabromide	1	0.115	5	5-15	4 1/2	None
Oxygen into Mineral Oil	1	0.081	5	5-20	4 1/2	None
Hydrogen Chloride into Soda Solution	1	0.081	5	5-25	4 1/2	1/4" Mineral Oil and Cork chips for some tests
Carbon Dioxide into Sodium Hydroxide Solution	1	0.081	5	5-25	4 1/2	None

Vessel No. 1	1' x 2'	Pyrex Cylinder
Vessel No. 2	6" x 18"	Pyrex Cylinder
Vessel No. 3	2' x 4'	Cylindrical
Vessel No. 4	1/2" x 12" x 20"	(Sectional)

*See additional tests of air blown into mercury using 0.315" nozzle discussed separately.

TABLE C-2

MEASURED PENETRATION OF GAS JET INTO VARIOUS LIQUIDS

Liquid	Gas	P_d psig	Nozzle Height	V_j ft/sec.	D_j Approx.	Meas. Pene.
Water	Air	5	5 in.	87	2.2 in.	1.15 in.
		10	5 in.	103	2.2 in.	1.7 in.
		15	5 in.	131	2.2 in.	2.3 in.
		20	5 in.	155	2.2 in.	2.85 in.
		25	5 in.	187	2.2 in.	3.5 in.
		20	7 in.	111	3.2 in.	1.9 in.
Glycerine	Air	5	5 in.	87	2.2 in.	.9 in.
		10	5 in.	103	2.2 in.	1.1 in.
		15	5 in.	131	2.2 in.	1.7* in.
Trichloro-ethane	Air	5	5 in.	87	2.2 in.	1.15 in.
		10	5 in.	103	2.2 in.	1.55 in.
		15	5 in.	131	2.2 in.	2.1 in.
		20	5 in.	155	2.2 in.	2.65 in.
Acetylene-Tetrabromide	Air	5	5 in.	87	2.2 in.	.5 in.
		10	5 in.	103	2.2 in.	.7 in.
		15	5 in.	131	2.2 in.	1.05 in.
Water	Helium	5	5 in.	219	2.4 in.	1.1 in.
		10	5 in.	298	2.4 in.	1.7 in.
		15	5 in.	325	2.4 in.	2.3 in.
		20	5 in.	393	2.4 in.	2.9 in.
Trichloro-ethane	Helium	10	5 in.	298	2.4 in.	1.6 in.
		15	5 in.	325	2.4 in.	2.2 in.
		20	5 in.	393	2.4 in.	2.5 in.

P_d = Nozzle driving pressure

V_j = Velocity of free jet at center and at same distance from nozzle as the liquid surface

D_j = Jet diameter at distance from nozzle equal to blowing height—as determined by nozzle tests made in room air.

For these tests: 1) Nozzle throat diameter = 0.115 in.; Exit diameter = 0.150 in.
2) Bath depth approximately 4 1/2 in.
3) A 1 ft diameter by 2 ft tall Pyrex cylinder vessel used.

*False bottom of vessel raised to within 1/2 in. of bottom of penetrated region. No change in depth of penetration.

TABLE C-3

REFERENCE DATA

Material	Temp.	State	Specific Gravity	Viscosity Centipoises (Approx.)	Sp. Gr. / Sp. Gr. Air
Iron (4%C)	2500°F	Liquid	6.8 (Approx.)	2.0	5,530.0
Oxygen	60°F	Gas	0.00135	0.019	1.1
Air	60°F	Gas	0.00123	0.017	1.0
Helium	60°F	Gas	0.000169	0.019	0.137
Water	20°C	Liquid	1.0	1.0	812.0
Glycerine	25°C	Liquid	1.26	1,000	1,024.0
Trichloroethane	20°C	Liquid	1.32	1.2	1,073.0
Trichloroethylene	25°C	Liquid	1.46	0.6	1,186.0
Acetylene-tetrabromide (tetrabromoethane) (1, 1, 2, 2)	20°C	Liquid	2.96	9.64	2,410.0
Mercury	20°C	Liquid	13.57	1.554	11,050

Note:

1) These values taken as listed in various references—reference conditions were varied; in some cases the values are only approximate.
2) For gases, specific gravity listed is at a pressure of one atmosphere.
3) For comparison:

$$\frac{\text{Sp. Gr. Iron}}{\text{Sp. Gr. Oxygen}} = 5,040$$

and

$$\frac{\text{Sp. Gr. Water}}{\text{Sp. Gr. Helium}} = 5,920$$

SECTION D

HEATED ATMOSPHERE TESTS

The procedure used to estimate or compute the depth to which an oxygen jet penetrates into a bath of molten iron from $(P_i)_{max}$ data was discussed in Section C. The use of the method described there together with $(P_i)_{max}$ data resulted in Figure 23.

Several "Bottom Marking" tests were made in the regular full size commercial Oxygen Converters of the McLouth Steel Corporation plant in September-October, 1961 at Trenton, Michigan. The results of these tests consistently indicated greater penetration of the oxygen jet into the iron bath than that shown by the appropriate curves of Figure 23. A comparison between penetrations indicated by those "Bottom Marking" tests and penetration as shown by Figure 23 resulted in the suggested relation:

Penetration = 1.33 times "Computed" Penetration

Another suggested relationship evolving from the September-October "Bottom Marking" tests was

Penetration = A + "Computed" Penetration

where A appeared to be about 10 to 13 inches, depending on the size of the Oxygen Converter used in the "Bottom Marking" test.

Regardless of what the precise relation was between computed (from $(P_i)_{max}$ data) and indicated penetration, there was clearly a significant difference between the two.

One of the significant differences between the behavior of an oxygen jet in room air and the behavior of an oxygen jet in the Oxygen Converter is due to the difference in the density of the gas surrounding

the jet. In room air tests the density of the surrounding gas is normally very nearly the same as the density of the gas within the jet (with the possible exception of that portion of the jet which is within the supersonic core). This is not so in the oxygen converter.

In both the room air tests and the oxygen converter tests, the ambient pressure is about 14.7 psia. Furthermore, the molecular weights of the surrounding gas atmosphere for the room air tests and the converter tests should be about the same, provided that the gas surrounding the jet in the converter is predominantly carbon monoxide. Consequently, the ratio of the density of the jet to the density of the gas surrounding the jet varies primarily with the temperature and is roughly proportional to the inverse of the ratio of the jet temperature (absolute) to the surrounding gas temperature (absolute). Thus, if the temperature of the surrounding gas were in the neighborhood of 5 times the temperature of the jet, the density of the gas surrounding the jet would be about 1/5 the density of the gas within the jet.

A few preliminary tests were made which showed a striking increase in $(P_i)_{max}$ due to surrounding the jet with heated gas from a propane-air burner. As a result of these preliminary tests several small scale heated atmosphere tests were made.

In these small scale tests the air inside of a Pyrex vessel, 12 inches diameter by 24 inches tall, was heated by electric heating coils mounted just above the bottom of the vessel. The temperature of the air leaving the vessel was measured to provide some indication of the average temperature of the gas within the vessel.

The flat plate impact pressure, $(P_i)_{max}$, was recorded as a function of blowing height, nozzle driving pressure and outlet temperature. The nozzle used was a convergent nozzle having a throat diameter of 0.081 inches. The results of these tests are summarized as follows:

1. Increasing the temperature of the gas surrounding the jet resulted generally in an increase in $(P_i)_{max}$ for any given nozzle blowing height and nozzle blowing distance.
2. The effect of heating the atmosphere was barely discernable when the blowing height (for the 0.081 inch nozzle) became greater than 9 inches (i.e., a ratio of nozzle height to throat diameter of 111). The blowing height can also be so low that there is no appreciable effect due to heating the atmosphere.
3. At the very low driving pressures the effect of the heated atmosphere was not discernable.
4. It was concluded that, within the limits tested, increasing the temperature of the atmosphere surrounding a jet resulted in higher values of $(P_i)_{max}$ except at extreme conditions of blowing pressure and nozzle heights.

Several "Heated Atmosphere" tests were also made with a 0.162 inch nozzle in the Cast Metals Laboratory. The heated atmosphere was created above a molten iron bath by blowing into the bath a jet of oxygen at a pressure sufficient to cause ignition to occur within a few seconds. Ignition, as used here, is said to have occurred when a visible flame and accompanying smoke billow out from the iron bath.

The purpose of these tests was to determine if the heated atmosphere, which exists above the molten iron in an Oxygen Converter, produced a value of P_t (gauge pressure measured by a total head probe) on the jet centerline different from that measured in room air. The essential results of these tests are shown by the following data:

Distance Between Nozzle and Total Head Tube = 4.5 inches

Nozzle Driving Pressure = 50 psig

The total head was measured in these tests by a "J" shaped silica tube probe connected to a mercury manometer.

Total Head-Cold Atmosphere = 11.2 inches Mercury

Here the nozzle and total head tube were remote from the bath, thus the jet was surrounded by air at essentially room temperature.

Total Head-Heated Atmosphere = 19.5 inches Mercury

Here the nozzle was 9 inches above the bath while the total head probe was still 4.5 inches below the nozzle. Thus the probe was 4.5 inches above the bath. The total head showed a sudden increase at the time of ignition, rising to the value of 19.5 inches of Mercury.

The results shown above are the average values obtained from two separate, successive runs.

These tests clearly indicate that the total head at a particular point in the oxygen jet, relative to the nozzle, can increase by more than 70% when the jet is surrounded by an atmosphere similar to that of an Oxygen Converter as compared to the "same" oxygen jet surrounded by room air.

The various "heated atmosphere tests" discussed above were more than adequate to demonstrate the importance of the ambient temperature (or more correctly, density) on the penetration capabilities of an oxygen jet. It was, however, considered desirable to obtain $(P_i)_{max}$ data for a range of ambient temperatures, using an 8 mm water cooled lance built for hot iron tests. In particular it was planned to obtain data within the range of blowing heights and driving pressures which might be used in the hot iron tests in the Cast Metals Laboratory.

The ideal test facility for such a series of tests would enable the lance to be surrounded by a gas of any temperature desired under conditions such that the gas surrounding the jet had no velocity other than that induced by the jet. This would require an exorbitant cost.

Consequently, it was concluded that a circular vessel closed at the bottom end and open at the top end, where the lance was mounted, would be used. The oxygen jet would strike a target area, where the $(P_i)_{max}$ probe was located and then be deflected in an outward and upward direction over a bed of glowing charcoal. The resulting combustion process would provide heat to keep the atmosphere surrounding the jet at some elevated temperature. Figure 7 is a schematic drawing of this Heated Atmosphere test facility.

It can be seen from this drawing that the target area which is slightly "cupped" is located in a recessed region. This configuration was chosen to deflect the oxygen jet upward from the charcoal bed, rather than onto the bed. The vortex flow set up by this scheme was quite adequate for supplying oxygen to the charcoal. Air instead of oxygen was used in some of these tests.

Two thermocouples were installed in the heated atmosphere vessel, outside the primary oxygen jet. They were located 2 inches off the jet centerline and 7 and 11 inches, respectively, above the impact cup. The average of the temperatures indicated by these two thermocouples was considered to be at least indicative of the average temperature of the gas surrounding the jet. A detailed survey of the velocity and temperature distribution throughout all the gas surrounding the jet would be required in order to obtain a precise average. Such a study was beyond the scope of this work.

Although it was difficult to measure the exact temperature of the ambient atmosphere in these tests and thus obtain precise impact data, several general observations can be made as a result of these tests:

1. The $(P_i)_{max}$ increases in general with increasing temperature of the surrounding atmosphere, at least up to the maximum temperature measured during these tests, which was almost $900^{o}F$.

2. The increase in $(P_i)_{max}$ of the jet with increase in ambient temperature was less pronounced at the low driving pressures, e. g., 15 psig, than at the higher driving pressure, e. g., 70 to 100 psig.

3. Most of the heated atmosphere data was taken using an 8 mm (0. 316 in.) nozzle at a blowing distance of 13 inches or 21 inches. The effect of an increase in ambient temperature on $(P_i)_{max}$ was significant at both these blowing distances, although the effect was more significant at the 13 inch blowing distance.

A cross plot of the heated atmosphere $(P_i)_{max}$ data was made and the estimated penetration was computed by Equation (11) as discussed previously. The result of these tests is the curve of Figure 28 which is described as an "Air jet into heated atmosphere at 620^{o}F." This temperature was chosen so that the curve would represent the situation where the density of the gas surrounding the jet would be about one half that of the gas within the jet.

Clearly a ratio of 2:1 produces a significant increase in the penetration capabilities of the jet, thus a temperature ratio of 5:1 should produce a much greater penetration capability. An indication of the increased penetrating capability of the jet at higher temperature ratios is shown by the curve in Figure 28 plotted from measured penetration data obtained with the same nozzle when used to blow molten iron in a two-ton converter.

Theoretical studies have been made by others regarding the effect on the jet due to changes in the density of the surrounding gas. References 10 and 11 deal with this subject. The major difficulty in applying directly the results of such studies is the fact that the fluid dynamic flow system of interest here includes a combination of:

1. Supersonic flow
2. Subsonic flow
3. Compressible flow
4. Turbulent flow
5. Two phase flow (i. e., gas and liquid)
6. Chemical reaction within the flow

None of the references listed above include studies which take account of all six of these conditions at one time.

Those studies do, however, demonstrate that decreasing the density (e. g., by increasing the temperature) of the gas surrounding a gas jet results in a generally less rapid spread of the jet, and thus a greater $(P_i)_{max}$ at given distances from the nozzle.

Because of all the interacting factors which are present in the jet flow in an Oxygen Converter all the proper scale relationships are not yet known (Ref. 9). It is certainly obvious, however, that the penetration of the oxygen jet into molten iron in a commercial oxygen converter would be greater than "cold" $(P_i)_{max}$ data would indicate. Thus the fact that penetration measured in the McLouth Plant exceeded the penetration previously estimated from "cold" $(P_i)_{max}$ data by the authors can now be satisfactorily explained (at least in part) on the basis of the heated atmosphere of the converter.

SECTION E

PENETRATION MEASUREMENTS IN MOLTEN IRON

The authors have participated in a number of tests involving the blowing of oxygen (and nitrogen) into molten iron. These tests were conducted in the Cast Metals Laboratory of The University of Michigan's Department of Chemical and Metallurgical Engineering. These tests were conducted under the direction of Professors R. A. Flinn and R. D. Pehlke of that department. During several of these "Hot Iron" tests, measurements were made of the extent to which the oxygen jet penetrated into the molten iron. A brief discussion of these penetration tests are included in this report in order to provide a more complete picture of the relation between nozzle performance and jet penetration in a molten iron bath. *

The problem of measuring the depth to which a gas jet penetrates into a liquid is simply that of determining the position of the interface between gas and liquid at the bottom extremity of the cavity created by the jet. Clearly, this is not difficult to accomplish in a transparent liquid such as water where the depth to which the cavity extends can be determined visually.

The depth to which an oxygen jet penetrates into a molten iron bath may sometimes be visually determined. Such visual determinations may be made and photographed prior to ignition if an open vessel is used and, occasionally, even after ignition. However, when large quantities of smoke and fume are being generated and molten iron and slag particles are erupting from the cavity, precise visual observations

*The University of Michigan, ORA Report 04806-1-F, Part 2, covers these "Hot Iron" tests in detail.

are practically impossible. Consequently, in order to obtain reliable data, some other method of measuring penetration is required.

The method developed for measuring the depth of penetration of the oxygen jet in molten iron is referred to herein as the "Nitrogen Bubbler Probe."

Principle of Operation of the Nitrogen Bubbler Probe

Consider the bottom of the cavity created by the oxygen jet penetrating into a molten iron bath. The pressure exerted by the gas on the liquid at the bottom of the cavity must just equal the pressure exerted in the opposite direction by the liquid on the gas, under steady state conditions. Otherwise the unbalanced force would cause the depth of penetration to change.

The gauge pressure at a point in a quiescent liquid bath (expressed in terms of the bath material) must equal the bath depth at that point. Similarily, the pressure in the bath at any particular point below a cavity in the bath is essentially equal to the pressure corresponding to the "bath depth" at that point. The bath depth at that point being measured down from the bath surface outside of the penetrated region.

However if a point is selected above the bottom of the cavity created by the jet the pressure at this point cannot be expected to be equal to the pressure at a corresponding depth in the liquid, outside the cavity. In fact, the pressure at a point near the bottom of the cavity will differ in two ways, depending on whether the point is below or above the bottom of the cavity.

a. Average Pressure. The average pressure at a point in the bath appreciably below the cavity will not noticeably change with depth of penetration, provided the penetration does not

extend to the point of measurement. The average pressure at a point above the bottom of the cavity will in general increase as depth of penetration increases beyond the point of measurement.

b. Pressure Fluctuations. The pressure at a point below the cavity is reasonably constant until the jet penetrates essentially to the point of measurement. However after the jet penetrates to the point of measurement the inherent pressure fluctuations within the jet (Reference 3) are impressed upon the pressure sensing probe. Hence, when the gas jet penetrates to the pressure probe, fluctuations may be recorded on the pressure trace.

These principles may be used to determine when a cavity produced by a jet of gas extends to a designated point in a liquid bath. A pressure sensing device (a pressure probe) located a fixed distance from the surface of a liquid bath and connected to a suitable recording instrument will show an essentially constant pressure provided the cavity made by a jet of gas does not penetrate to the sensing point. When the cavity penetrates to the sensing point a variation in pressure at that point will occur and will be recorded.

The Need for Nitrogen Flow Through the Pressure Probe

A pressure probe open to the liquid in the bath can normally be expected to be filled with the bath liquid. For water, mercury, etc., this is acceptable. It is not practical for molten iron, however, since at some point in the pressure probe line the iron would solidify and thus block any further transmission of pressure changes. For this reason it was necessary to continuously force some inert fluid, such as nitrogen, through the pressure probe to keep it at least partially free of iron.

Demonstration of the Performance of the Bubbler Probe System in a Water Bath

Figure 24A is a photograph of the model set up to demonstrate the principle of operation of the bubbler probe system. The bubbler probe assembly mounted in the bottom of this 12 inch diameter Pyrex vessel is essentially as shown in Figure 24B.

The results of a test made with this model are shown by the two curves of Figure 25. This plot was obtained by successively increasing the nozzle driving pressure until the probe back pressure (P_b) trace showed complete penetration. Each time it was visually observed that the jet had penetrated completely to the bottom of the vessel where the Bubbler Probe was located a disturbance was indicated by the P_b trace. Except for the fact that visual observation is impossible in a molten iron bath, the principal of operation of the nitrogen bubbler probe is the same in a molten iron bath as in the water bath.

Variations in Bubbler Probe Design

Initial penetration tests made in hot iron with the nitrogen bubbler probe systems utilized a "J" shaped silica tube. The results were encouraging but the "J" probe would frequently bend early in the test. The opening in the end of the silica probe would also enlarge during the test, thus changing the nature of the recorded back pressure. Centering of the "J" probe within the oxygen jet was also a problem.

It was decided that a nitrogen bubbler probe installed in the bottom of the Oxygen Converter would eliminate some of these problems. With this system a given bath depth and a given nozzle blowing height were established before the test. During the test the driving pressure was increased until the P_b trace showed that penetration to the bottom of the bath had occurred. This was then repeated within the limits

of time and equipment. The bubbler tube frequently plugged after one or two bottom "touches" with the jet had been indicated.

The first bubbler probes mounted in the Converter bottom consisted mainly of a 1/8 inch hole through a brick in the vessel bottom. Within the lower portions of the bottom lining this hole was joined to a stainless steel tube which extended outside of the converter. Here a nitrogen feed line and a line to the pressure recorder were connected. With this system nitrogen bubbles were formed individually and the pressure pulsations thereby created were indicated by the pressure recorder.

The results of a test in molten iron made with a bubbler system of this sort are shown in Figure 26. The test conditions are listed on the figure. The continuing pressure fluctuations are shown inside of the two dotted lines which form the envelope of the P_b trace. The average back pressure rises as the driving pressure continues to increase after penetration to the bottom of the bath has occurred. Also, the nature of the pressure fluctuations is altered when the jet impinges on the probe itself.

The final nitrogen bubbler probe configuration as shown by Figure 24B utilizes an alumina tube having an inside diameter of 0.041 inch. With this system the pressure recorder does not show these pressure fluctuations resulting from the forming of the nitrogen bubbles. Thus the P_b trace is essentially a smooth line until penetration occurs, as shown by Figure 27.

Throughout these penetration tests in molten iron frequent failures occurred due to the bubbler probe becoming plugged with solidified iron. The very small size bubbler tube was used to help eliminate this problem. It was concluded that plugging of the bubbler was caused by molten iron particles becoming entrained in the oxygen jet and being

literally driven into the bubbler tube. This would occur when the converter bottom was essentially exposed in the vicinity of the probe. For this reason the driving pressure would be rather slowly increased until an indication of penetration was observed on the P_b trace. The driving pressure would then be quickly reduced in order that the bubbler would not become plugged. If the bubbler were not plugged then the test would be immediately repeated. This procedure resulted in the curves of Figure 27. The data points for penetration tests made with the 8 mm nozzle at a blowing height of 13 inches are plotted on Figure 28. This figure shows that under the conditions existing in the two ton Oxygen Converter, the penetration of the oxygen jet is actually much greater than the penetration "computed" from $(P_i)_{max}$ data. Also, the penetration of oxygen into molten iron is much greater than the corresponding penetration of air into a bath at room temperature.

Estimating Penetration from the "Empirical Penetration Curve"

The bubbler technique was used to measure the depth of penetration of an oxygen jet into a molten iron bath when using various nozzles and converters with various blowing heights and bath depths.

An analysis of this test data shows that the depth of penetration of an oxygen jet discharged through a Laval nozzle toward a molten iron bath is dependent on the size of the nozzle (throat diameter), the driving pressure (pressure of the gas imposed on the nozzle) and the distance of the nozzle from the bath surface (the blowing height). The data also indicate that penetration increases with an increase in driving pressure and throat diameter and decreases with an increase in blowing height. This relationship may be expressed graphically be plotting the measured depth of penetration against the computed value $P_d D_t/\sqrt{H}$;

where P_d = nozzle driving pressure - psia

D_t = nozzle throat diameter - inches

H = distance of nozzle to bath surface - inches.

The parameter $P_d D_t/\sqrt{H}$ was empirically derived.

Figure 29 presents the results of several penetration tests made wherein an oxygen jet penetrated a bath of molten iron. Each point on this figure was obtained by:

a. Determining nozzle diameter.

b. Measuring the depth of the molten iron bath.

c. Measuring the height of the nozzle above the bath.

d. Increasing the oxygen flow rate until penetration of the entire bath was indicated by the Nitrogen Bubbler Probe System.

e. Plotting the bath depth against the computed value of $P_d D_t/\sqrt{H}$.

The purpose of these penetration tests was to determine for a given set of conditions the minimum driving pressure required for the oxygen jet to penetrate the entire bath. Increasing the oxygen pressure too rapidly would frequently result in an indication of penetration at a nozzle driving pressure greater than the minimum. For this reason a curve is drawn through those data points of Figure 29 which represents essentially the minimum conditions necessary to penetrate the entire bath rather than through the average of these data points. This curve, which is approximately a straight line for bath depths greater than 6 inches is referred to herein as the "Empirical Penetration Curve."

The data points for Figure 29 were obtained by the use of:

a. Nozzles - 0.162 inch and 0.316 inch

b. Nozzle heights above the molten iron - 6 1/8 to 13 inches

c. Bath depths - 3 to 14 1/4 inches

d. Ratios of nozzle height to nozzle diameter range from 22 to 41

The nozzles (water cooled lances) used in these molten iron penetration tests were converging-diverging (Laval) nozzles which were usually operated at driving pressures somewhat different from their design pressure (see Section A). It is felt, however, that the empirical curve of Figure 29 is useful for converging-diverging nozzles operated reasonably near their design pressure and for converging nozzles operated with nozzle driving pressure well below 100 psig.

REFERENCES

1. Glass, D. R., and Howard, E. T., "A Study of Supersonic Nozzle Design as Applied to the Oxygen Conversion Process," Univ. of Mich., ERI 2409-1-F, November, 1955.

2. Glass, D. R., and Hays, P. O., "An Evaluation of the Average Impact Pressure Produced by a Supersonic Nozzle Operating at Conditions Specified for the Oxygen Conversion Process," Univ. of Mich., ERI 2625-1-F, February, 1957.

3. Glass, D. R., and Hays, P. O., "A Design Study of Supersonic Nozzles for the Oxygen Conversion Process," Univ. of Mich., ERI 2638-1-F, June, 1957.

4. Glass, D. R., and Hays, P. O., "An Evaluation of Supersonic Nozzles used in the Oxygen Conversion Process," Preliminary Progress Report, Univ. of Mich., ORA 04806-1-P, January, 1962.

5. Shapiro, A. H., The Dynamics and Thermodynamics of Compressible Fluid Flow, New York, The Ronald Press Co., 1953.

6. "Fluid Meters, their Theory and Application," An American Society of Mechanical Engineers Research Publication, 4th Edition, 1937.

7. "Flow Measurement," Published by the ASME, 1940. "Power Test Codes," PTC 19. 5. 4 - 1940, Information on Instruments and Apparatus, Part 5, Measurement of Quantity of Materials, Chapter 4, Flow Measurement by Means of Standardized Nozzles and Orifice Plates.

8. "Equations, Tables, and Charts for Compressible Flow," NACA Report 1135, 1953.

9. "The Physics of Oxygen Steelmaking," Holden, C., and Hogg, A., Journal of Iron and Steel Inst., Vol. 196, November, 1960, p. 318-332.

10. Pai, Shih-I, Fluid Dynamics of Jets, New York, D. Van Nostrand Company, Inc., 1954.

11. Hinze, J. O., Turbulence, New York, McGraw-Hill Book Company, Inc., 1959.

12. Ferri, Antonio, Elements of Aerodynamics of Supersonic Flows, New York, MacMillan Company, 1949.

13. Kuethe, A. M., and Schetzer, J. D., Foundations of Aerodynamics, John Wiley and Sons, Inc., 2 ed., November, 1961.

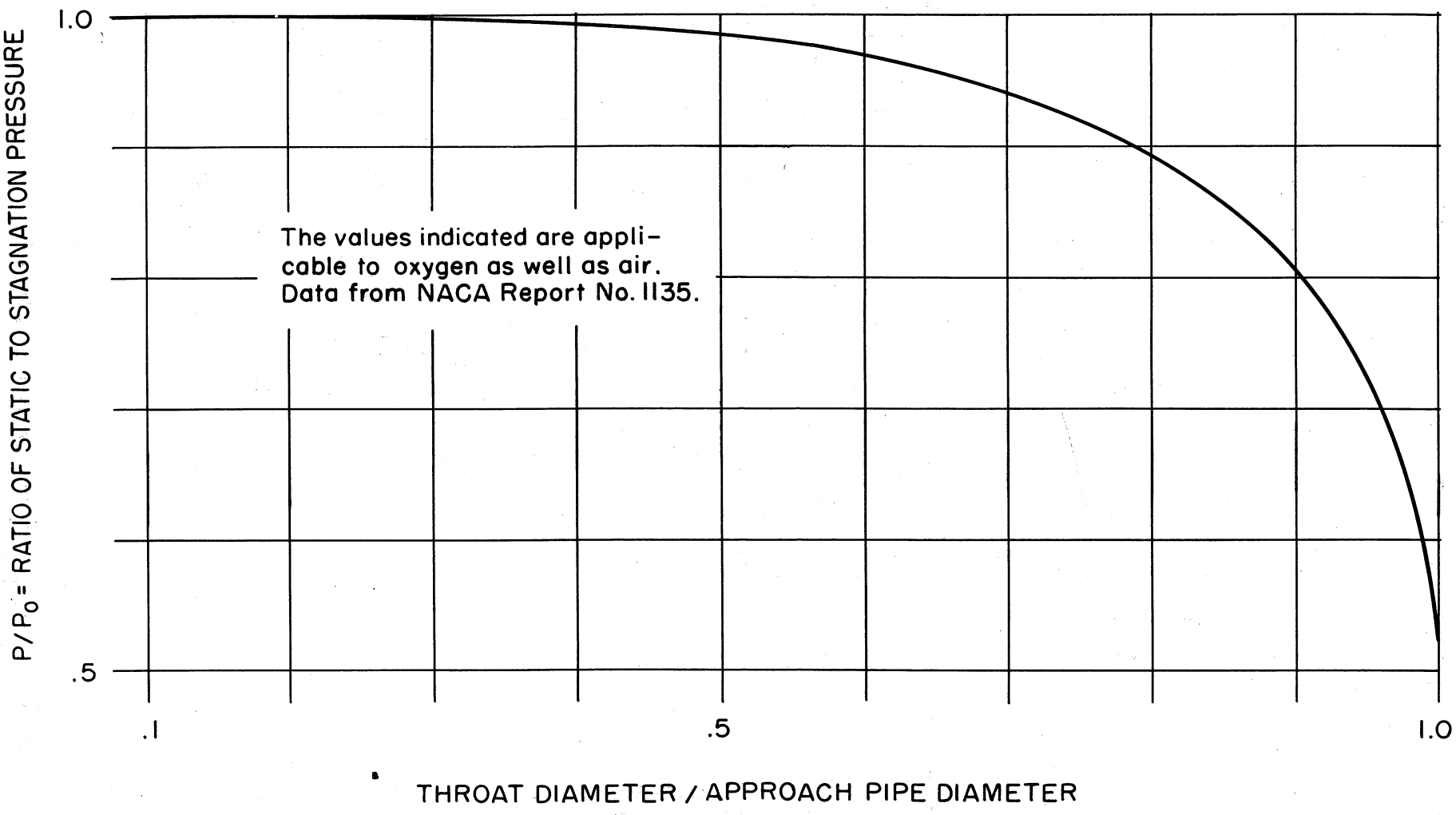

FIGURE 1 RATIO OF STATIC TO STAGNATION PRESSURE VS. RATIO OF THROAT TO APPROACH PIPE DIAMETER.

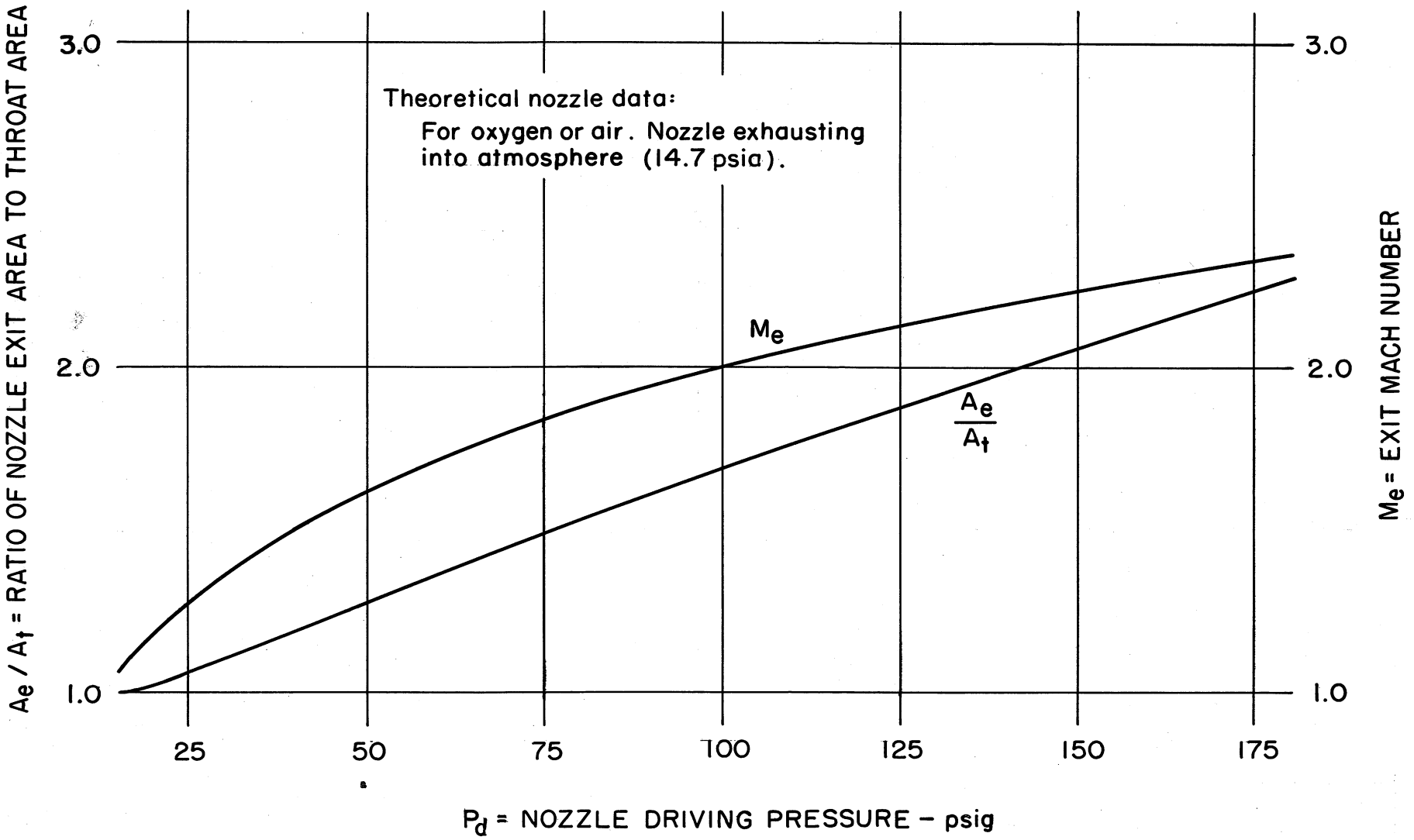

FIGURE 2 RATIO OF NOZZLE EXIT AREA TO THROAT AREA AND EXIT MACH NUMBER VS. NOZZLE DRIVING PRESSURE.

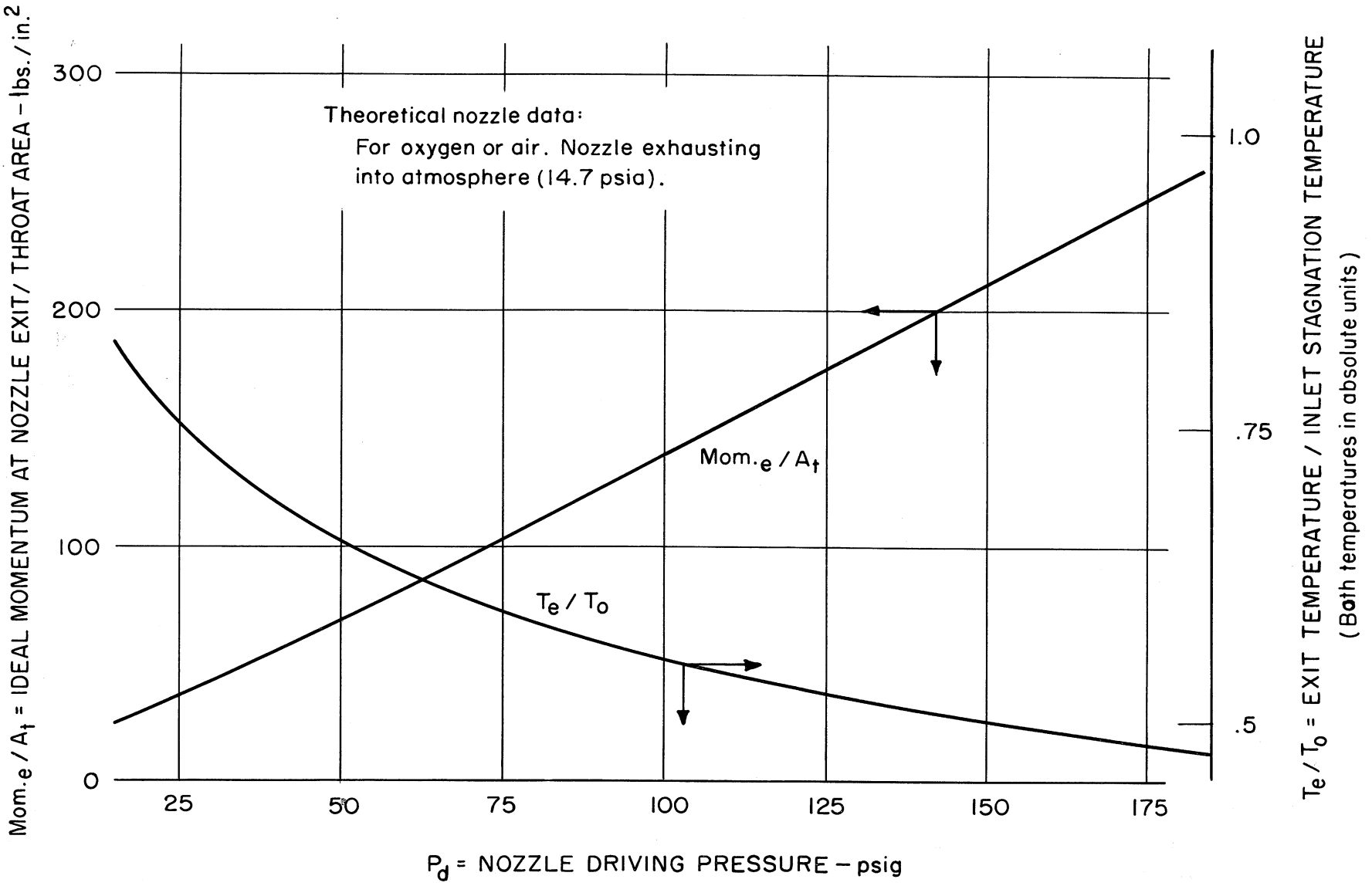

FIGURE 3 RATIO OF IDEAL EXIT MOMENTUM TO THROAT AREA AND RATIO OF EXIT TEMPERATURE TO STAGNATION TEMPERATURE VS. NOZZLE DRIVING PRESSURE .

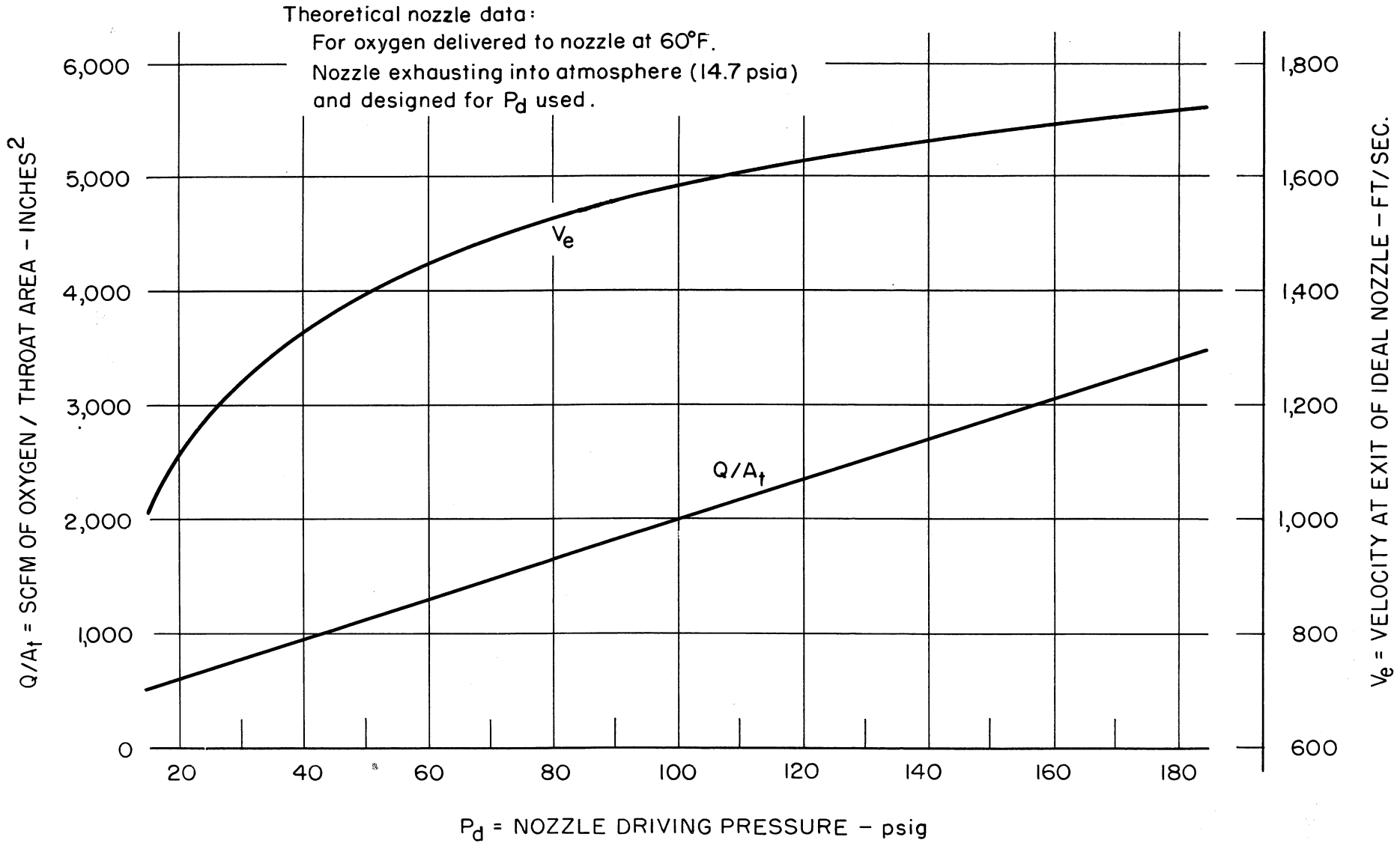

FIGURE 4 FLOW RATE PER SQUARE INCH OF NOZZLE THROAT AREA AND EXIT VELOCITY VS. NOZZLE DRIVING PRESSURE.

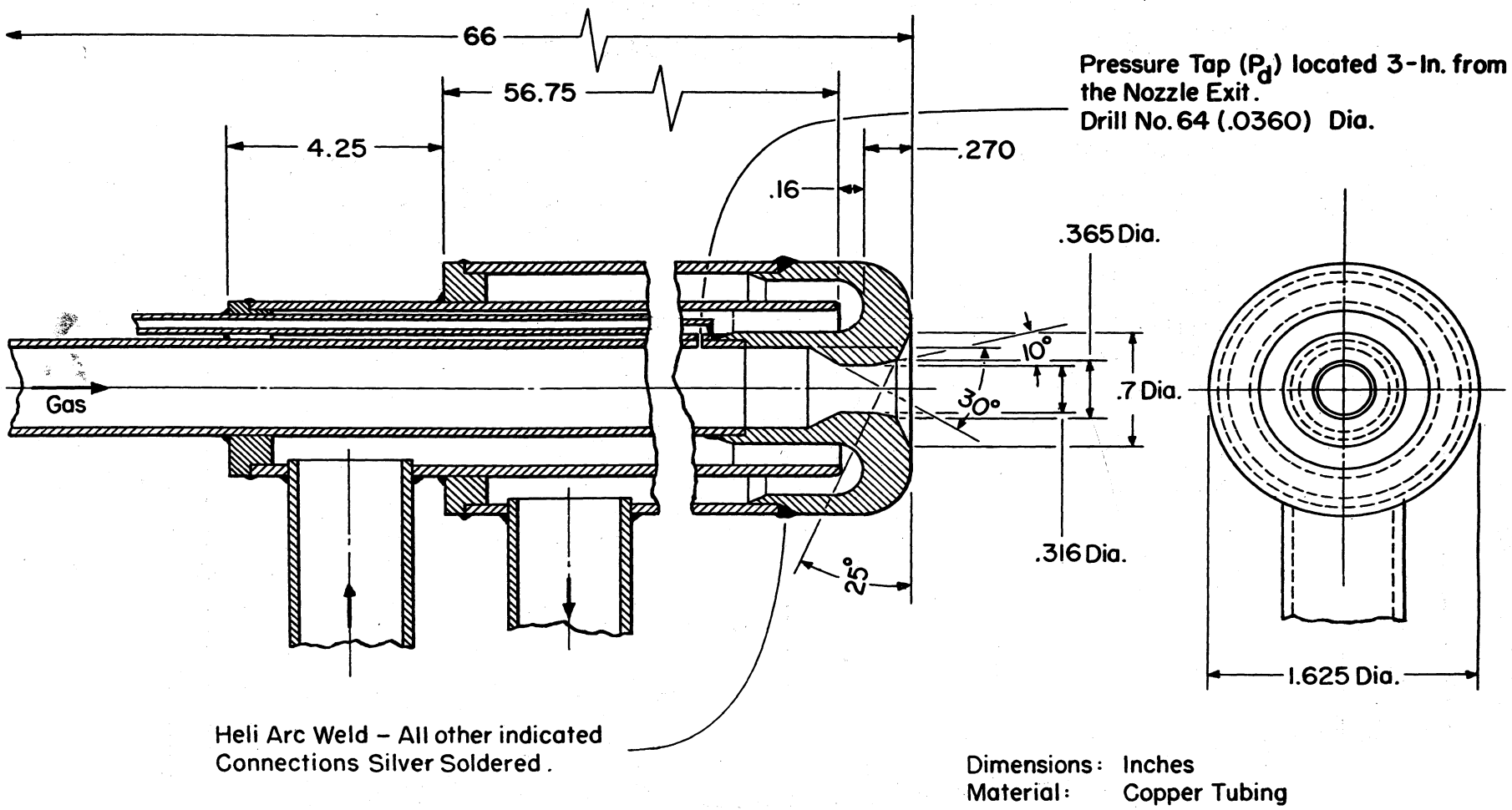

FIGURE 5 WATER COOLED LANCE.

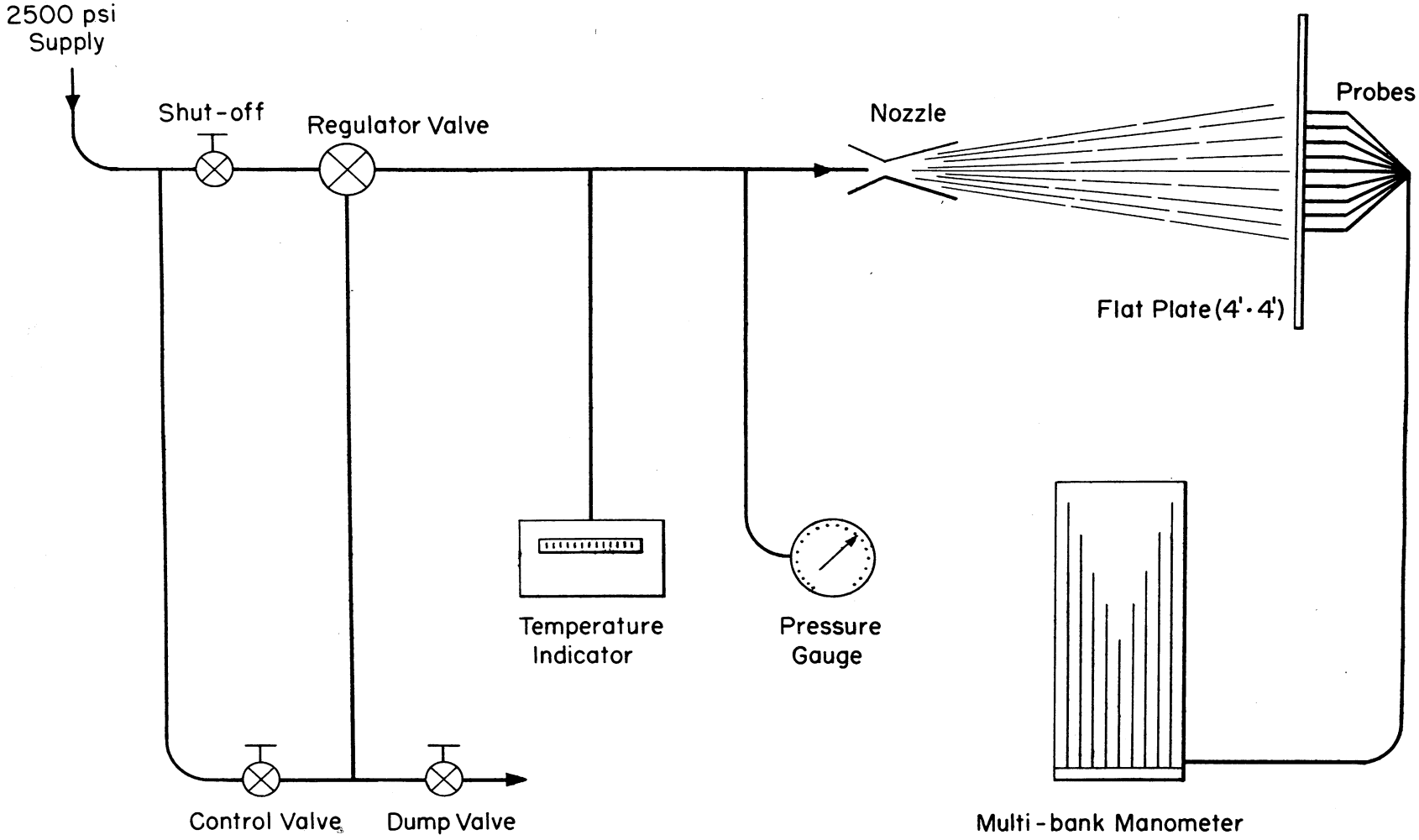

FIGURE 6 SCHEMATIC DRAWING OF TEST INSTALLATION FOR DETERMINING IMPACT PRESSURES.

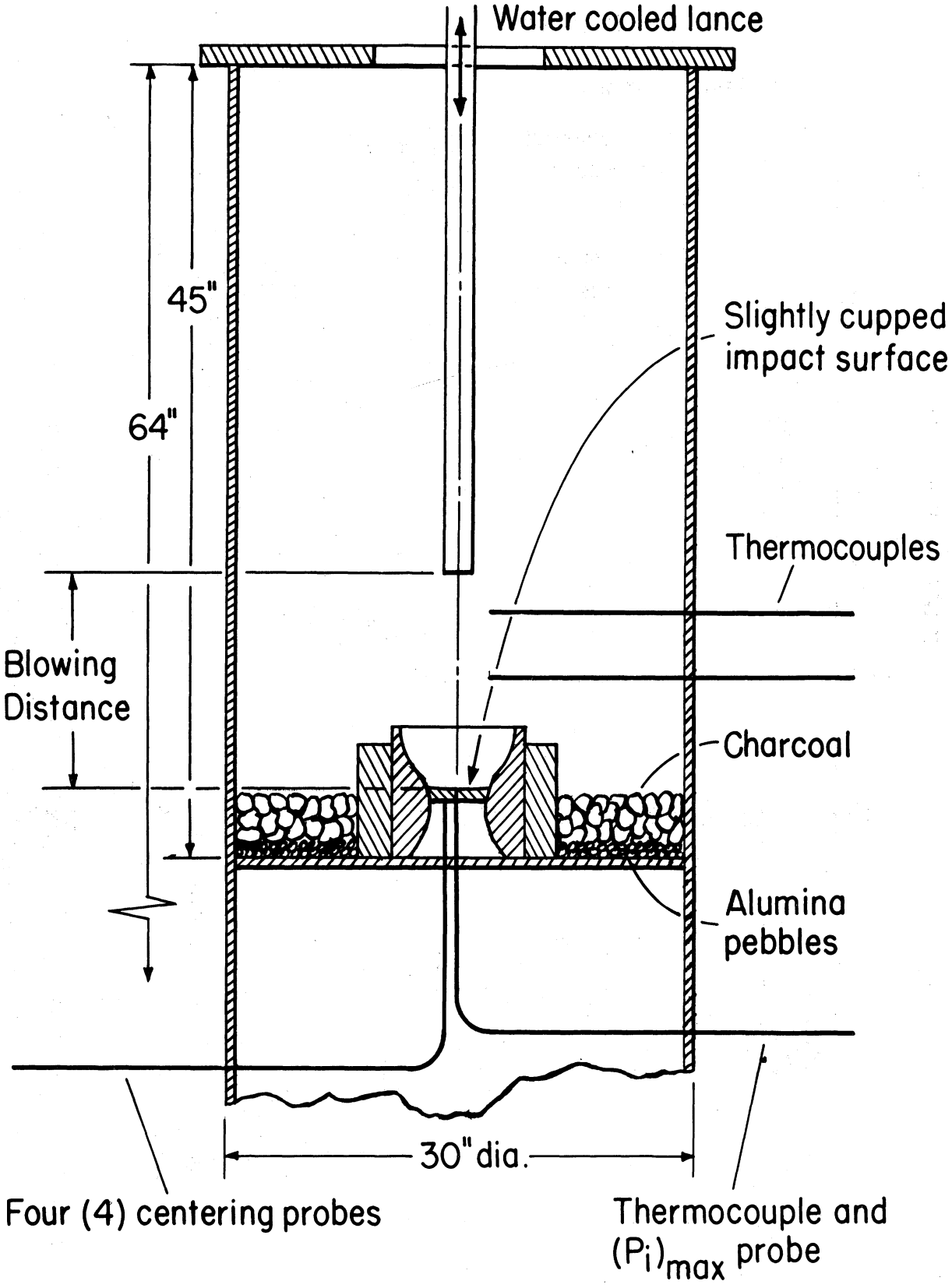

FIGURE 7 SCHEMATIC DRAWING OF HEATED ATMOSPHERE FACILITY.

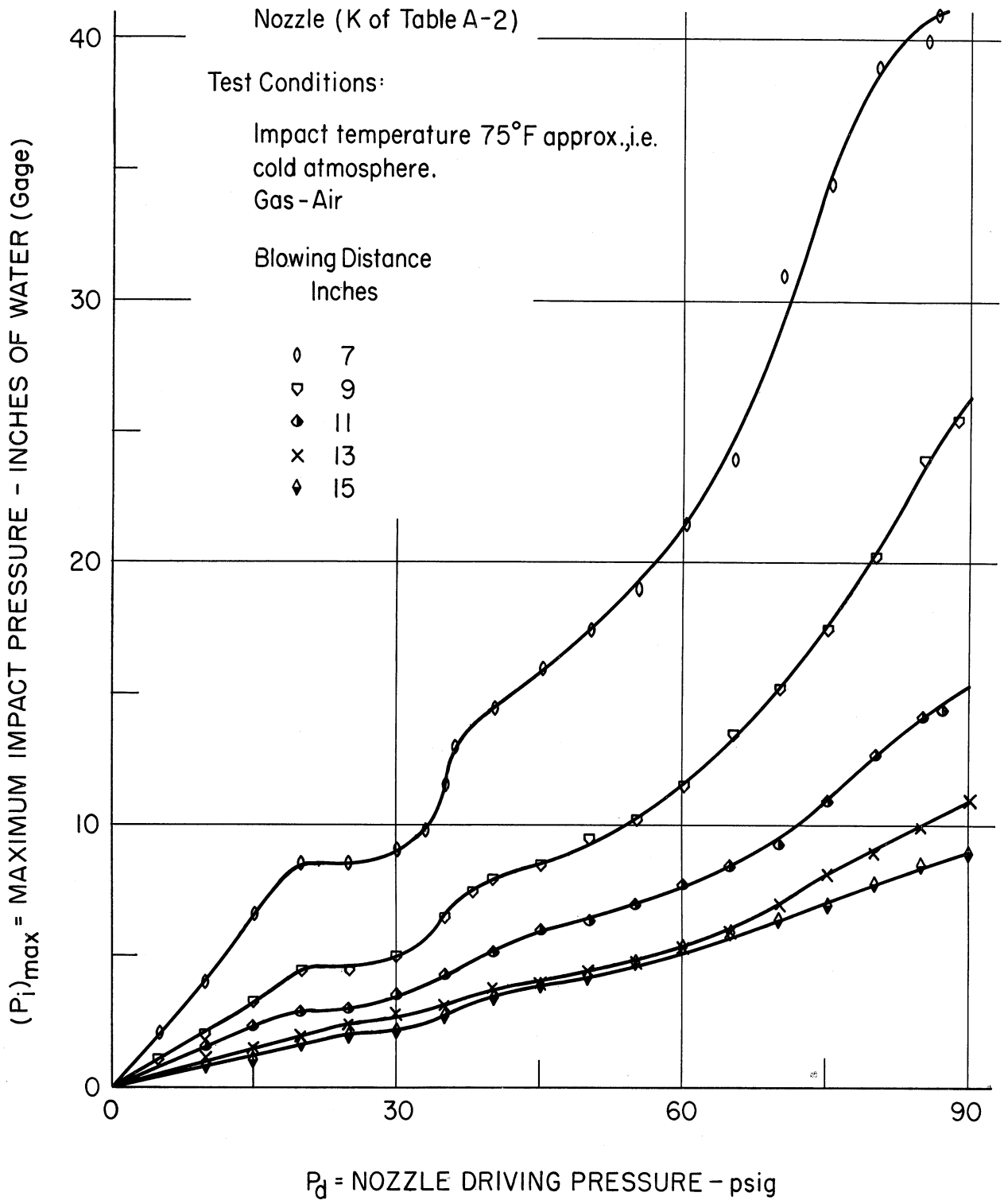

FIGURE 8 MAXIMUM IMPACT PRESSURE VS. NOZZLE DRIVING PRESSURE FOR .162 - INCH DIAMETER LANCE.

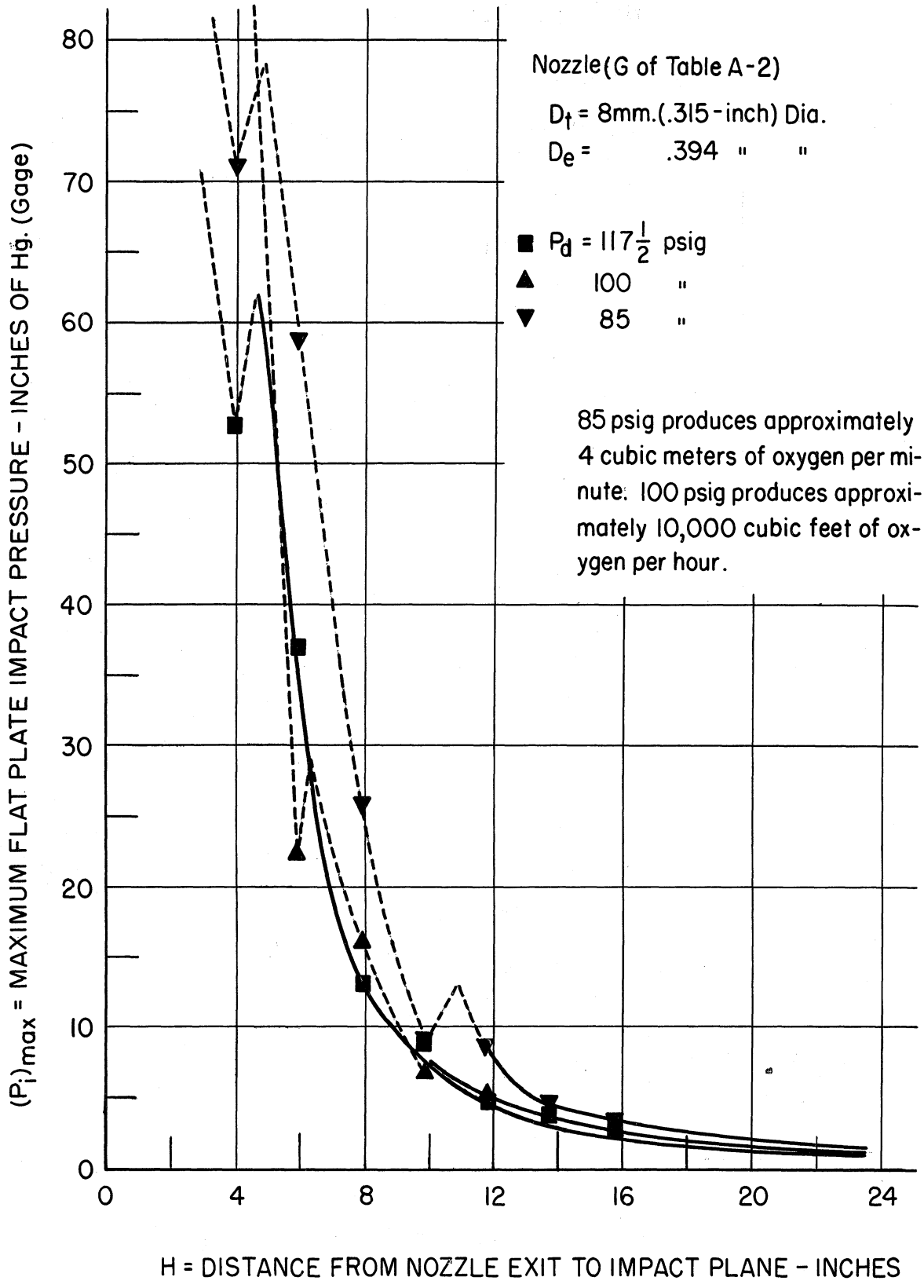

FIGURE 9 MAXIMUM FLAT PLATE IMPACT PRESSURE VS. BLOWING DISTANCE FOR 8 mm. NOZZLE .

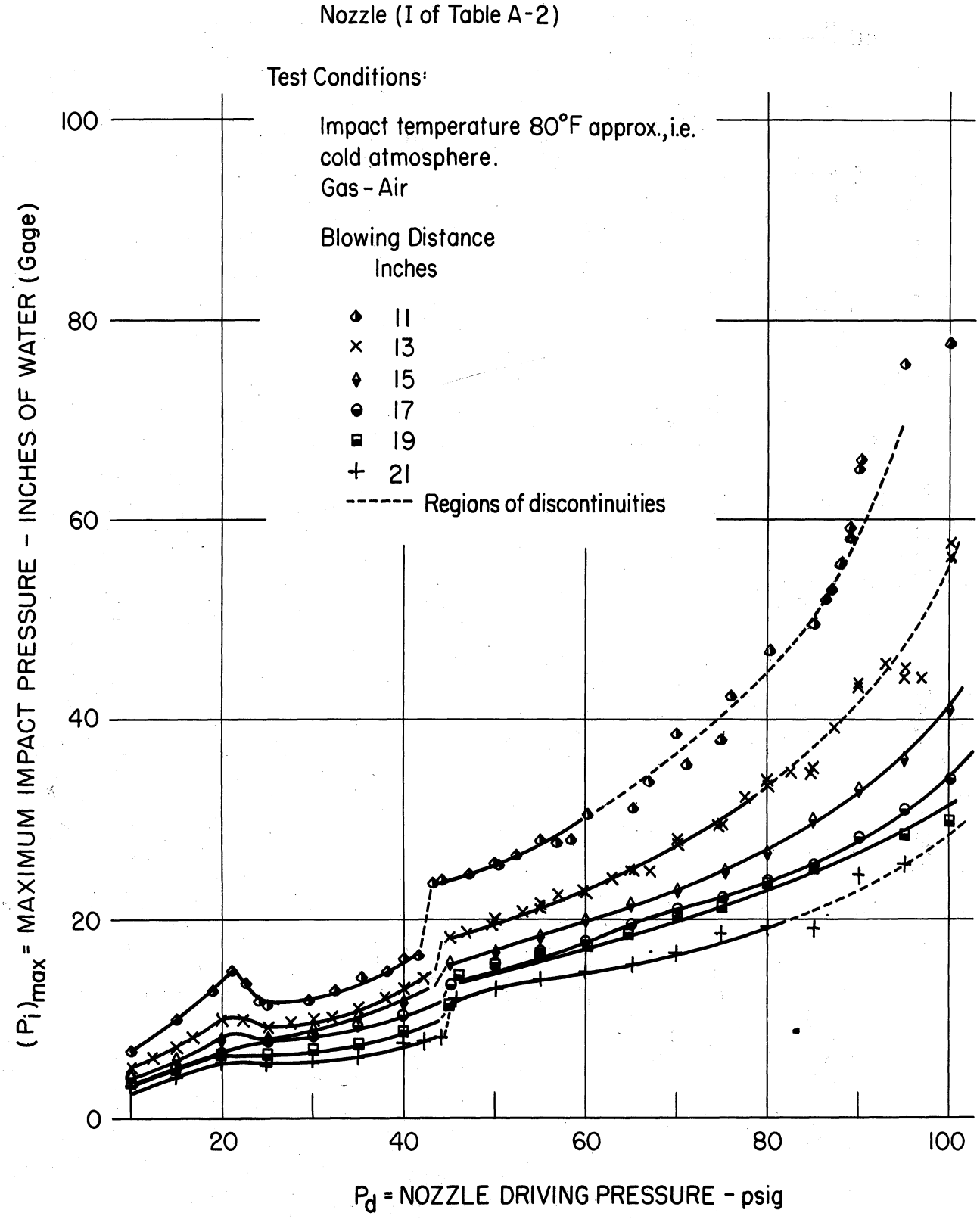

FIGURE 10 MAXIMUM IMPACT PRESSURE VS. NOZZLE DRIVING PRESSURE FOR 8-mm. DIAMETER LANCE.

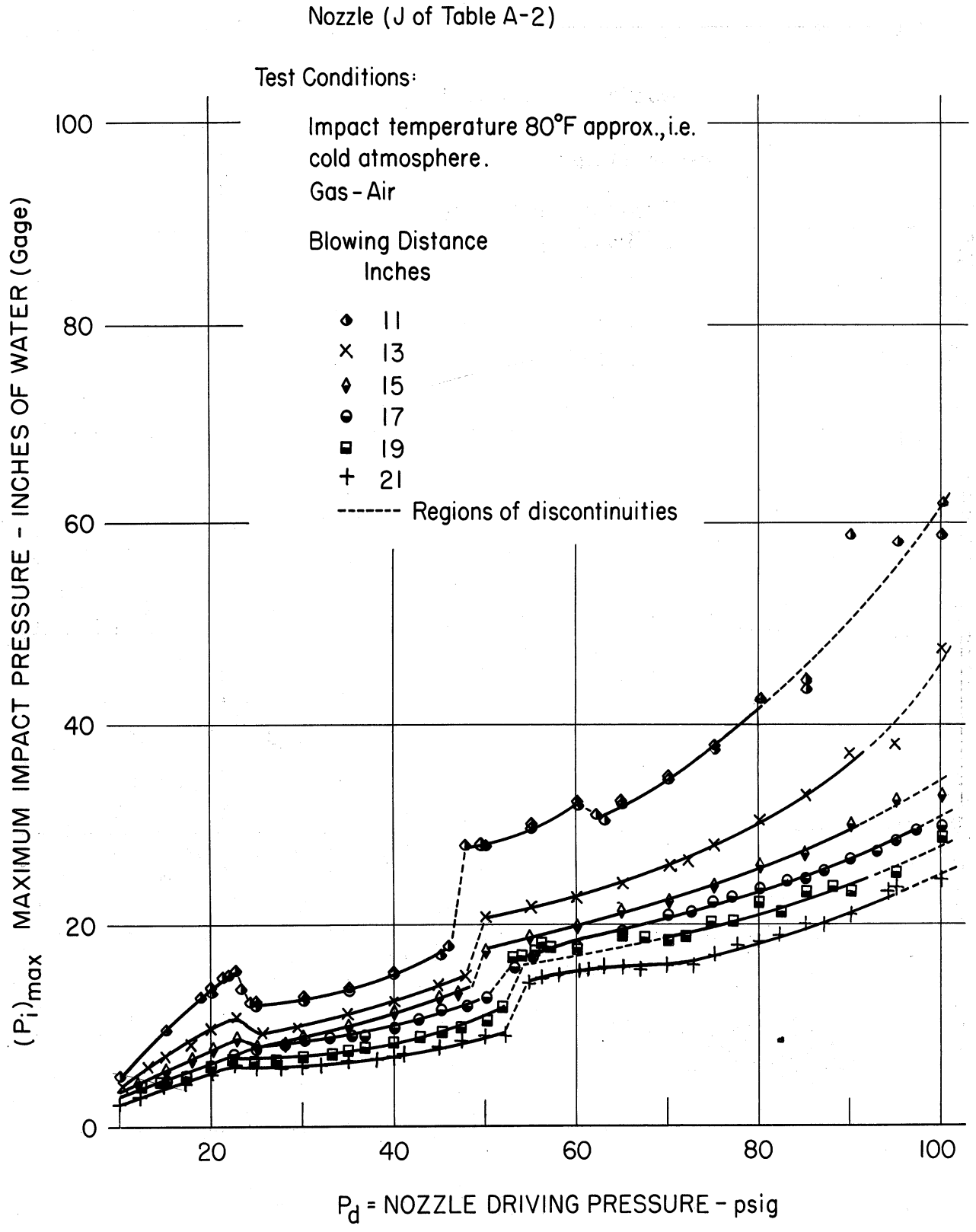

FIGURE 11 MAXIMUM IMPACT PRESSURE VS. NOZZLE DRIVING PRESSURE FOR 8-mm. DIAMETER LANCE.

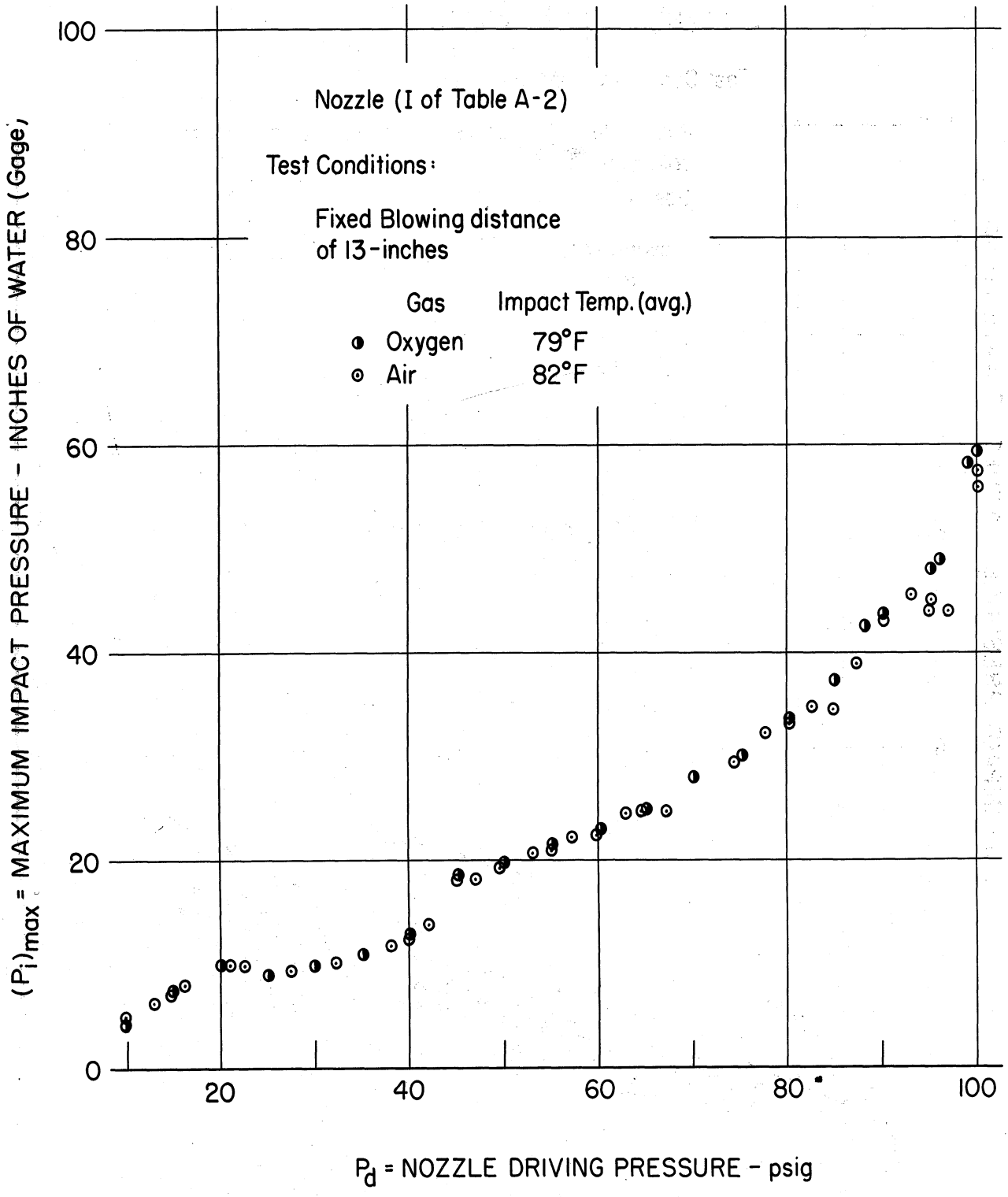

FIGURE 12 MAXIMUM IMPACT PRESSURE VS. NOZZLE DRIVING PRESSURE FOR 8-mm. DIAMETER LANCE; USING OXYGEN OR AIR.

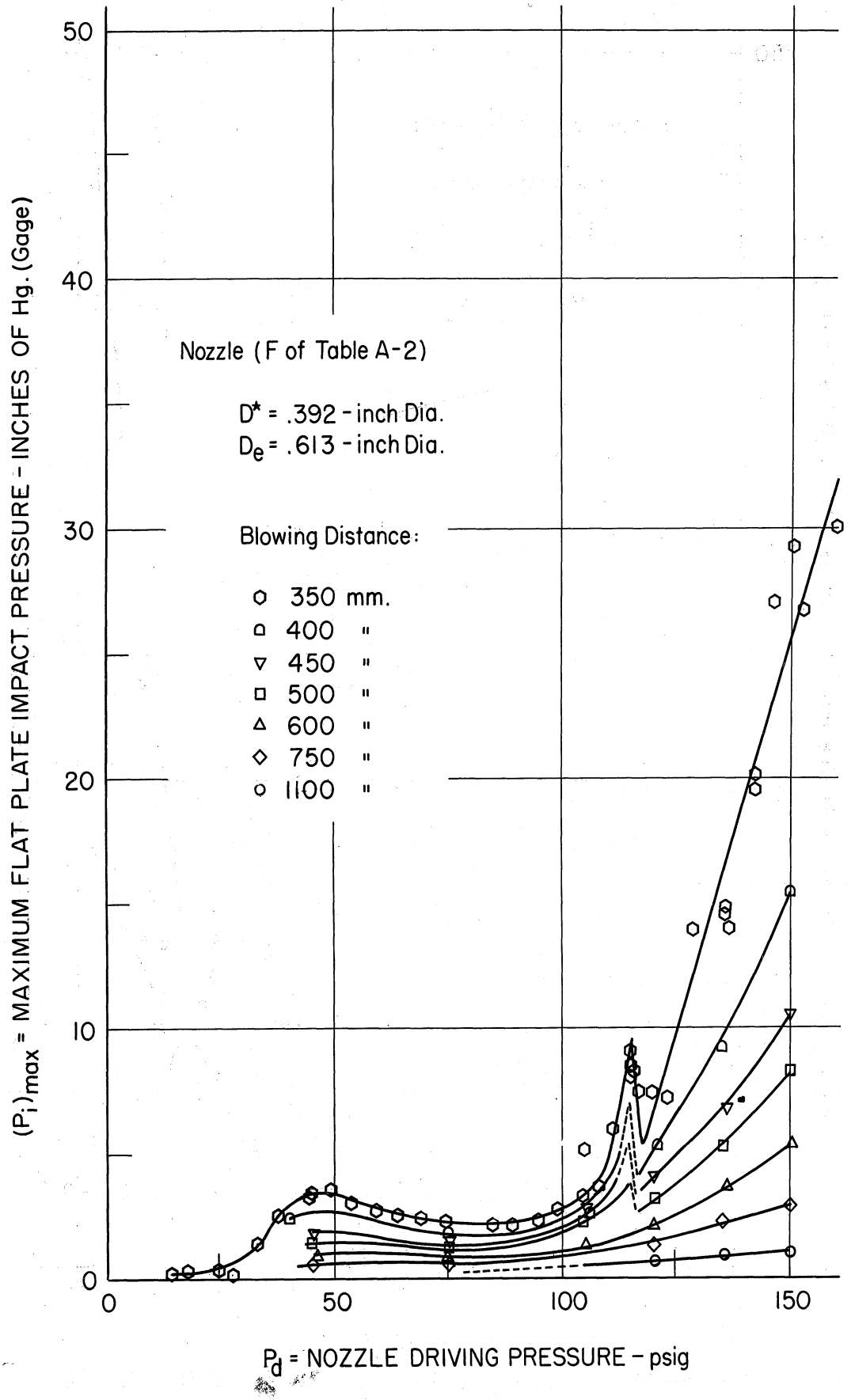

FIGURE 13 MAXIMUM FLAT PLATE IMPACT PRESSURE VS. NOZZLE DRIVING PRESSURE FOR .392 - INCH DIA. NOZZLE.

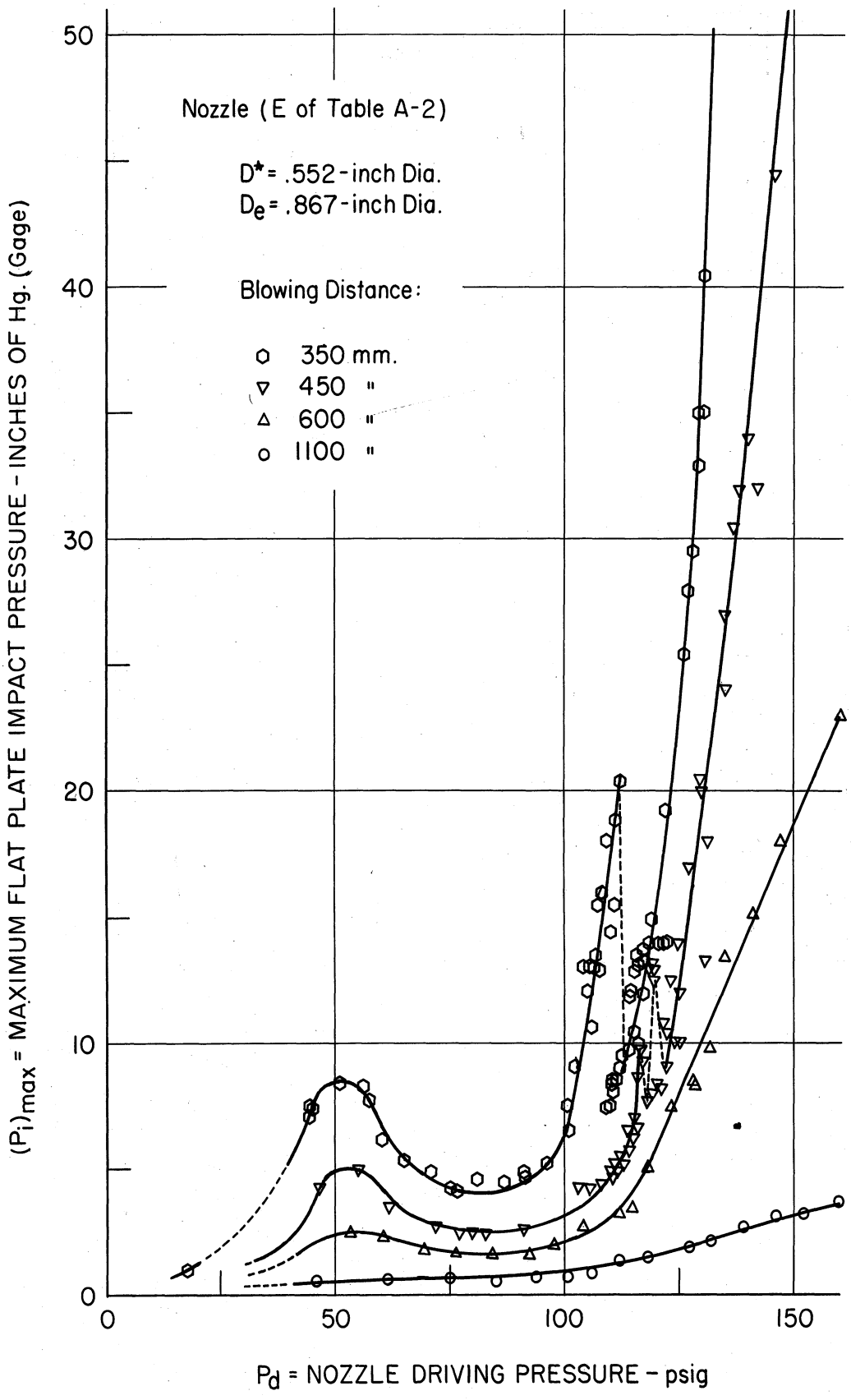

FIGURE 14a MAXIMUM FLAT PLATE IMPACT PRESSURE VS. NOZZLE DRIVING PRESSURE FOR .552-INCH DIA. NOZZLE.

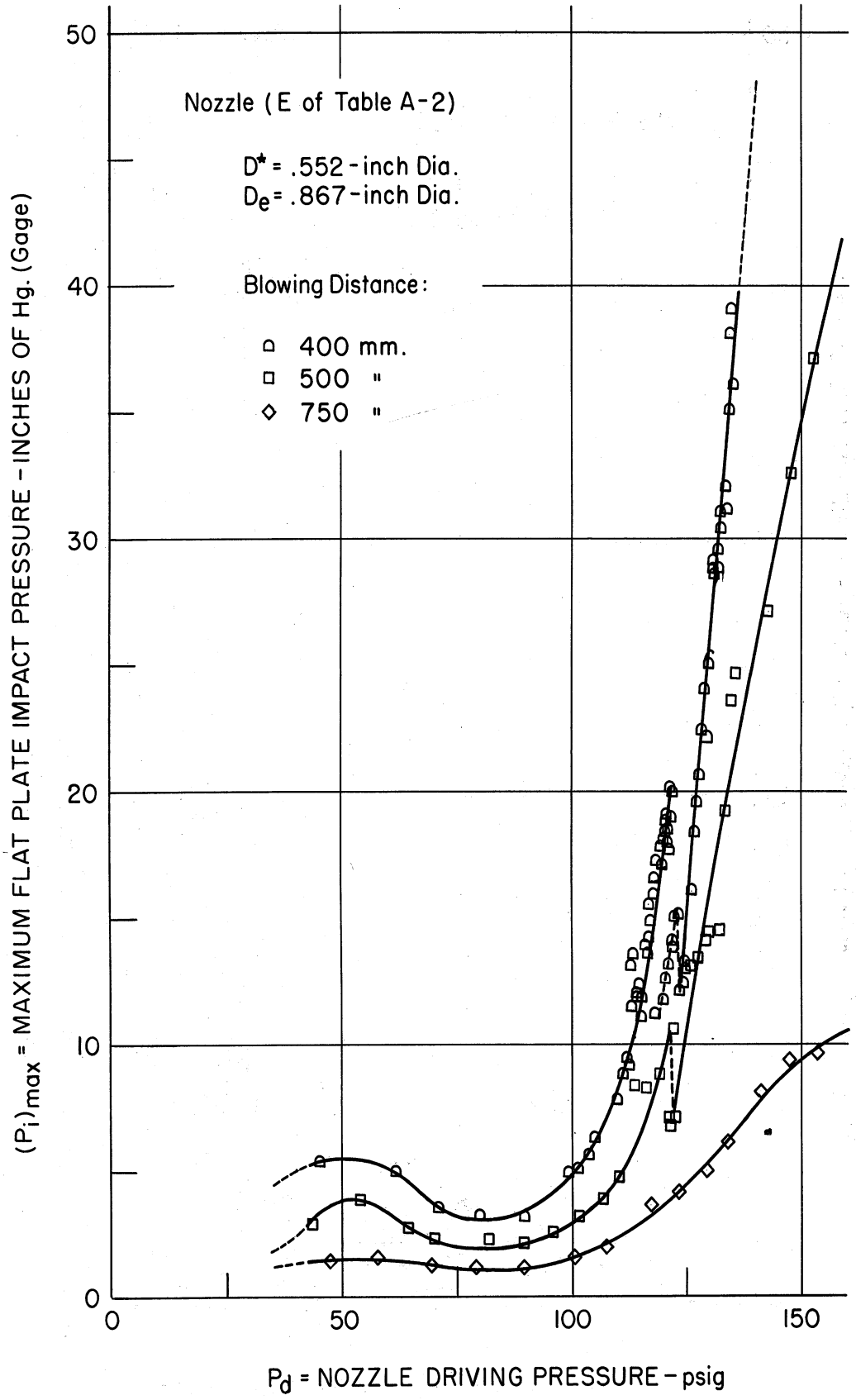

FIGURE 14b MAXIMUM FLAT PLATE IMPACT PRESSURE VS. NOZZLE DRIVING PRESSURE FOR .552 - INCH DIA. NOZZLE .

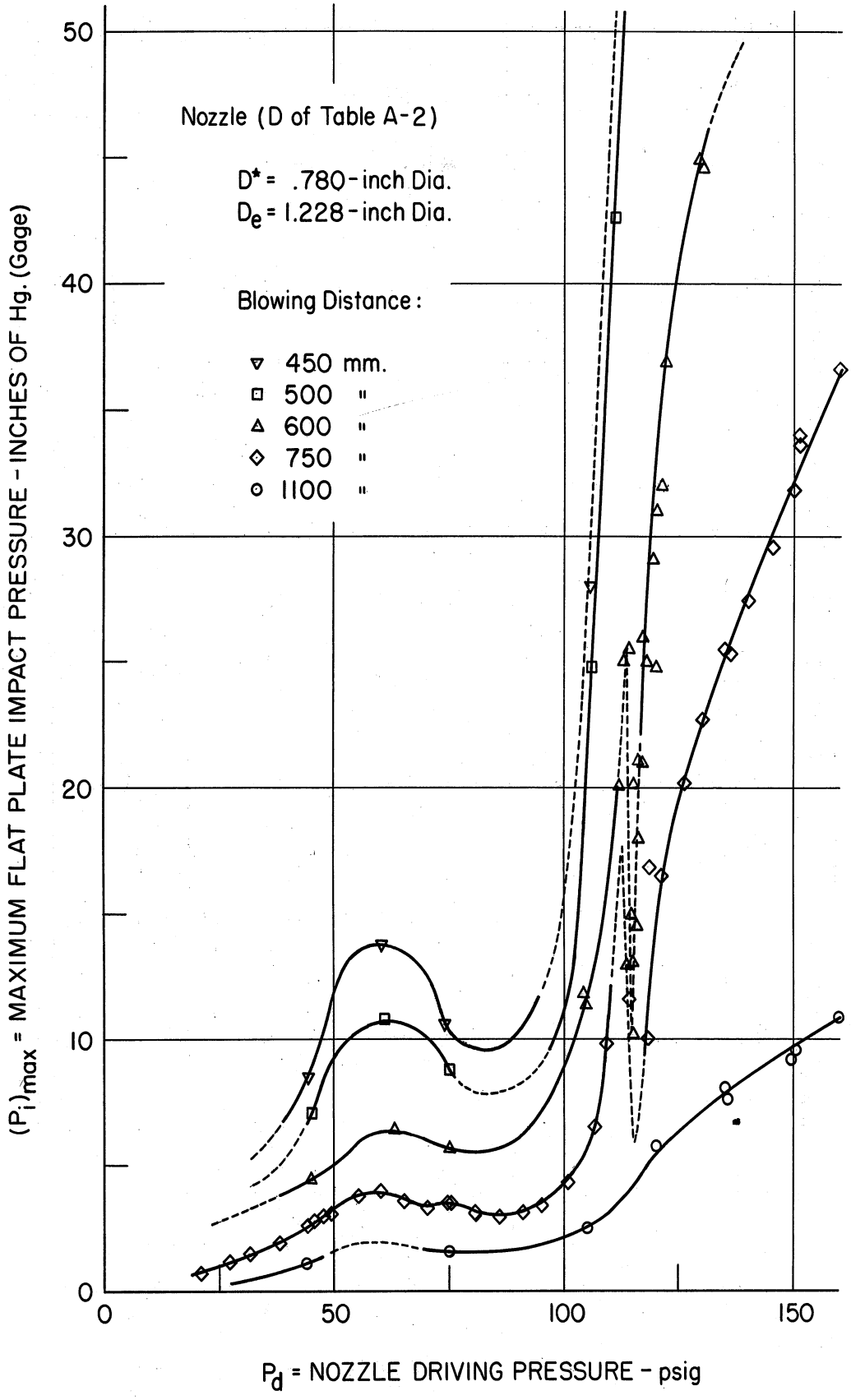

FIGURE 15 MAXIMUM FLAT PLATE IMPACT PRESSURE VS. NOZZLE DRIVING PRESSURE FOR .780-INCH DIA. NOZZLE.

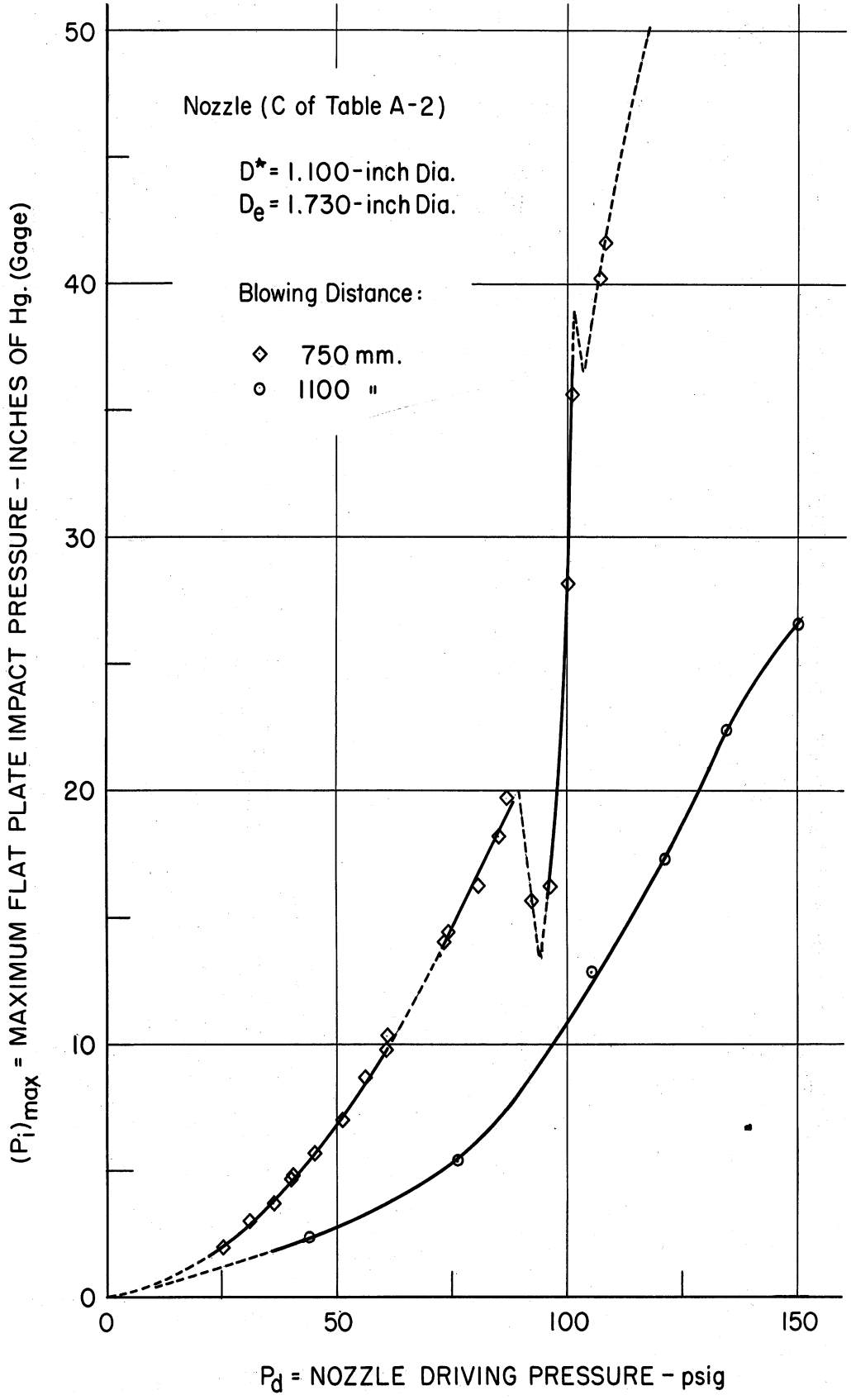

FIGURE 16 MAXIMUM FLAT PLATE IMPACT PRESSURE VS. NOZZLE DRIVING PRESSURE FOR 1.100-INCH DIA. NOZZLE.

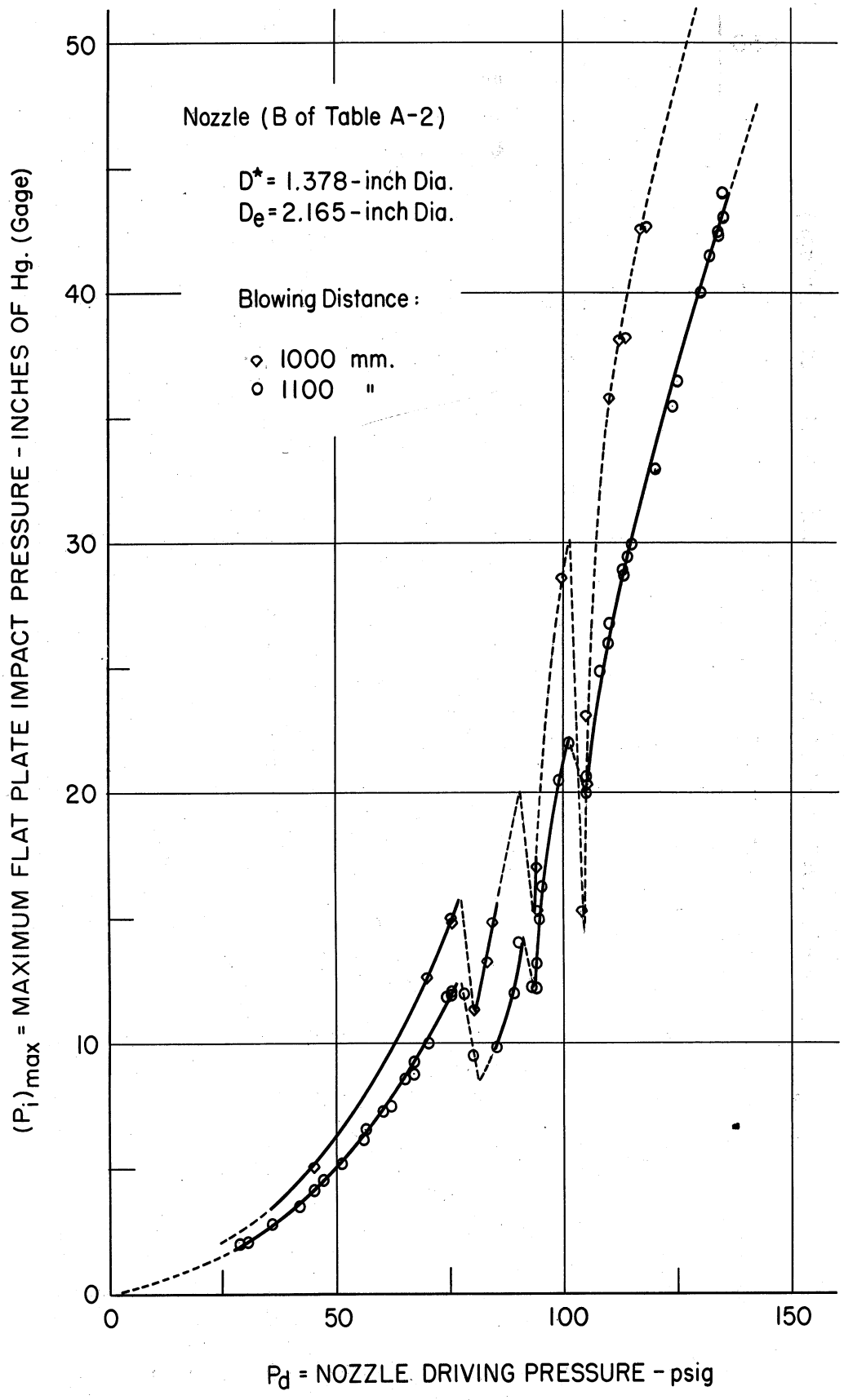

FIGURE 17 MAXIMUM FLAT PLATE IMPACT PRESSURE VS. NOZZLE DRIVING PRESSURE FOR 1.378-INCH DIA. NOZZLE.

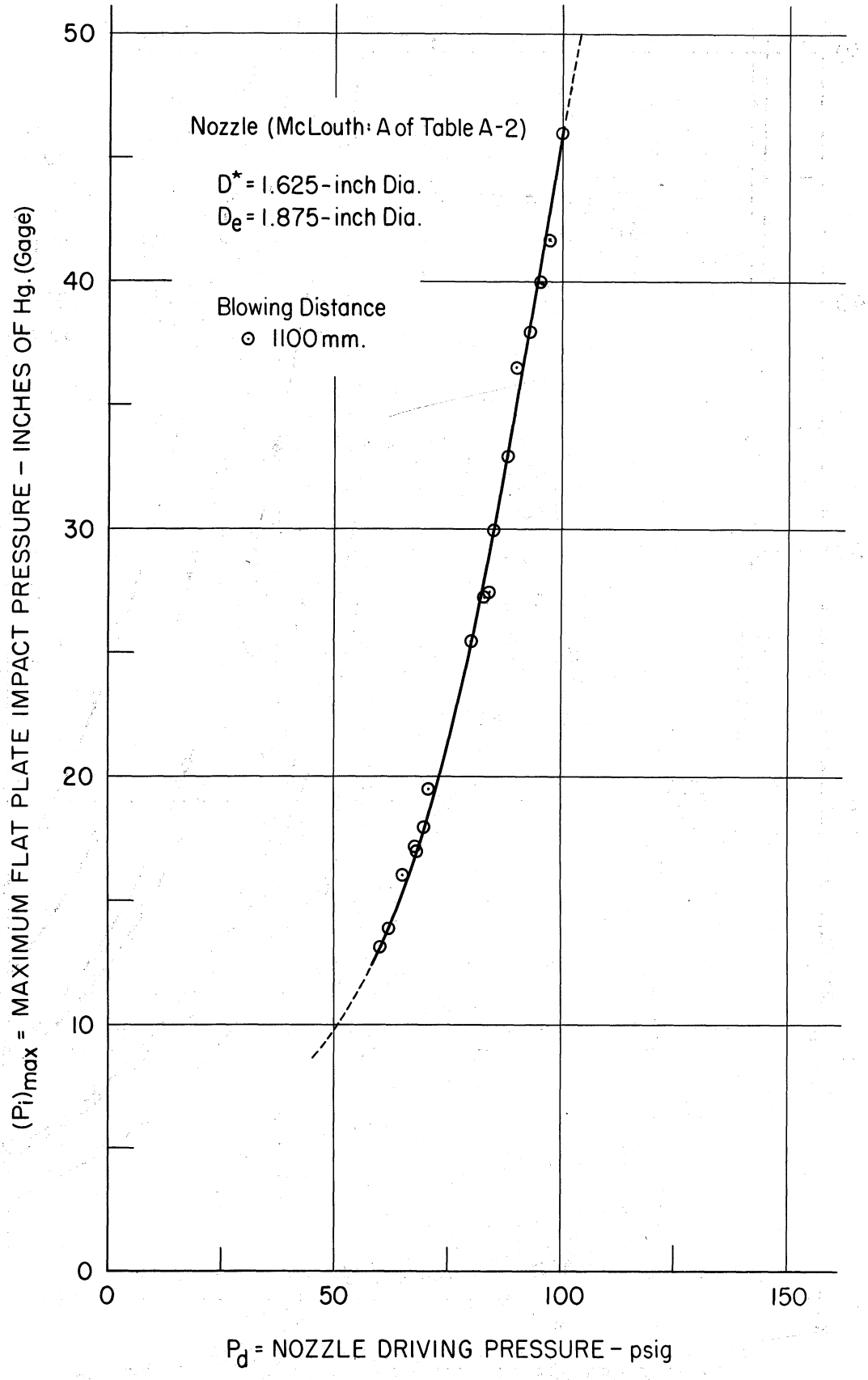

FIGURE 18 MAXIMUM FLAT PLATE IMPACT PRESSURE VS. NOZZLE DRIVING PRESSURE FOR 1.625-INCH DIA. NOZZLE .

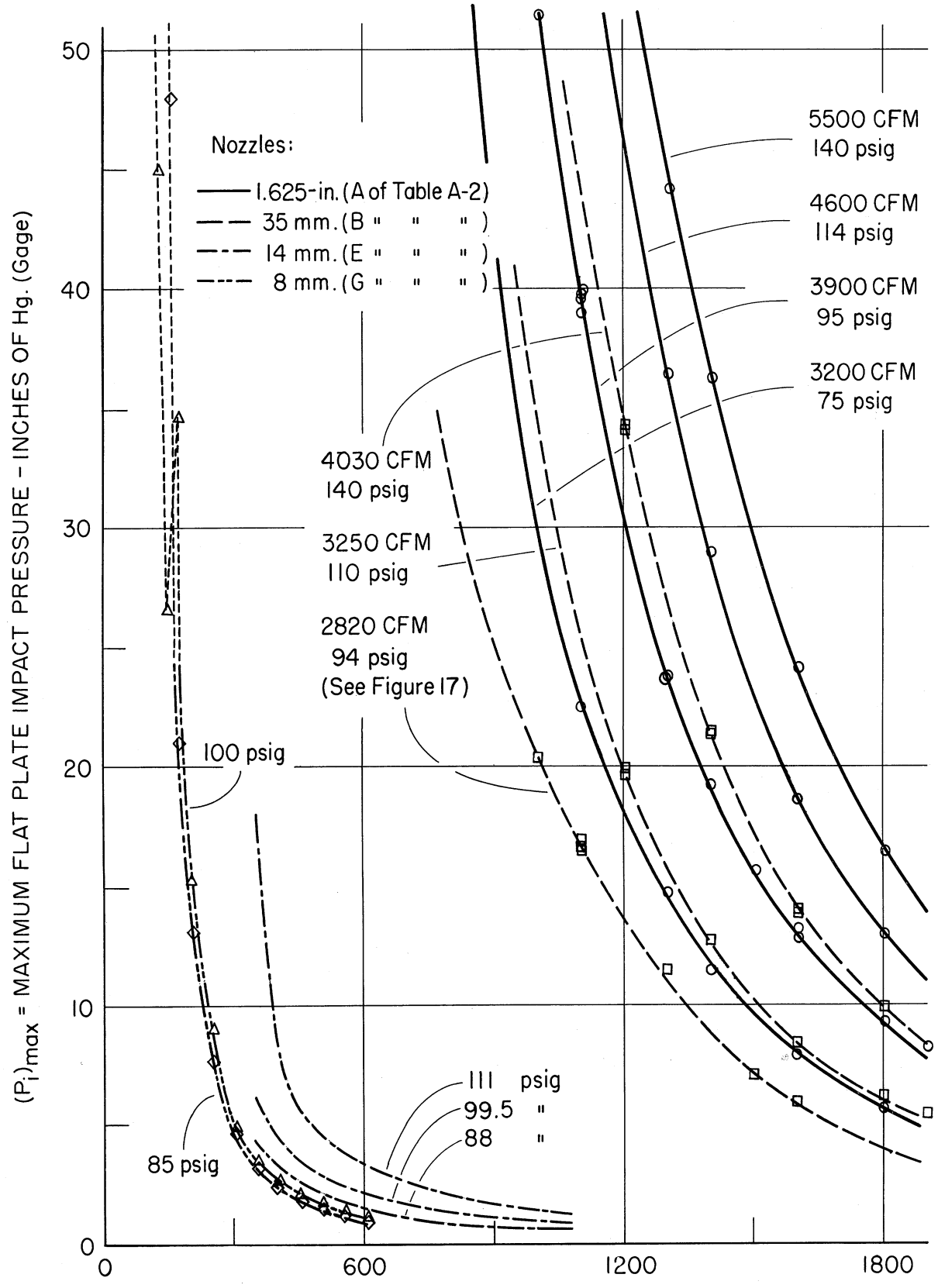

FIGURE 19 MAXIMUM FLAT PLATE IMPACT PRESSURE VS. BLOWING DISTANCE FOR NOZZLES A, B, E, AND G.

McLOUTH STEEL CORP. NOZZLE (A OF TABLE A-2)
AIR DRIVING PRESSURE 98 PSIG
THROAT AREA: 2.072 SQ. IN.
EXIT AREA: 2.76 SQ. IN.
AMBIENT AIR AT 29.3 IN. HG.
THEORETICAL EXIT MACH NUMBER 1.69
AIRCRAFT PROPULSION LABORATORY
UNIVERSITY OF MICHIGAN AUG. 9, 1955

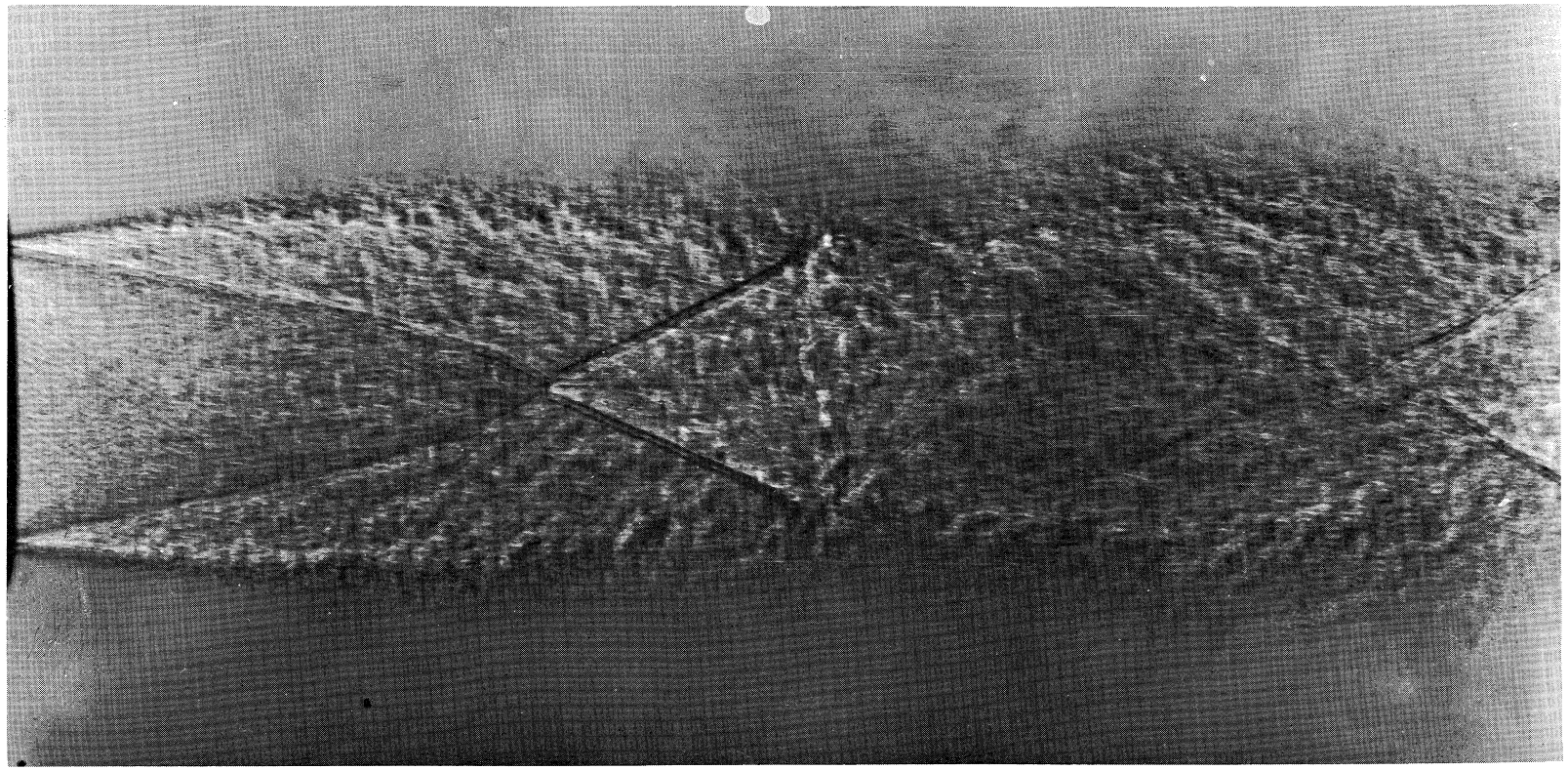

FIGURE 20 SHADOW PHOTOGRAPH.

McLOUTH STEEL CORP. NOZZLE (L OF TABLE A-2)
AIR DRIVING PRESSURE 71 PSIG
THROAT AREA: 2.74 SQ. IN.
EXIT AREA: 5.98 SQ. IN.
AMBIENT AIR AT 29.3 IN. HG.
THEORETICAL EXIT MACH NUMBER 2.3
AIRCRAFT PROPULSION LABORATORY
UNIVERSITY OF MICHIGAN AUG. 9, 1955

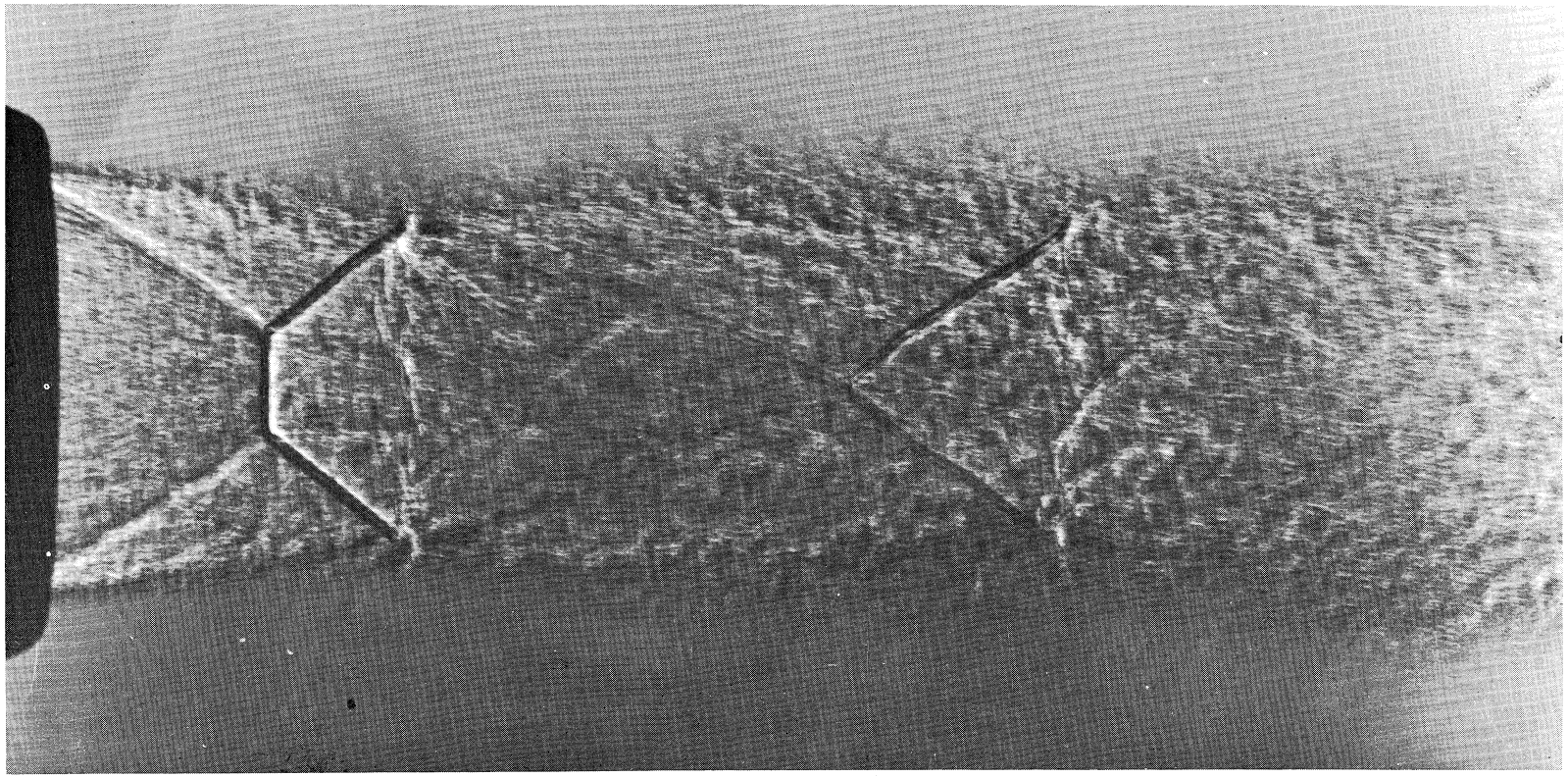

FIGURE 21 SHADOW PHOTOGRAPH.

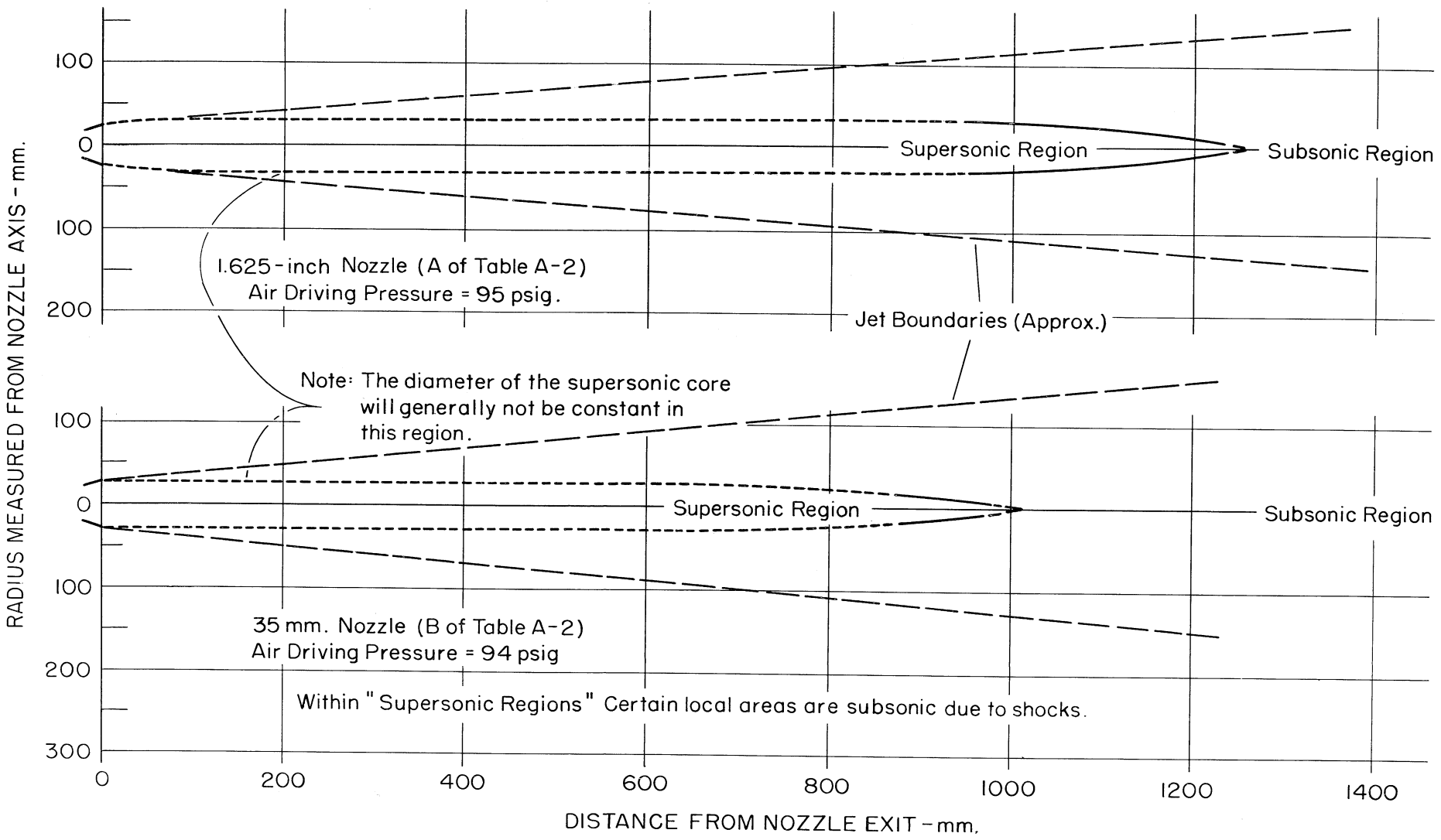

FIGURE 22 GRAPH SHOWING APPROXIMATE SHAPE AND LENGTH OF SUPERSONIC CORE IN FREE AIR FOR A 1.625-INCH DIAMETER NOZZLE (A OF TABLE A-2) AT 95 psig DRIVING PRESSURE AND A 35 mm. NOZZLE (B OF TABLE A-2) AT 94 psig DRIVING PRESSURE.

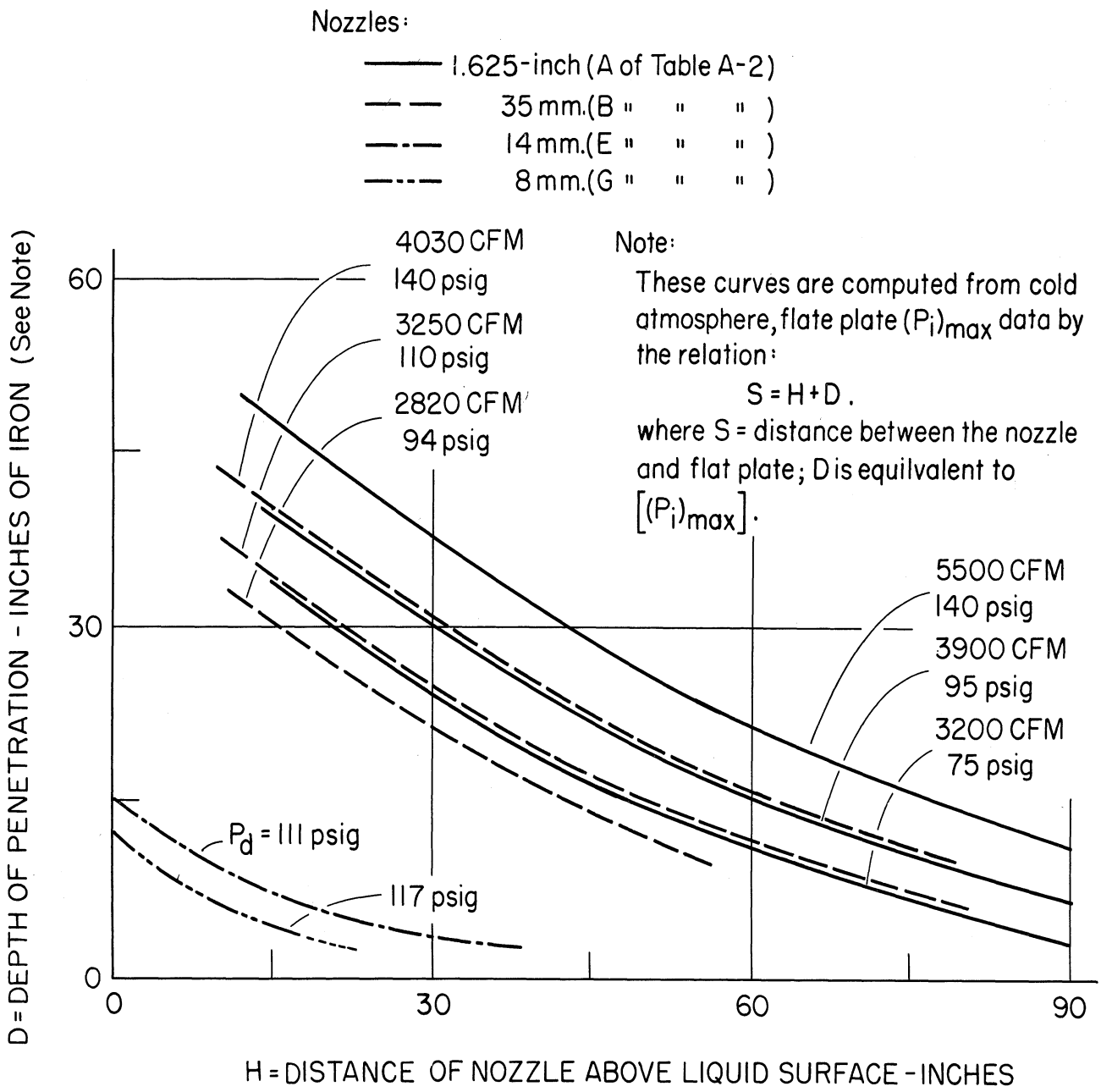

FIGURE 23 GRAPH OF PENETRATION (COMPUTED FROM COLD ATMOSPHERE MAXIMUM IMPACT PRESSURE DATA) VS. BLOWING DISTANCE FOR 8, 14, AND 35 mm. AND 1.625-INCH NOZZLES (A,B,E, &G).

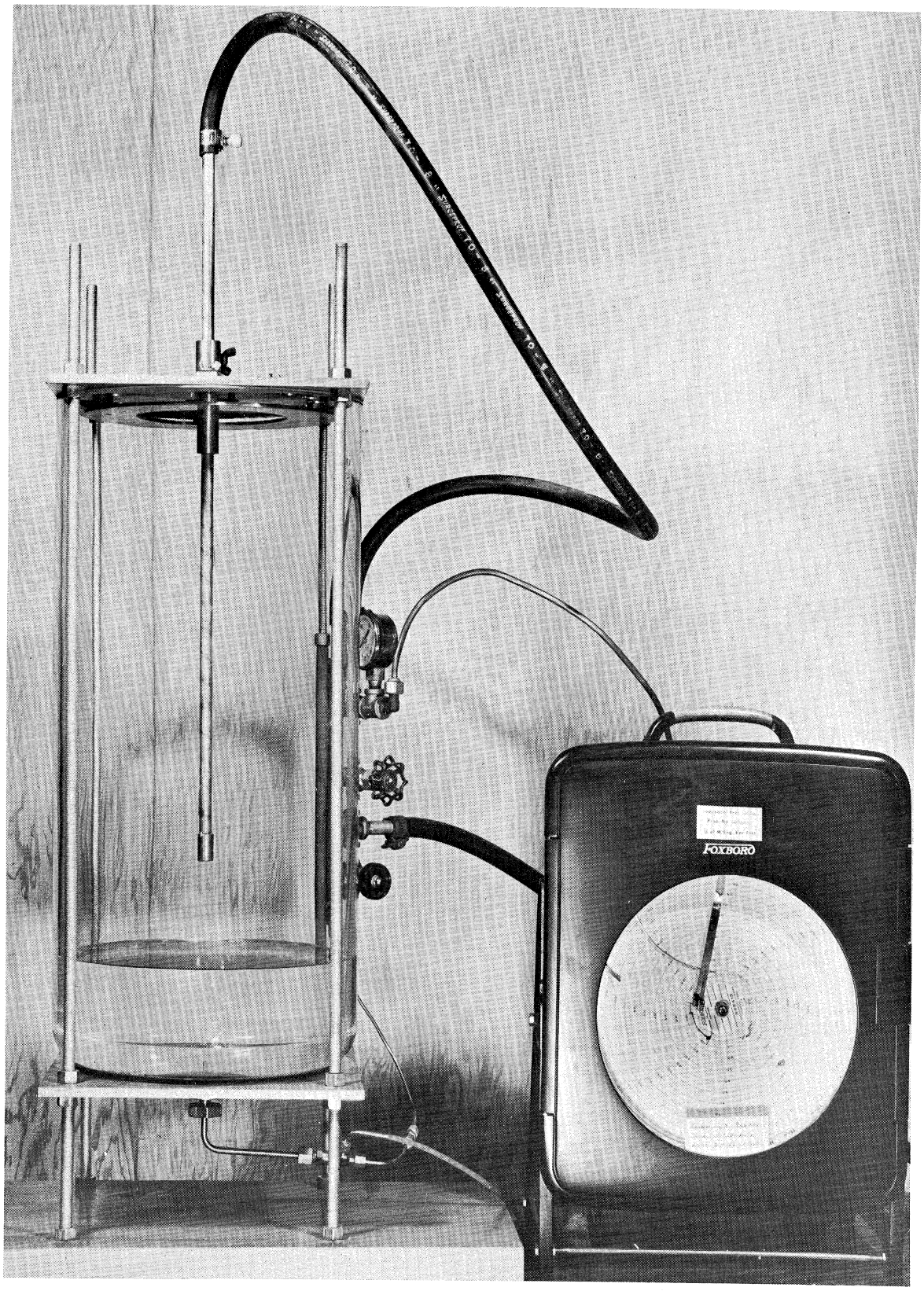

FIGURE 24a PHOTOGRAPH OF MODEL USED TO DEMON - STRATE "BUBBLER PROBE" TECHNIQUE.

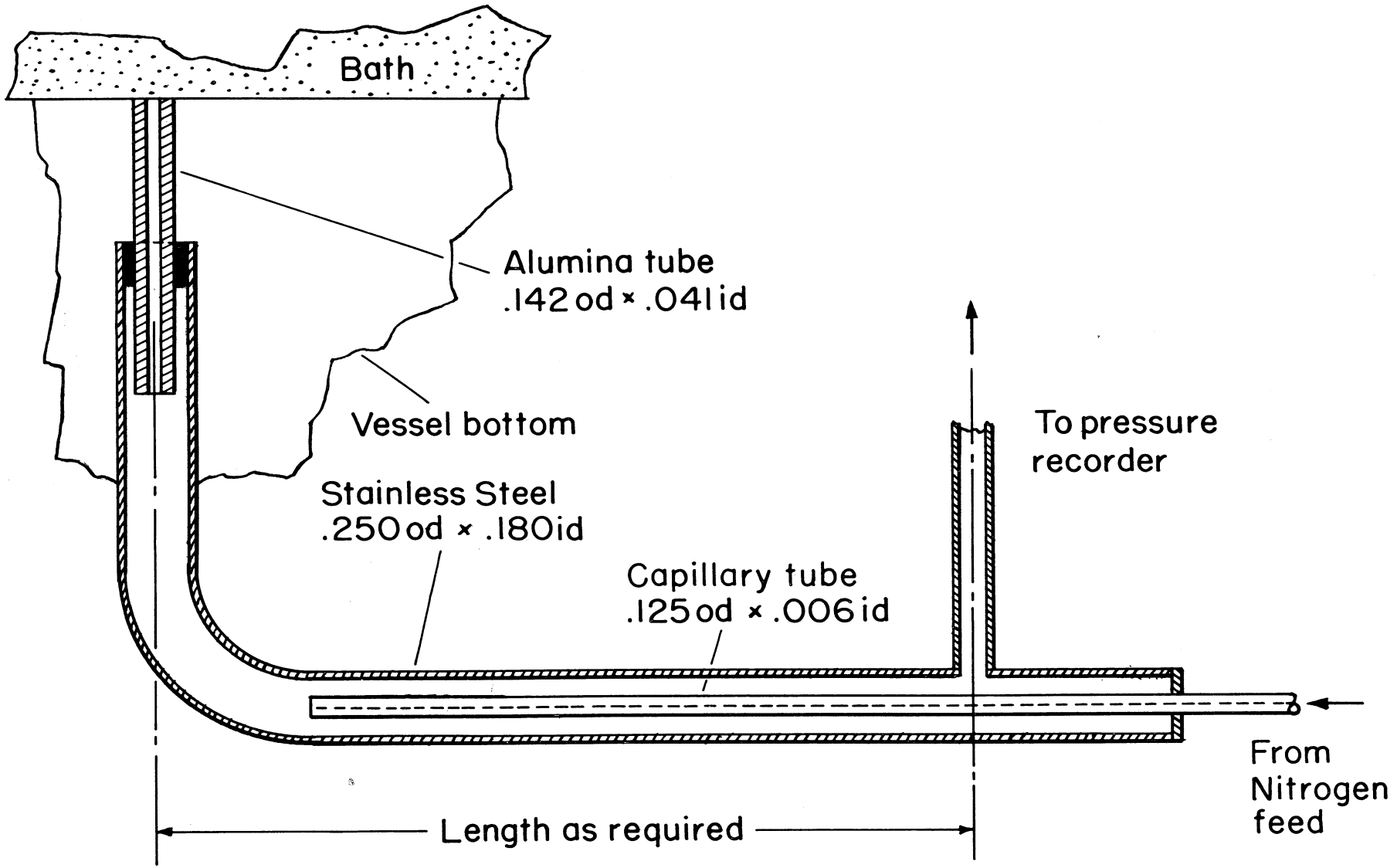

FIGURE 24b NITROGEN BUBBLER PROBE.

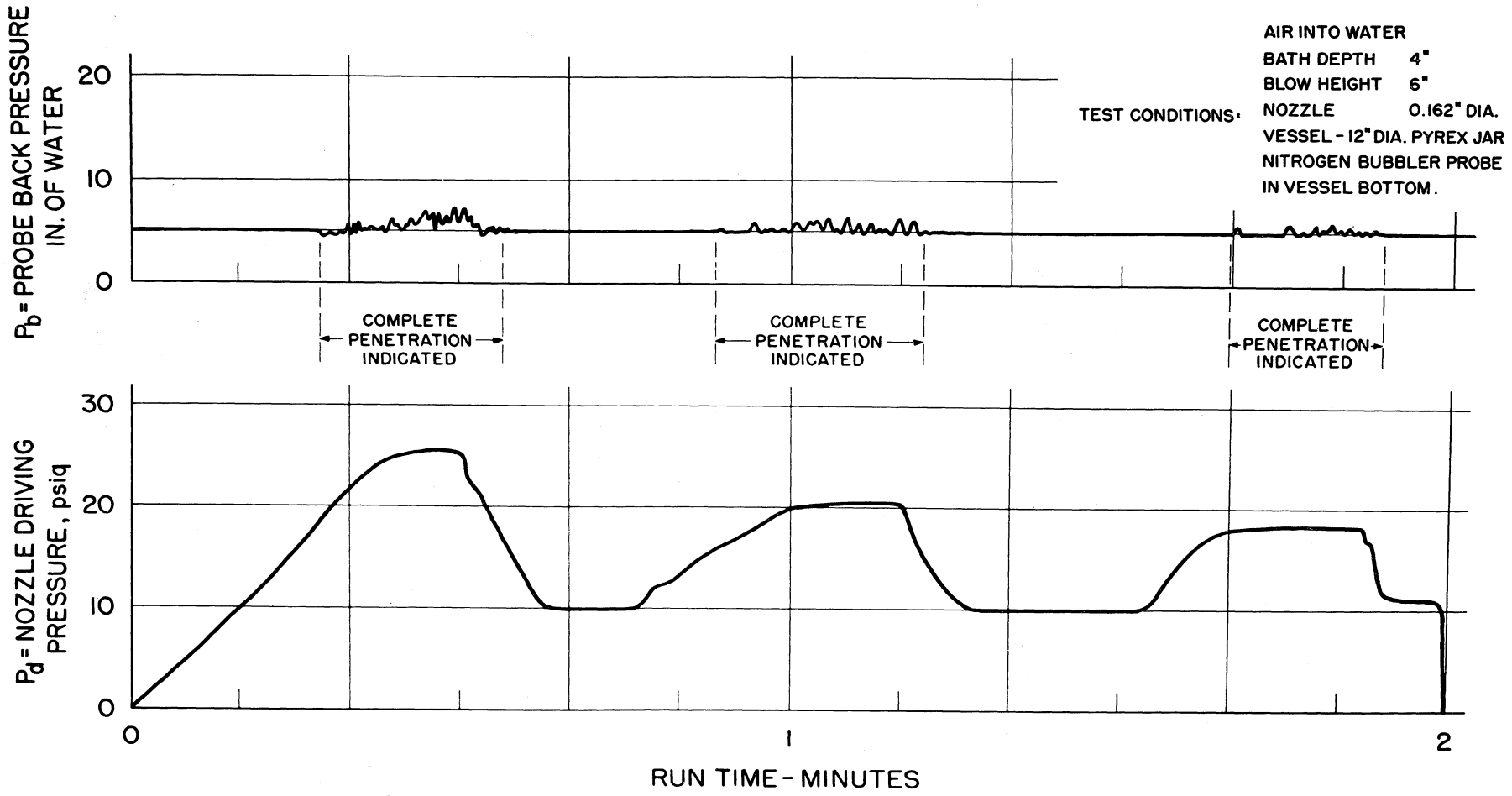

FIGURE 25 MEASUREMENT OF JET PENETRATION IN WATER.

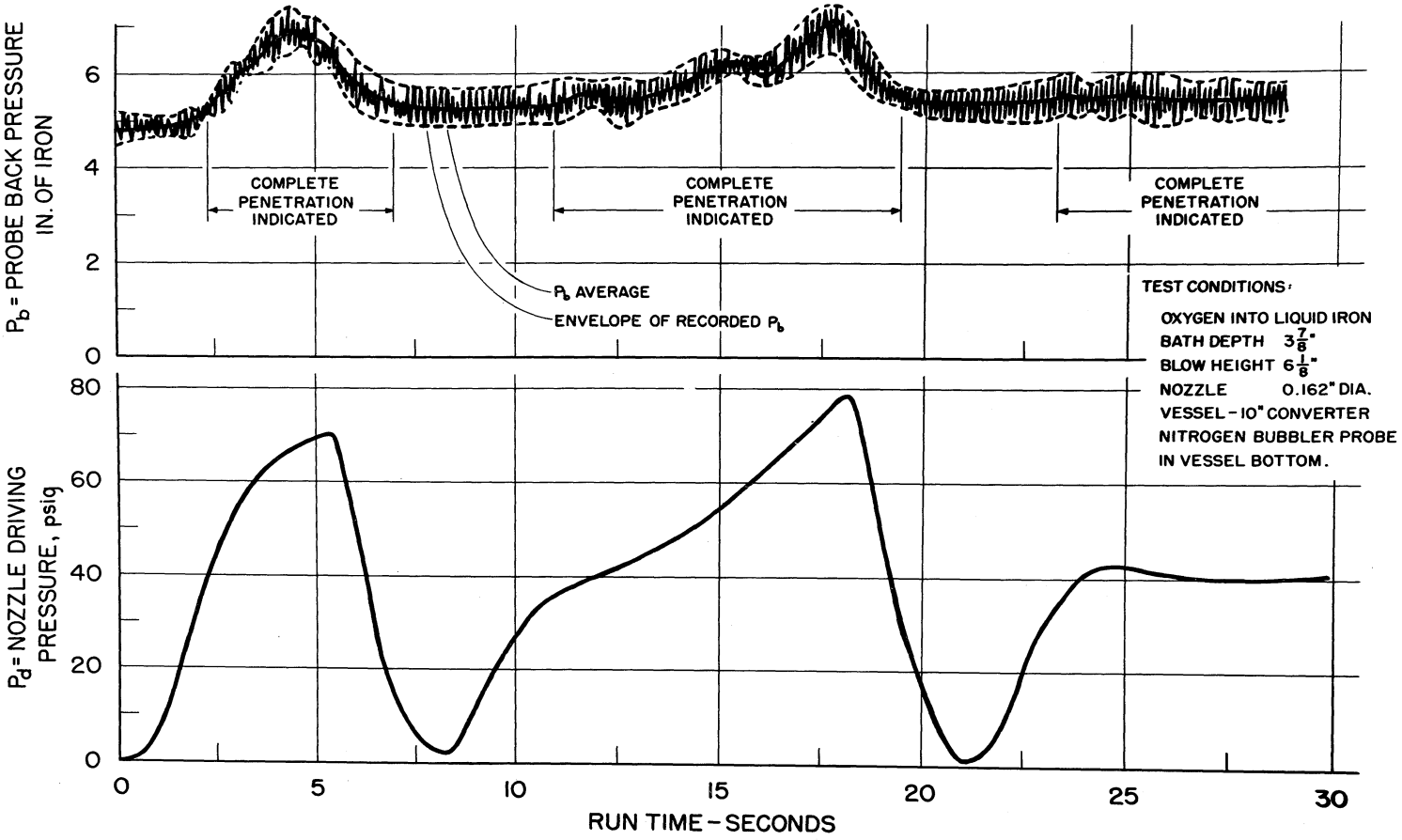

FIGURE 26 MEASUREMENT OF JET PENETRATION IN 3 7/8-INCH MOLTEN IRON BATH.

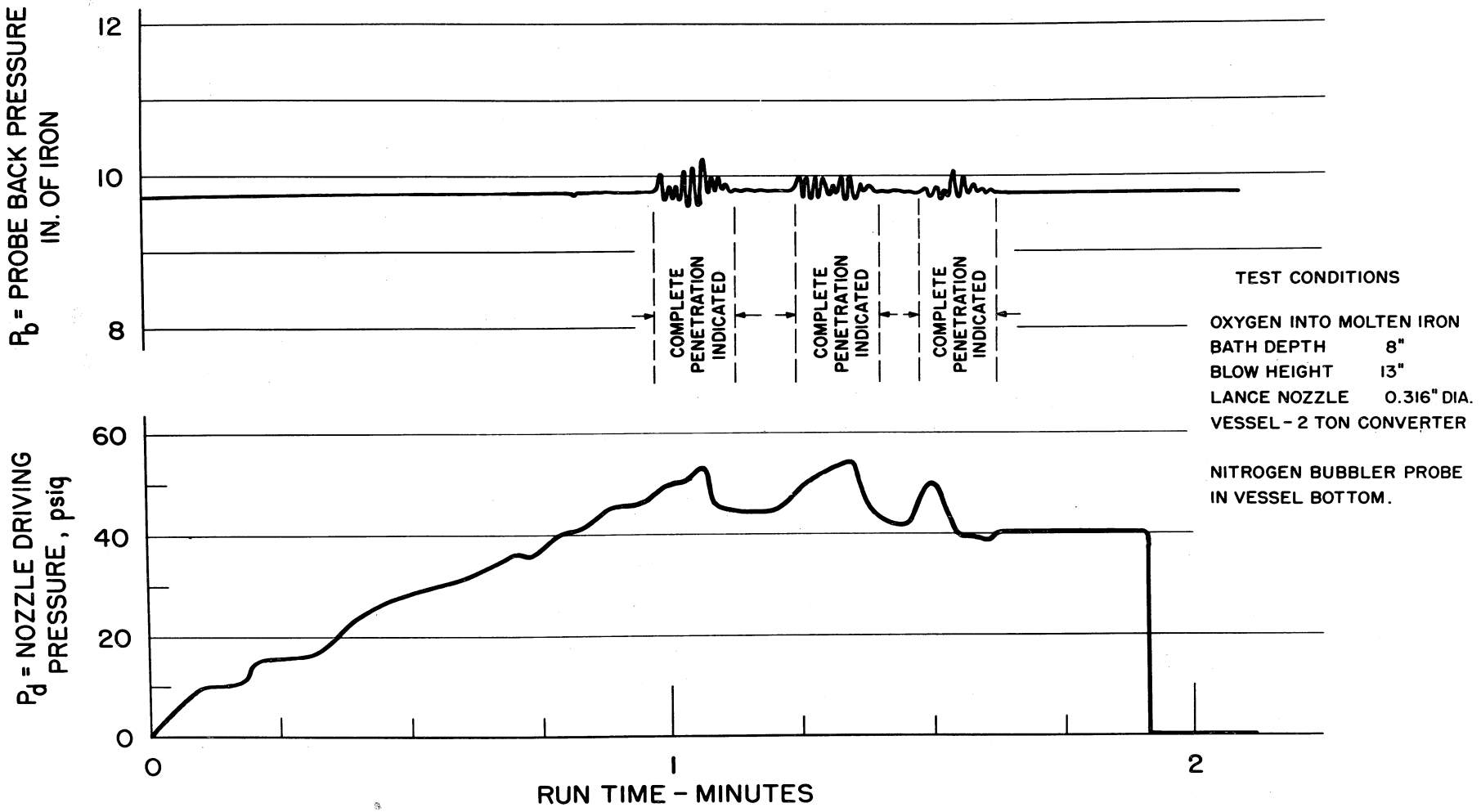

FIGURE 27 MEASUREMENT OF JET PENETRATION IN 8-INCH MOLTEN IRON BATH.

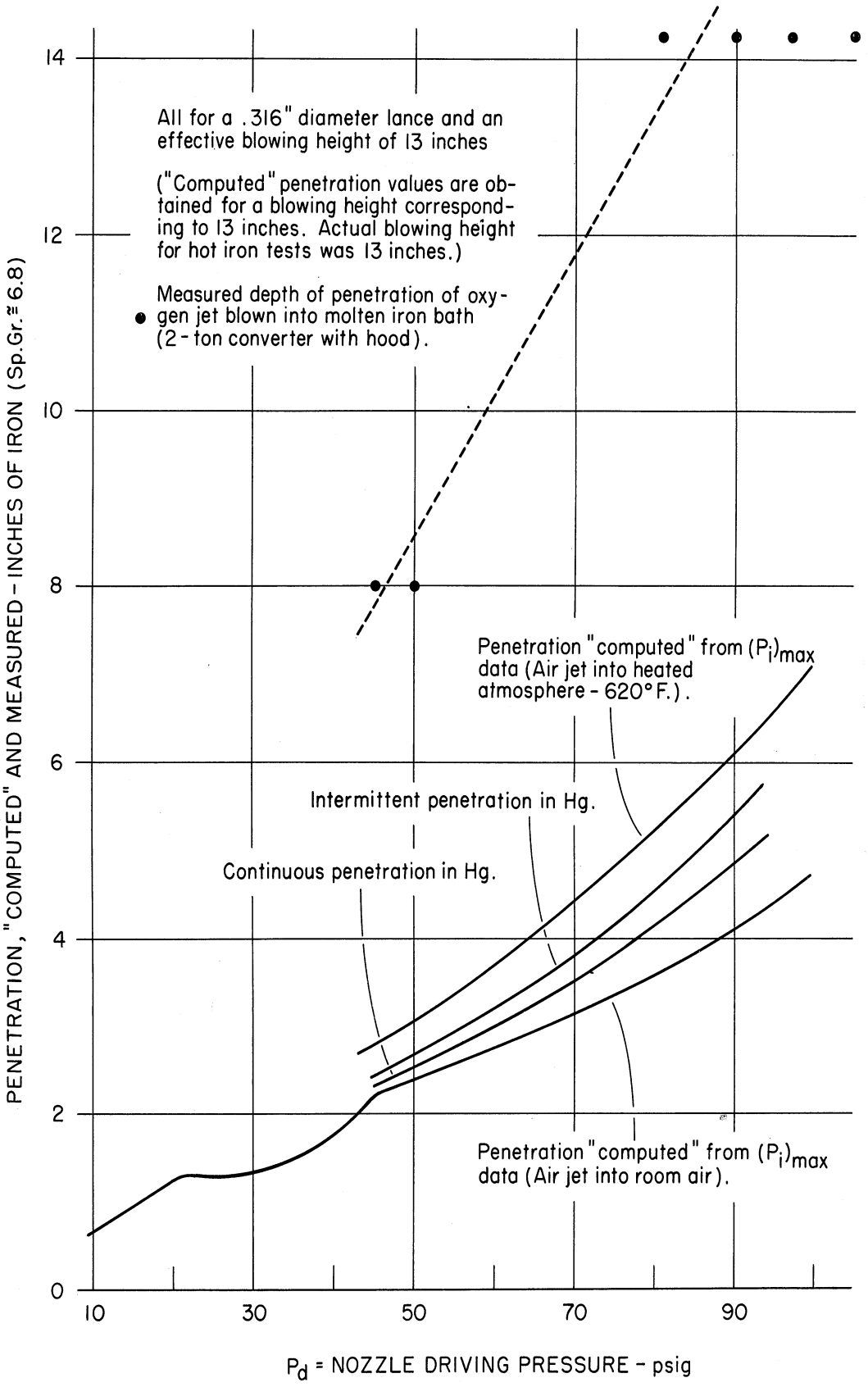

FIGURE 28 PENETRATION, "COMPUTED" AND MEASURED VS. NOZZLE DRIVING PRESSURE.

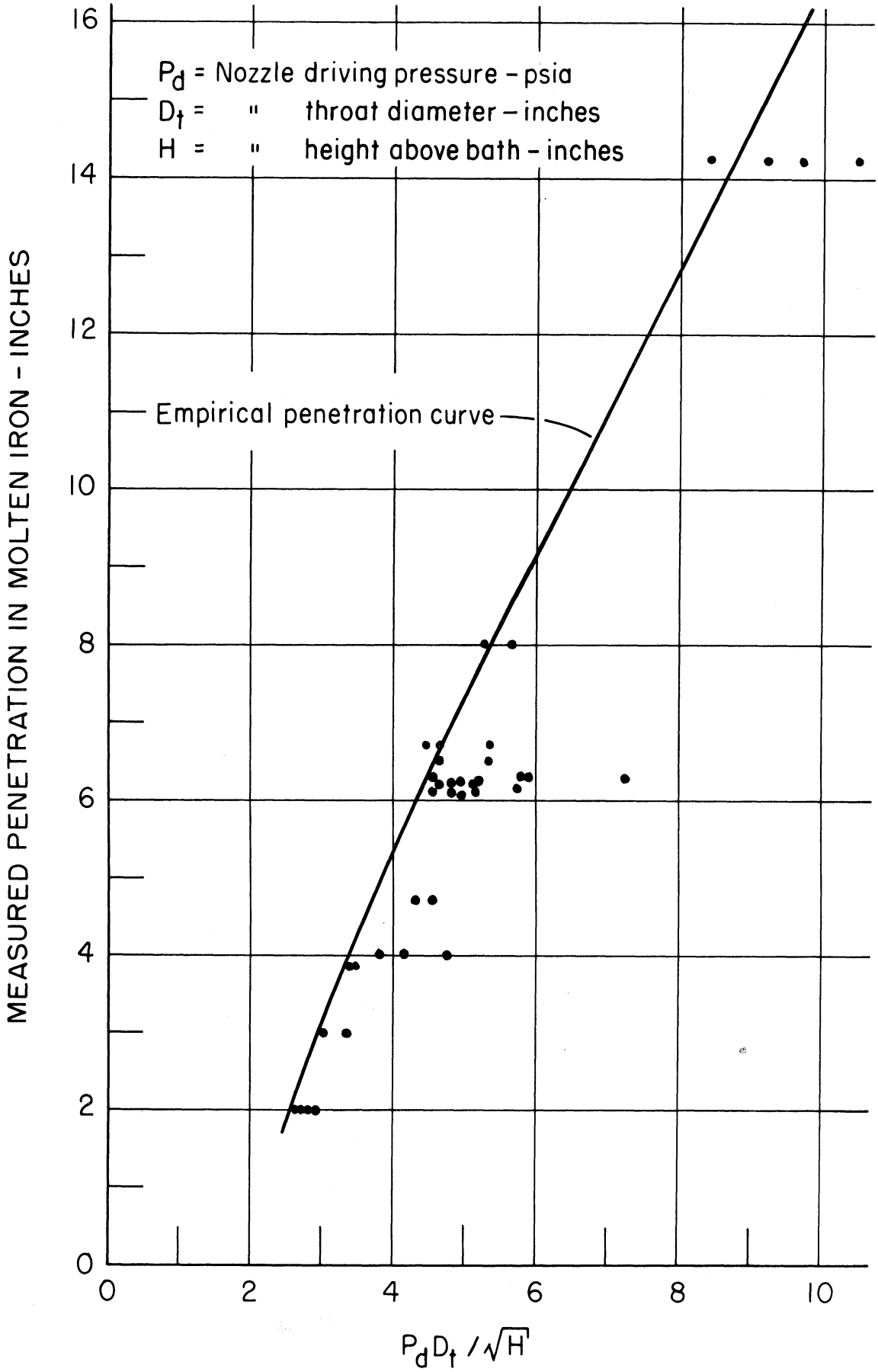

FIGURE 29 GRAPH OF MEASURED PENETRATION IN MOLTEN IRON VS. THE PARAMETER – $P_d D_t / \sqrt{H}$.

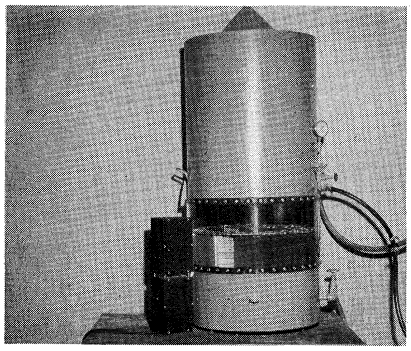

1

Model and Light source. All Vanes pointed toward Vessel.center. No Jet.

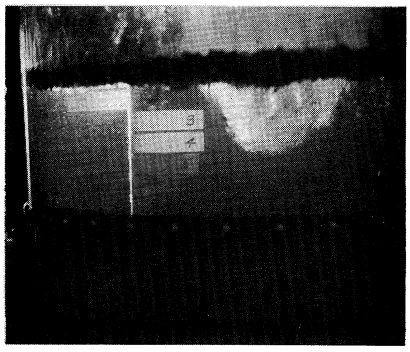

4

Bath and Vanes 8 seconds after starting the Jet.

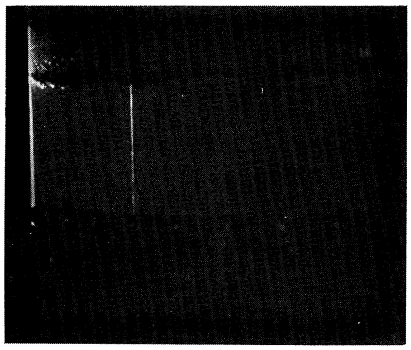

2

Bath and Rudder assembly before Jet started. All Vanes perpendicular to Vessel radius through pivot line of Vanes.

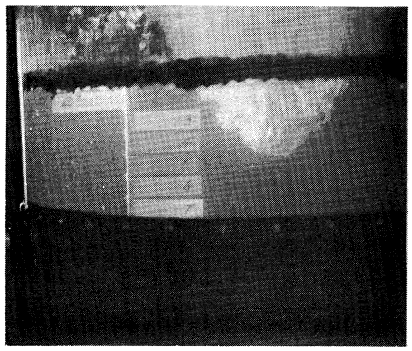

5

Bath and Vanes 19 seconds after starting the Jet.

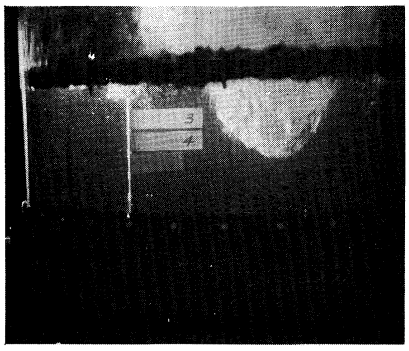

3

Bath and Vanes 6 seconds after starting the Jet.

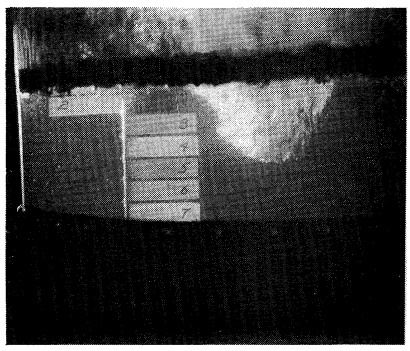

6

Bath and Vanes 30 seconds after starting the Jet.

Rudder assembly mounted in a 2-foot Vessel (No. 3 of Table C-1) to show the direction of motion of the liquid in a vertical section of the Bath.

FIGURE 30 MULTI-VANED RUDDER ASSEMBLY.

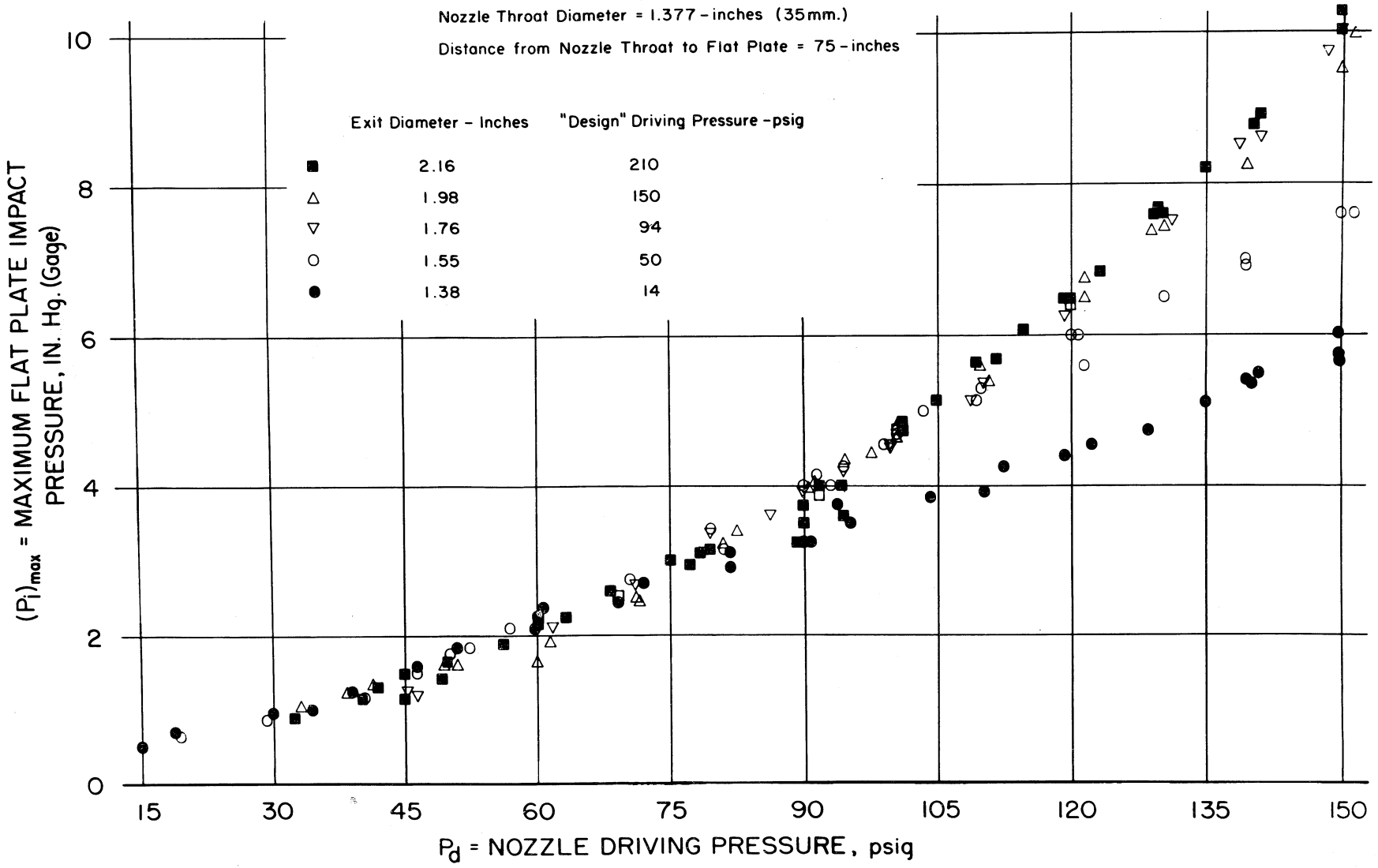

FIGURE 31 MAXIMUM FLAT PLATE IMPACT PRESSURE VS. NOZZLE DRIVING PRESSURE.

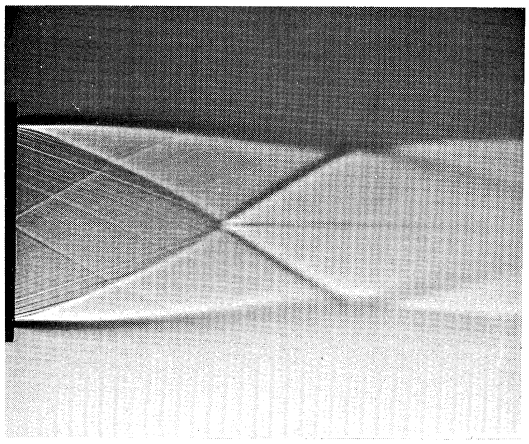

D_e = 2.16 – inches

Nozzle B'

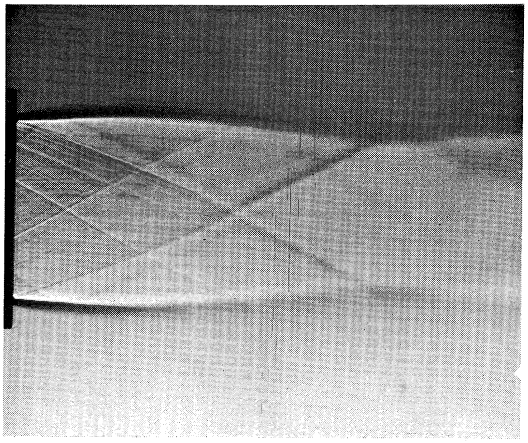

D_e = 1.98 – inches
(Correct for P_d = 150)

Nozzle B'_1

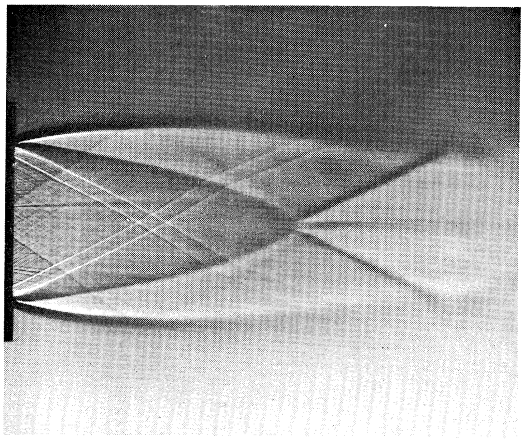

D_e = 1.76 – inches

Nozzle B'_2

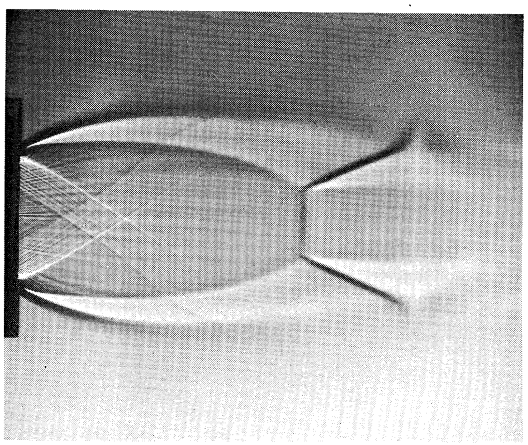

D_e = 1.55 – inches

Nozzle B'_3

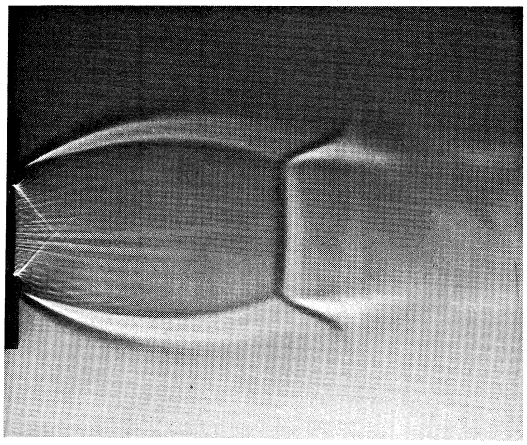

$D_e = D^\star$ = 1.377 – inches

Nozzle B'_4

$D^\star$ = Throat Diameter = 1.377 – inches
P_d = Nozzle Driving Pressure = 150 psig
D_e = Exit Diameter – as Specified

(Nozzles Exhausting Into Room Air)

FIGURE 32 SHADOW PHOTOGRAPHS.

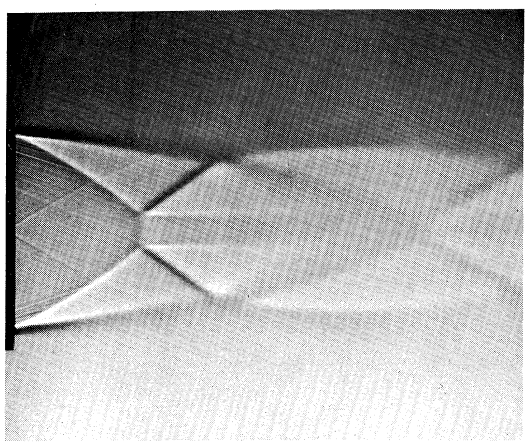

D_e = 2.16 – inches

Nozzle B'

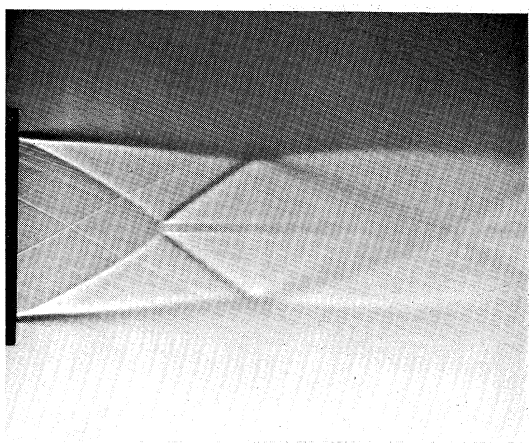

D_e = 1.98 – inches

Nozzle B'_1

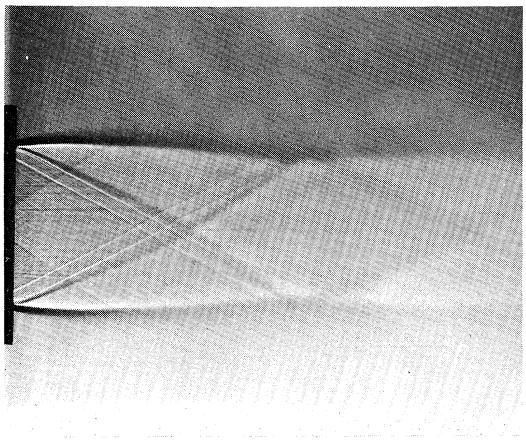

D_e = 1.76 – inches
(Correct for P_d = 94)

Nozzle B'_2

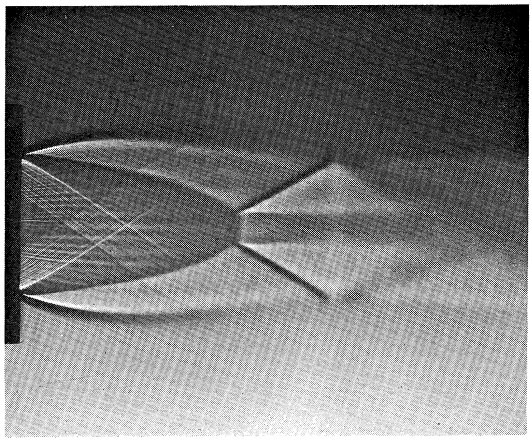

D_e = 1.55 – inches

Nozzle B'_3

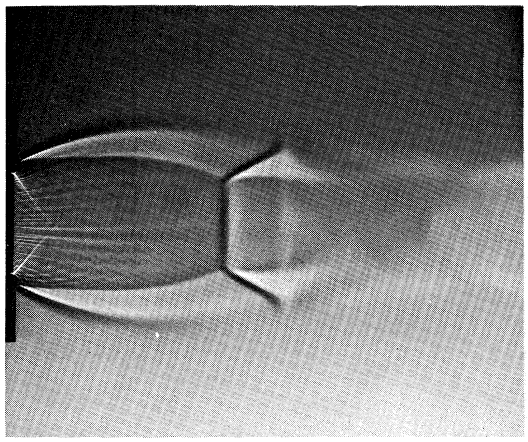

$D_e = D^* = 1.377$ – inches

Nozzle B'_4

D^* = Throat Diameter = 1.377 – inches
P_d = Nozzle Driving Pressure = 94 psig
D_e = Exit Diameter – as Specified

(Nozzles Exhausting Into Room Air)

FIGURE 33 SHADOW PHOTOGRAPHS.

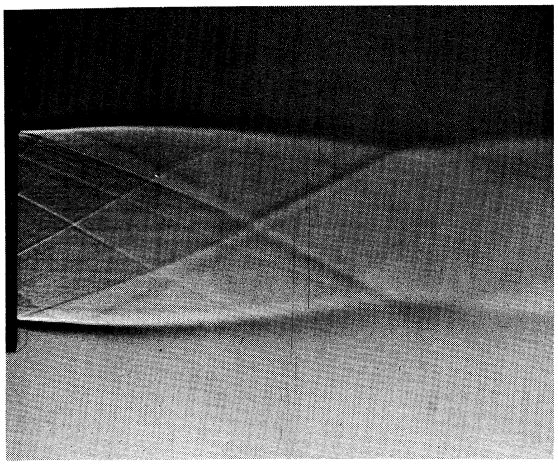

D_e = 1.98 – inches
P_d = 150 psig

Nozzle B'_1

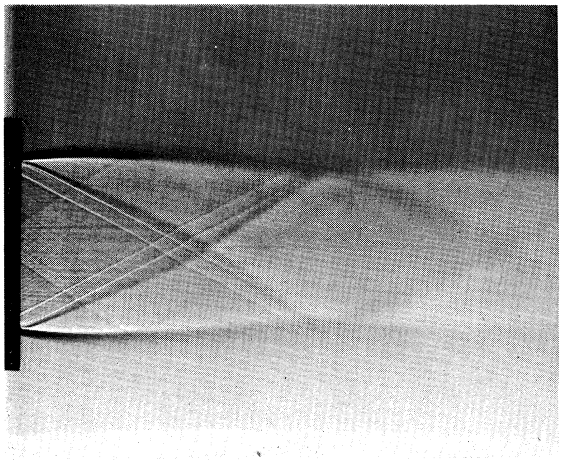

D_e = 1.76 – inches
P_d = 94 psig

Nozzle B'_2

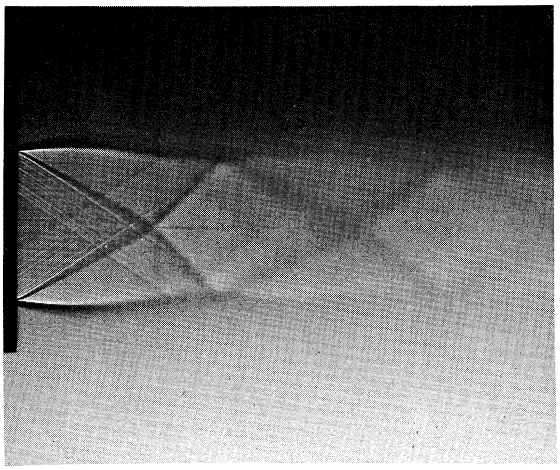

D_e = 1.55 – inches
P_d = 50 psig

Nozzle B'_3

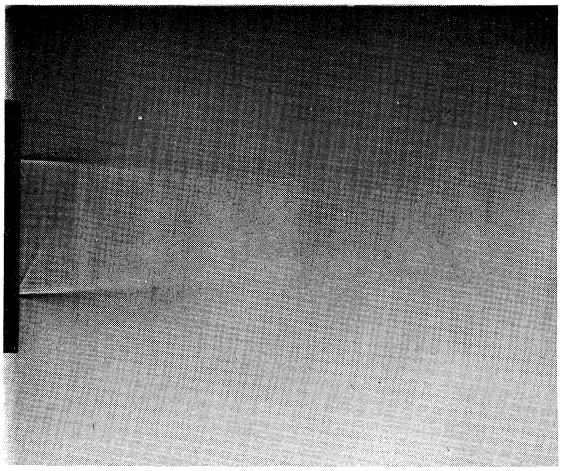

$D_e = D^\star$ = 1.377 – inches
P_d = 15 psig

Nozzle B'_4

$D^\star$ = Throat Diameter = 1.377 – inches
P_d = Nozzle Driving Pressure – as Specified
D_e = Exit Diameter – as Specified

(Nozzles Exhausting Into Room Air)

FIGURE 34 SHADOW PHOTOGRAPHS.